การพัฒนาอนุภาคนาโนไขมันแข็งที่บรรจุแอสตาแซนธินจากสารสกัดเปลือกกุ้ง
เพื่อการนำส่งทางผิวหนัง

นายกฤษฎา รูปใหญ่

วิทยานิพนธ์นี้เป็นส่วนหนึ่งของการศึกษาตามหลักสูตรปริญญาเภสัชศาสตรมหาบัณฑิต
สาขาวิชาเภสัชกรรม ภาควิชาวิทยาการเภสัชกรรมและเภสัชอุตสาหกรรม
คณะเภสัชศาสตร์ จุฬาลงกรณ์มหาวิทยาลัย
ปีการศึกษา 2555

DEVELOPMENT OF SOLID LIPID NANOPARTICLES CONTAINING ASTAXANTHIN

FROM SHRIMP SHELL EXTRACT FOR SKIN DELIVERY

Mr. Kritsada Roopyai

A Thesis Submitted in Partial Fulfillment of the Requirements

for the Degree of Master of Science in Pharmacy Program in Pharmaceutics

Department of Pharmaceutics and Industrial Pharmacy

Faculty of Pharmaceutical Sciences

Chulalongkorn University

Academic Year 2012

Thesis Title   DEVELOPMENT OF SOLID LIPID NANOPARTICLES
                    CONTAINING   ASTAXANTHIN   FROM   SHRIMP
                    SHELL EXTRACT FOR SKIN DELIVERY
By   Mr. Kritsada Roopyai
Field of Study   Pharmaceutics
Thesis Advisor   Prapasri Sinswat, Ph.D.
Thesis Co-advisor   Associate Professor Parkpoom Tengamnuay, Ph.D.

Accepted by the Faculty of Pharmaceutical Sciences, Chulalongkorn University in Partial Fulfillment of the Requirements for the Master's Degree

...………………………………Dean of the Faculty of Pharmaceutical Sciences

(Associate Professor Pintip Pongpech, Ph.D.)

THESIS COMMITTEE

…………………………………Chairman

(Assistant Professor Nontima Vardhanabhuti, Ph.D.)

………………………….…… Thesis Advisor

(Prapasri Sinswat, Ph.D.)

………………………………... Thesis Co-advisor

(Associate Professor Parkpoom Tengamnuay, Ph.D.)

…………………………….…… Examiner

(Anyarporn Tansirikongkol, Ph.D.)

………………………….…… External Examiner

(Associate Professor Varaporn Junyaprasert, Ph.D.)

กฤษฎา รูปใหญ่: การพัฒนาอนุภาคนาโนไขมันแข็งที่บรรจุแอสตาแซนธินจากสารสกัดเปลือกกุ้งเพื่อการนำส่งทางผิวหนัง. (DEVELOPMENT OF SOLID LIPID NANOPARTICLES CONTAINING ASTAXANTHIN FROM SHRIMP SHELL EXTRACT FOR SKIN DELIVERY) อ.ที่ปรึกษาวิทยานิพนธ์หลัก: ดร.ประภาศรี สินสวัสดิ์, อ.ที่ปรึกษาวิทยานิพนธ์ร่วม: รศ. ดร.ภาคภูมิ เต็งอำนวย, 154 หน้า.

งานวิจัยนี้มีวัตถุประสงค์ในการพัฒนาสูตรตำรับอนุภาคนาโนไขมันแข็ง (เอสแอลเอ็น) ที่บรรจุแอสตาแซนธินจากสารสกัดเปลือกกุ้งเพื่อการนำส่งทางผิวหนัง ศึกษาถึงสภาวะที่เหมาะสมในการไฮโดรไลซิสสารสกัดหยาบจากเปลือกกุ้ง ศึกษาผลของสารสกัดและส่วนประกอบในสูตรตำรับต่อการเกิดและความคงตัวของแอสแอลเอ็นที่ผลิตด้วยวิธีไมโครอิมัลชัน และศึกษาการปลดปล่อยและการซึมผ่านผิวหนังของแอสตาแซนธินอิสระจากตำรับแอสแอลเอ็น จากการศึกษานี้พบว่าสภาวะที่เหมาะสมในการไฮโดรไลซิสสารสกัดหยาบจากเปลือกกุ้งคือการใช้สารละลายโซเดียมไฮดรอกไซด์ที่มีความเข้มข้น 0.03 นอร์มัลลิตี สารสกัดที่ผ่านการไฮโดรไลซ์ประกอบด้วยแอสตาแซนธินอิสระ 21.66 เปอร์เซ็นต์โดยน้ำหนักและแสดงฤทธิ์ยับยั้งอนุมูลอิสระดีพีพีเอชที่สูงที่สุด (0.7297 ไมโครโมลต่อมิลลิลิตร) เมื่อเทียบกับสารมาตรฐานแอสตาแซนธินและอะโปแคโรทีนอล ปัจจัยที่มีผลต่อขนาดของเอสแอลเอ็นเปล่าที่เตรียมด้วยวิธีไมโครอิมัลชันคือชนิดและปริมาณของส่วนประกอบต่างๆในสูตรตำรับ การเพิ่มความเข้มข้นของไขมันแข็ง สารลดแรงตึงผิวและสารลดแรงตึงผิวร่วมส่งผลต่อการเพิ่มขึ้นของขนาดอนุภาค โดยอนุภาคของเอสแอลเอ็นที่เกิดจากไขมันแข็งชนิดกลีเซอริลโมโนสเตียเรท (จีเอ็มเอส) มีขนาดใหญ่กว่าไดนาซาน 118 การใช้สารลดแรงตึงผิวที่เป็นของแข็ง (เมิร์จ 52 และบริจจ์เอส 721) จะมีขนาดอนุภาคที่ใหญ่กว่าการใช้สารลดแรงตึงผิวที่เป็นของเหลว (ทวีน 80 และครีโมฟอร์อาร์เอช 40) เอสแอลเอ็นเปล่าจำนวน 14 สูตรตำรับที่ผ่านการศึกษาความคงตัวทางกายภาพที่อุณหภูมิห้องเป็นเวลา 1 เดือนถูกเลือกมาเพื่อบรรจุแอสตาแซนธินจากสารสกัดที่ผ่านการไฮโดรไลซ์ที่ความเข้มข้น 25 มิลลิกรัมต่อมิลลิลิตร ผลการทดลองพบว่าสูตรตำรับดังกล่าวมีขนาดอนุภาคอยู่ในช่วงนาโนเมตรและประสิทธิภาพการกักเก็บแอสตาแซนธินอิสระอยู่ในช่วง 46-91 เปอร์เซ็นต์ ผลจากพาวเดอร์เอ็กซ์เรย์ดิฟแฟรคชันแสดงให้เห็นว่าไขมันแข็งสูญเสียความเป็นรูปผลึกภายหลังการเตรียมเอสแอลเอ็นและมีแนวโน้มที่จะอยู่ในรูปอสัณฐานมากขึ้นเมื่อเปรียบเทียบกับการผสมแบบกายภาพ สูตรตำรับที่เตรียมโดยการใช้ทวีน 80 และครีโมฟอร์อาร์เอช 40 แสดงความสามารถในการกักเก็บแอสตาแซนธินอิสระได้มากกว่าการใช้เมิร์จ 52 ภายหลังการเก็บที่อุณหภูมิห้องพ้นแสงเป็นเวลา 3 เดือนพบว่าความคงตัวทางกายภาพและเคมีของ เอสแอลเอ็นที่บรรจุแอสตาแซนธินดีกว่าสารละลายควบคุม ประสิทธิภาพการกักเก็บแอสตาแซนธินอิสระในแต่ละสูตรตำรับค่อยๆลดลงร่วมกับการเพิ่มขึ้นของค่าดัชนีความเป็นผลึก การศึกษาการปลดปล่อยแบบนอกกายแสดงการปลดปล่อยของแอสตาแซนธินอิสระอย่างช้าๆจากเอสแอลเอ็นและสัมพันธ์อย่างดีกับสมการของฮิกูชิ การซึมผ่านผิวหนังแบบนอกกายใช้ผิวหนังหน้าท้องของสุกรแรกเกิดพบว่าตำรับเอสแอลเอ็นสามารถเพิ่มการซึมผ่านผิวหนังของแอสตาแซนธินอิสระได้เมื่อเทียบกับสารละลายควบคุมอย่างมีนัยสำคัญ

ภาควิชา วิทยาการเภสัชกรรมและเภสัชอุตสาหกรรม ลายมือชื่อนิสิต _____

สาขาวิชา เภสัชกรรม _____ ลายมือชื่อ อ.ที่ปรึกษาวิทยานิพนธ์หลัก _____

ปีการศึกษา 2555 _____ ลายมือชื่อ อ.ที่ปรึกษาวิทยานิพนธ์ร่วม _____

5476200533: MAJOR PHARMACEUTICS

KEYWORDS: ASTAXANTHIN/ SHRIMP SHELL/ SOLID LIPID NANOPARTICLES

KRITSADA ROOPYAI: DEVELOPMENT OF SOLID LIPID NANOPARTICLES CONTAINING ASTAXANTHIN FROM SHRIMP SHELL EXTRACT FOR SKIN DELIVERY. ADVISOR: PRAPASRI SINSWAT, Ph.D., CO-ADVISOR: ASSOC. PROF. PARKPOOM TENGAMNUAY, Ph.D., 154 pp.

The objective of this study was to develop solid lipid nanoparticles (SLNs) containing astaxanthin from shrimp shell extract for skin delivery. The suitable condition for hydrolysis the shrimp shell crude extract was examined. The effect of extract and components in the formulation to SLNs formation, which were prepared by microemulsion technique, and its stability was investigated. The studies of release and skin permeation of free astaxanthin from SLNs were also carried out. This study indicated that the suitable condition for hydrolysis the shrimp shell crude extract was 0.03 N NaOH. The hydrolyzed extract was composed of free astaxanthin at 21.66%w/w and showed the highest DPPH scavenging activity (0.7297 μmole/mL) in comparison to standard astaxanthin and apocarotenal. Factors affecting the particle size of blank-SLNs prepared by microemulsion method were types and quantities of formulation ingredients. Increasing the concentration of solid lipid, surfactant, and co-surfactant resulted in the augmentation of particle size. The SLNs generated from glycerylmonostearate (GMS) as solid lipid gave a bigger size than Dynasan®118. The use of solid surfactants (Myrj®52 and Brij®S721) also provided the larger particle size than the use of liquid surfactants (Tween®80 and Cremophor®RH40). Fourteen formulations of blank-SLNs, which passed the physical stability study at room temperature for 1 month, were selected for loading astaxanthin from hydrolyzed extract at a concentration of 25 mg/mL. The results indicated that those formulations were in nanometer size range and the entrapment efficiencies of free astaxanthin were in the range of 46-91%. Powder X-ray diffraction study revealed that solid lipids lost their crystallinity after SLNs preparation and tended to be in more amorphous form when compared to the physical mixture. ASX-SLNs formulations prepared using Tween®80 and Cremophor®RH40 demonstrated the better capacity to entrap free astaxanthin than the use of Myrj®52. After 3 months of storage at room temperature and protected from light, the physical and chemical stability of ASX-SLNs formulations was superior to the control solution. The entrapment efficiency of free astaxanthin in each formulation gradually decreased with the increase in crystallinity index. *In vitro* release study showed sustained release profiles of free astaxanthin from SLNs and was well fitted to the Higuchi equation. The *in vitro* permeation study using newborn abdominal pig skin revealed that SLNs could significantly enhance the skin penetration of free astaxanthin as compared with the control solution.

Department: Pharmaceutics and Industrial Pharmacy   Student's Signature

Field of Study: Pharmaceutics   Advisor's Signature

Academic Year: 2012   Co-advisor's Signature

ACKNOWLEDGEMENTS

CONTENTS

LIST OF TABLES

Table   **Page**

LIST OF FIGURES

Figure **Page**

Figure   **Page**

LIST OF ABBREVIATIONS

ANOVA	=	analysis of variance
ASX	=	astaxanthin
°C	=	degree celcius
%CI	=	the percentage of crystallization index
conc	=	concentration
cm	=	centimeter
df	=	degree of freedom
DPPH	=	2,2-diphenyl-1-picrylhydrazyl
DSC	=	differential scanning calorimetry
EE	=	entrapment efficiency
et al.	=	*et alii*, 'and others'
g	=	gram
GMS	=	glyceryl monostearate
h	=	hour
HLB	=	hydrophilic-lipophilic balance
HPLC	=	high performance liquid chromatography
IC_{50}	=	half maximum inhibition concentration
J	=	joule
mg	=	milligram
m.p.	=	melting point
min	=	minute
mL	=	milliliter
n	=	sample size
nm	=	nanometer
No.	=	number
o/w	=	oil in water
PBS	=	phosphate buffer solution
PCS	=	photon correlation spectroscopy
PDA	=	photodiode array

PDI	=	polydispersity index
PG	=	propylene glycol
PXRD	=	powder x-ray diffractometry
R^2	=	coefficient of determination
rpm	=	round per minute
RSD	=	relative standard deviation
s	=	second
SD	=	standard deviation
SEM	=	scanning electron microscopy
SLNs	=	solid lipid nanoparticles
SPSS	=	statistical package for the social science
SS	=	sum of square
TLC	=	thin layer chromatography
USP/NF	=	The United States Pharmacopoeia/National Formulary
w/v	=	weight by volume
w/w	=	weight by weight
%	=	percentage
μg	=	microgram
μg/mL	=	microgram per milliliter
μmole	=	micromole
μm	=	micrometer

CHAPTER I

INTRODUCTION

Nowadays, shrimp processing industry of Thailand expands in the marketing plentifully. Shrimp products immensely increased to 600 million kilograms in 2011 (Aquaculture trade, 2011). Shrimp shell is the problem in terms of transportation and management. However, the shrimp shell has a great number of benefits, for example, using as supplementary food in some animals (duck, chicken), shrimp flavoring agent, and changing into the high value materials (such as chitin, chitosan, astaxanthin, etc.). Astaxanthin (3,3'-dihydroxy-β-β'-carotene-4,4'-dione) is the main carotenoids pigment found in numerous seafoods including shrimp, trout, lobster, salmon, red sea bream, and especially *Haematococcus pluvialis*. At present, astaxanthin has various essential benefits for human health such as prevention aginst cerebral ischemia (Kudo et al., 2002), inhibition of lipid peroxidation (Lim et al., 1992), anti-inflammation (Ohgami and Shiratori, 2003), attenuating eye fatique (Shiratori et al., 2005), suppression of hyper-pigmentation, inhibit of melanin synthesis, and photo-aging (Yamashita, 2006), etc. The astaxanthin is composed of three forms: diesters, monoesters, and free form (Lorenz and Cysewski, 2000). Free astaxanthin shows an antioxidant activity more than its ester forms (Kobayashi and Sakamoto, 1999). Thus, it is essential to convert the astaxanthin ester forms into free form by using hydrolysis reaction in basic solutions. For this study, the suitable hydrolysis condition was examined in order to prevent astaxanthin degradation. Moreover, astaxanthin structure comprises an unsaturated chain. It is unstable to light, high temperature, and oxidative conditions. Furthermore, the physicochemical properties of astaxanthin are water-insoluble $(6.67 \times 10^{-4}$ g/L) but soluble in various organic solvents with molecular weight of 596.84 g/mole, and melting point at 216°C, etc., which may affect low skin permeation. Many studies improved the solubility, stability, and bioavailability of astaxanthin by incorporation it into nanoemulsion (Affandi et al., 2011; Kim et al., 2012), microencapsulation (Ciapara et al., 2004), liposomal encapsulation (Peng et al., 2010), nanodispersions (Anajarn et al., 2010), etc.

Solid lipid nanoparticles (SLNs) have been used for delivery the water-insoluble substances which have particle size in the nanometer range. SLNs structure consists of a core of physiological solid lipid, for example, triglycerides, glyceryl monostearate, cetyl palmitate, stearic acid with the bioactives being a part of the lipid matrix. The particle (core of solid lipid) is stabilized by a surfactant layer, which may be composed of a single surfactant such as soy bean lecithin, egg lecithin, phosphatidylcholine, poloxamer, polysorbate, sodium cholate, or a mixture of surfactants (Shah et al., 2007; Dong et al., 2003; Sylvia and Muller, 2003; Wolfgang and Karsten, 2001). SLNs show distinct advantages over classical colloidal carriers such as the protection of incorporated labile active from the outer surroundings (water, light, temperature), possession of controlled release profile, a broad application route (dermal, oral, peroral, intravenous), the use of physiological lipids, avoidance of organic solvents, and possibility to scale-up production. The development of SLNs containing astaxanthin from shrimp shell extract may increase the astaxanthin stability and skin penetration. There are different production methods of finely dispersed lipid nanoparticles, for instance, high pressure homogenization (hot/cold homogenization), microemulsion technique, solvent emulsification-evaporation/diffusion, and membrane contactor (Charcosset et al., 2005). Microemulsion technique does not require special manufacturing equipment, no use of organic solvent, no risk of damaging shear sensitive drugs (Morel et al., 1996). Moreover, it also generates smaller particles than other methods (Ma et al., 2007). This method was selected for SLNs preparation.

Therefore, the main purpose of this study was to formulate SLNs containing astaxanthin from shrimp shell extract for topical delivery system. The effect of components in the formulation and astaxanthin extract on SLNs formation by microemulsion technique and its stability was also investigated. Finally, the release and the skin permeation of astaxanthin from SLNs were also examined.

The specific objectives of this investigation were as follows:
1. To optimize the hydrolysis condition from shrimp shell crude extract.
2. To study the effect of types and quantities of solid lipids and surfactants on the physical property of blank-SLNs.

3.   To investigate the effect of astaxanthin from shrimp shell extract in the SLNs formulation and evaluate physical and chemical stability of SLNs containing astaxanthin.

4.   To evaluate the release profile and pig skin permeation of astaxanthin loaded in SLNs.

CHAPTER II

LITERATURE REVIEW

1. Astaxanthin

Astaxanthin (3,3'-dihydroxy-β-β'-carotene-4,4'-dione) is the main carotenoids pigment found in several seafoods especially *Haematococcus pluvialis*. The existence of the hydroxyl (-OH) and keto (-CO-) functional groups on the ionone rings at the end of structure (Figure 1A) describes its unusual characteristics such as the capability to be esterified into astaxanthin monoesters (Figure 1B), and astaxanthin diesters (Figure 1C), a superior antioxidant effect, and more polar configuration than other carotenoids, namely, zeaxanthin, lutein, canthaxanthin, and β-carotene.

(A) Free astaxanthin

(B) Astaxanthin monoesters (R_1 = fatty acid)

(C) Astaxanthin diesters (R_1, R_2 = fatty acid)
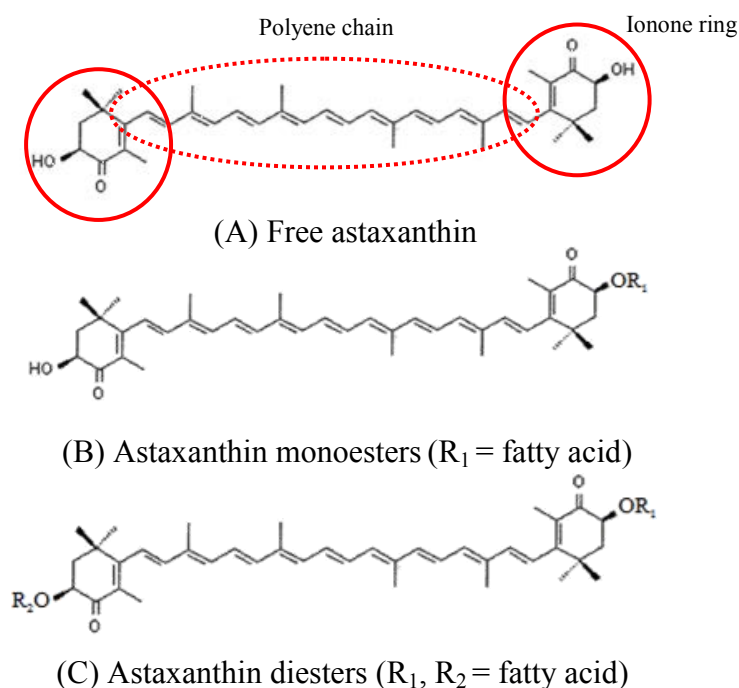
Figure 1 The astaxanthin structures (Goto et al., 2001).

When free radicals generate lipid peroxidation process, astaxanthin will show antioxidant effect both hydrophobic and hydrophilic regions of cell membrane. The hydroxyl group at each end of structure is positioned in hydrophilic region whereas

polyene chain is vertically located in hydrophobic region. Thus, the antioxidant activity of astaxanthin is more powerful than β-carotene (40x) and vitamin E (1,000x).

Vitamin E acts in the hydrophobic region of cell membrane by donating free electrons to counteract free radicals. The oxidized vitamin E is reused by receiving the electron from vitamin C in the hydrophilic region of cell membrane and continues its antioxidant effect, whereas oxidized vitamin C will be eliminated from the human body. β-carotene is presented in the hydrophobic region of cell membrane and entraps free radicals created inside cell membrane only (Figure 2).
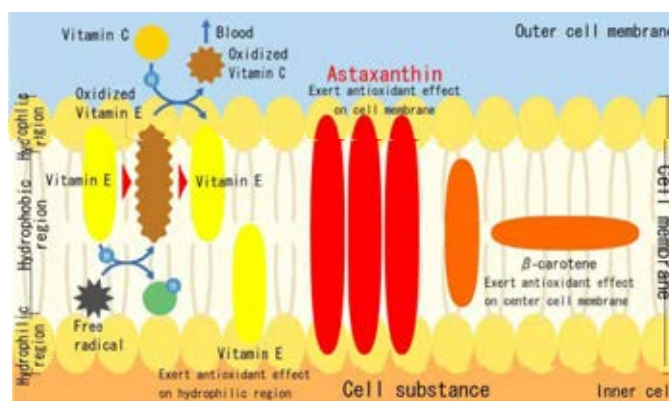
Figure 2 The antioxidant effect of astaxanthin, vitamin E, and β-carotene on cell membrane (Oryza, 2006).

1.1 Source of astaxanthin

Astaxanthin has been found in several microorganisms, including algae (*Haematococcus pluvialis*), yeast (*Xanthophyllomyces dendrorhous*), crustacean by-products. Crustacean wastes are originated from peeling and processing operations of crawfish (Samuel and David, 1981), shrimp shell (Khanafari et al., 2007), and red crabs (Coral and Bjerkeng, 2002). Generally, these wastes lead to the loss of valuable by-products and cause the ecological problems. These crustacean by-products are used as the primary source of chitin, protein, and astaxanthin. The quantity of total astaxanthin in these by-products depends on the species, development stage, and storage condition. The major carotenoid pigment is astaxanthin and its ester forms. A great number of literatures presented astaxanthin recovery from crustacean by-products, for example, shrimp, snow crab, and crawfish. Among their studies, various

methods were performed to extract astaxanthin such as fermentation method (Sachindra et al., 2007), enzymatic method (Holanda and Netto, 2006), and passive extraction by organic solvent (Sachindra et al., 2006). Acetone, isopropanol, methanol, and petroleum ether were the types of organic solvents that used to extract astaxanthin from crustacean by-products.

According to the antioxidant activity of free astaxanthin is more than ester forms (Kobayashi and Sakamoto, 1999), it is essential to convert the ester form of astaxanthin into free form by using hydrolysis reaction in basic solutions, for example, potassium hydroxide or sodium hydroxide in methanol (Yuan and Chen, 1999) or applying esterase enzyme (Jacobs et al., 1982). The former method need to control the reaction condition for prevention the astaxanthin degradation whereas the latter is a mild condition; however, the enzyme is expensive price. Hence, hydrolysis reaction in basic solution needs to control the condition for prevention the astaxanthin degradation.

1.2 Extraction methods

Many extraction methods have been developed for separation of astaxanthin from crustacean by-products. Organic solvents are applied in many publications for axtaxanthin extraction from Lousiana crawfish (Samuel and David, 1981), red crab langostilla (Coral and Bjerkeng, 2002), shrimp powder (Khanafari et al., 2007), *Haematococcus pluvialis* (Yuan and Chen, 1998). However, this method consumes high energy and has multiple separation steps. Alternatively, the fermentation with lactic acid bacteria is adapted to de-proteinase crustacean's residues and obtain carotenoids especially astaxanthin (Armenta et al., 2002). Treating by-products with organic or inorganic acids can prevent them from bacterial decomposition and increase astaxanthin recovery (Chen and Meyers, 1983). Torrisen et al. (1981) explained that acid addition can change the calcium salts into the dissolvable form and easy to extract astaxanthin from crustacean wastes. Moreover, the astaxanthin have been extracted with the use of vegetable or fish oils (Coral et al., 1997) which can be incorporated in feed ingredients. Supercritical fluid extraction is also applied for the extraction of astaxanthin from Brazillian redspotted shrimp waste (Carmago et al., 2012). This technique is accepted because of its quickness, efficiency, and low toxicity of the solvent. The percentage yields of astaxanthin

increased proportionally with the increase of ethanol in the ethanol and supercritical carbondioxide mixture. Krichnavarak et al. (2008) also supported that supercritical fluid extraction could be a competitive technology in comparison to organic solvent extraction from *Haematococcus pluvialis*.

1.3 *In vitro* and *in vivo* efficacy test of astaxanthin

At present, astaxanthin has an important application in the cosmetics due to its ability to suppress hyper-pigmentation, inhibit melanin synthesis, and photo-aging. Yamashita (2006) revealed that consumption of astaxanthin supplementation (4 mg/day) for 6 weeks significantly improved the wrinkle skin, skin elasticity, and moisture content in 49 US healthy middle-aged women. Astaxanthin preserves skin health by many methods such as decrease puffiness and erythema, protect the wrinkles formation induced by UVand reduce the risk of skin cancer both topical route and dietary route. Mizutani et al. (2005) also suggested that astaxanthin protected photo-aging, skin wrinkles, and improved skin elasticity in bald mice. Kusuda et al. (2010) reported that "Astalift whitening essence" containing astaxanthin would control formation of normal blemishes with other substances to act on everlasting blemishes.

Izumi et al. (2009) discovered that "Astalift supplement" and "Astalift drink", which contained astaxanthin and other ingredients for beauty, prevented the formation of dark spots, blotches and wrinkles, and maintained the moisture content of skin. Seki et al. (2001) studied the efficacy and irritation of astaxanthin extract from *Haematococcus pluvialis* in the human volunteers. Patch testing revealed no serious side effect existed on human skin. Moreover, they also found cream containing astaxanthin would decrease the skin wrinkles by visual observation.

1.4 Stability of astaxanthin

Since astaxanthin is a powerful free radical scavenging agent, the astaxanthin structure will link with oxygen molecules easily. When the oxidation process occurs, it will change the astaxanthin into an ineffective molecule called "astacene" that has no advantage to humans. Armenta et al. (2009) studied the stability of astaxanthin contained in carotenoproteins extracted from fermented shrimp by-products. Carotenoprotein powder, containing 1% free astaxanthin, was subjected to oxidation factors of oxygen availability, illumination, and temperature, using synthetic astaxanthin as a control. Air and full light were the two main factors causing

astaxanthin oxidation. Storage in the non-oxygen and dark condition at $25^{\circ}C$ were the conditions that efficiently reduced astaxanthin oxidation. Even though natural astaxanthin oxidized faster than the synthetic pigment, its stability may improve by adding the antioxidant and polymer.

1.5 Physicochemical properties of astaxanthin

The solubilities of astaxanthin in various solvents are as follows: water $(6.67 \times 10^{-4}$ g/L), acetone (0.2 g/L), and dichloromethane (30 g/L). The molecular weight and melting point are 596.84 g/mole and $216^{\circ}C$ respectively. Astaxanthin presents the absorption maximum wavelenght at 466-467 nm in hexane, 472 nm in methanol, 485 nm in chloroform, and 503 nm in carbon disulfide.

2. Solid lipid nanoparticles (SLNs)

SLNs are the type of drug delivery systems for topical, transdermal, parenteral, oral, ocular route, etc. with mean particle sizes in the submicron range. SLNs structure is composed of physiological lipids. The lipids remain in solid state at room temperature and turn to liquid state at temperature above its melting point (Muhlen et al., 1998). Hence, the mobility of loaded drug in SLNs is decreased, which is a requirement for controlled release profile. The lipid core of SLNs is coated by the surfactant layers. This delivery system also combines the benefits of various colloidal carriers and avoids some of their drawbacks (Venkateswarlu and Manjunath, 2004). Shah et al. (2007) found that SLNs of tretinoin improved topical delivery in terms of photostability and skin irritation when compared to the marketed tretinoin cream (Retino-A$^{®}$). Wissing et al. (2004) discovered that SLNs containing coenzyme Q10 increased chemical stability, skin hydration, and skin penetration effect. Furthermore, SLNs can be incorporated into cream, gel, and other formulations for topical application.

2.1 Preparation techniques of SLNs

Different methods are used for the SLNs preparation and can be divided into four groups.

2.1.1 High pressure homogenization technique (hot/cold homogenization)

High pressure homogenization (HPH) is an appropriate technique for

the production of SLNs and can be prepared at high temperature (hot HPH) or at below room temperature (cold HPH). The particle size is diminished by turbulences and cavitation. Figure 3 displays the SLNs preparation by high pressure homogenization technique. For both methods, the active compound is dissolved in melted lipid at 5-10°C above melting temperature. The hot HPH is suitable for lipophilic drugs whereas the cold HPH is appropriate for hydrophilic drugs or highly temperature-sensitive drugs. When compared to hot HPH, the bigger particle sizes and wider size distribution are obtained from cold homogenization method. However, cold HPH does not avoid thermal exposure from melting of drug/lipid mixtures in the first step.

The benefits of the HPH method are ease of scaling-up process and avoidance the use of organic solvent in preparation process. Nonetheless, the high pressure may generate the coalescence of small particles and the high temperature can expedite the drug degradation rate (Wolfgang and Karsten, 2001).

2.1.2 Microemulsion technique

Microemulsion technique is suitable for both lipophilic and hydrophilic drugs. In case of hydrophilic drugs, the w/o/w double emulsion is formed and the drug molecule is solubilized in aqueous phase. Whereas lipophilic drugs, the o/w microemulsion is generated and the drug is solubilized in lipid phase. This kind of o/w microemulsion is quite different from normal microemulsion for the solid lipid as oil phase. So it can be obtained only at the temperature 10-15°C over the melting point of pure lipid. SLNs formulation is prepared by dispersion the o/w microemulsion (based on pseudoternary phase diagram) in the excess cold aqueous system under mechanical stirring. After the temperature of this mixture is lower than the melting point of lipid, the lipid is recrystallized to solid and forms SLNs. Figure 4 shows the preparation of SLNs by microemulsion technique.
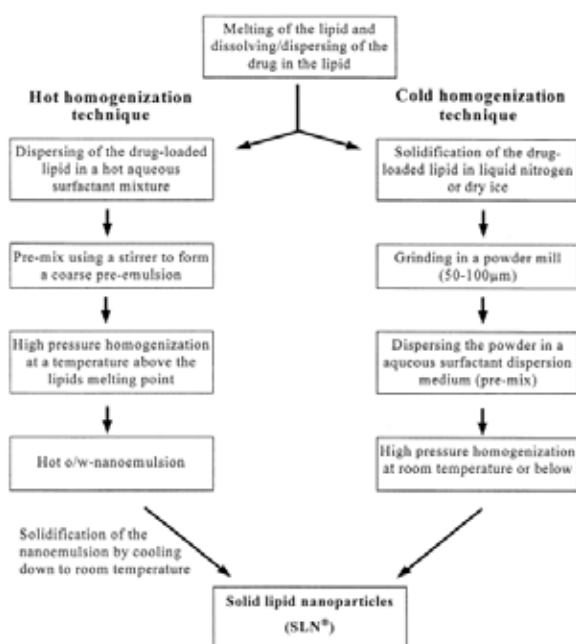
Figure 3   Schematic procedure of hot and cold homogenization techniques for SLNs production (Wolfgang and Karsten, 2001).
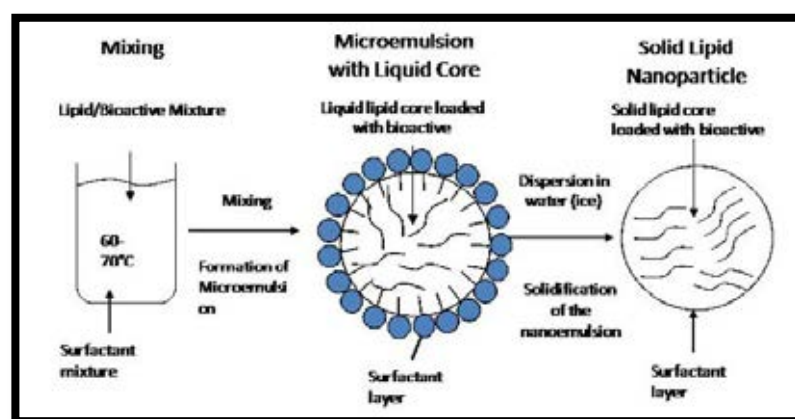
Figure 4   Preparation of SLNs by the microemulsion technique (Jochen et al., 2008).

2.1.3 Solvent emulsification-evaporation/diffusion technique

The process consistsof emulsification step and organic solvent removal step. The first step, the drug and lipid are solubilized in organic solvent that is suspended in water phase. The second step, organic solvent is removed from the sample by using rotary evaporator. SLNs dispersions are generated by

precipitation of the lipid in aqueous phase as shown in Figure 5. This method avoids any thermal stress; however, it cannot apply in the industry.

Types of organic solvents used in solvent emulsification-evaporation and emulsification-diffusion method are water-immiscible solvents (dichloromethane, chloroform, ethyl acetate, toluene, etc.) and partially water-miscible solvents (acetone, benzyl alcohol, butyl lactate, ethyl formate, etc.), respectively.
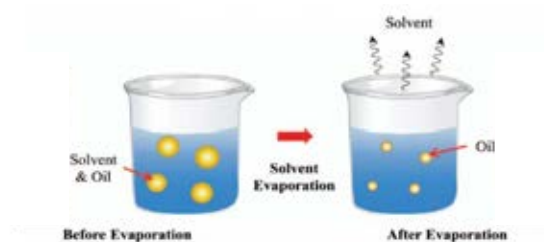
Figure 5   Preparation of SLNs by solvent emulsification-evaporation/diffusion technique (David and Jia, 2011).

2.1.4 Membrane contactor technique

Membrane contactor is the novel method for SLNs preparation. The schematic preparation is shown in Figure 6. The production of small droplets is generated by the compression of lipid phase at a temperature over the lipid melting point through the membrane pores. The aqueous phase gradually moves within the membrane and passes away the droplets forming at the pore exit. SLNs dispersions are formed by the subsequent cooling of the sample to normal temperature. Particle size depends on the effect of process parameters, for example, the temperature of aqueous phase and lipid phase, the aqueous phase velocity inside membrane, the pressure of lipid phase, and membrane pore size. For this process, the particle size is controlled by changing all of those process parameters.
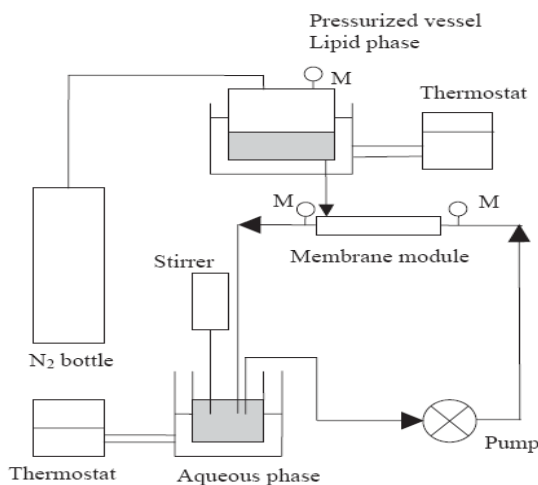
Figure 6   Preparation of SLNs by membrane contactor technique (Charcosset et al., 2005).

2.2 Drug incorporation and loading capacity

Commonly, the tightly packed and highly ordered crystalline particle matrix should be anticipated to express a rather unfavorable localization for drug incorporation. Owing to its high order degree of packing patterns (β modification or triclinic pattern), the quantity of imperfections in the crystal lattice is decreased leading to drug expulsion. The degree of crystallinity (crystallinity index) of SLNs is greatly important parameter since it affects the entrapment efficiency, the release rate, and the drug expulsion from SLNs during storage. The incorporation capacity depends on the physicochemical properties of the drug, the type of lipid, and the lipid matrix state (especially the polymorphic form and crystallinity index).

The chemical structure of the lipid is crucial for drug incorporation in SLNs. The lipid includes the mixtures of mono-, di-, triglycerides, and dissimilar carbon chain length of fatty acids can accommodate the space for drug incorporation in the lipid matrix more than the highly crystalline structure of lipid (eg. triglycerides, cetyl palmitate). This property decreases the drug expulsion from lipid matrix during storage (Westesen et al., 1997). Thus, the chemical nature of the lipid is an important factor to make a decision whether a drug will be expelled or still retained in the SLNs for long term storage. Differential Scanning Calorimetry (DSC), X-ray Diffraction, and Proton Nuclear Magnetic Resonance (NMR) are the techniques for

characterization the physical state, crystallinity, arrangement, and mobility of lipid molecule in SLNs.

2.3 The drug incorporation models

Three different models are contructed in order to explain the drug incorporation pattern into SLNs as follows:

1. Homogeneous matrix (Figure 7A)
2. Active-free lipid core with active-enriched shell (Figure 7B)
3. Active-enriched core with active-free lipid shell (Figure 7C)
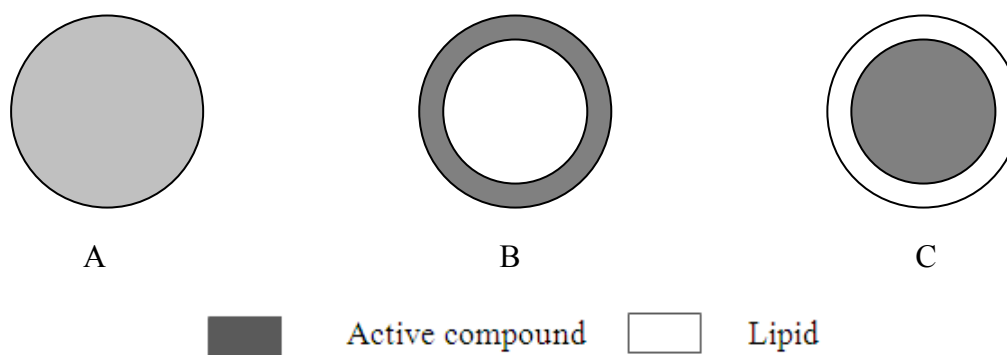
Figure 7   Models for incorporation of active compounds into SLNs.

The model of homogeneous matrix solution is thought to be mainly obtained when applying the homogenization method (hot/cold). In case of the cold homogenization method, the lipid carries the melted drug in dispersed form. Mechanical breaking by high pressure homogenization causes SLNs having the homogeneous matrix structure (Figure 7A). The same phenomenon will happen when the oil droplet produced by the hot homogenization method is being crystallized and no phase separation between lipid and drug occurs during this cooling process. This model is assumed for incorporation of drug which can show a prolonged release of prednisolone for 5 weeks (Muhlen et al., 1998).

An enrichment of drug molecule in the outer layer of the SLNs or drug deposition on the SLNs surface is generated when phase separation occurs during the cooling method from the liquid droplet to the formation of SLNs. In the first step, the lipid crystallization happens and leads to the formation of inner core of pure lipid

during solidification process. Then, the solid drug solution will be coated surrounding the lipid core (Figure 7B).

A drug enriched core model is arranged when the opposite occurs, which implies the drug starts crystallization first and the shell will have distinctly less drug (Figure 7C). This model causes a controlled release profile explained by the Fick's law of diffusion.

2.4 Drug release

The release profile of SLNs may play a significant role on the application. Controlled release is the main objective for minimizing the side effect of active molecule to skin such as skin irritation. Gradually release effect causes the increase of drug concentration. Muhlen et al. (1998) examined the function of production temperature on the release profile from SLNs. It could be concluded that the release was followed by a prolonged release.

The burst release was highest when producing at high temperatures and applying the hot homogenization method. It reduced with decreasing temperature and was almost non-existent when applying the cold homogenization method. The extent of burst release could also be controlled by the amount of surfactant used in the formulation. High surfactant concentration leads to high burst release while low surfactant concentration can minimize the burst effect. This was explained by redistribution effects of the compound between the lipid and the water phase during the cooling down process after production of the hot oil in water emulsion during the hot homogenization process. Heating the lipid and water mixture causes an increased solubility of the active compound in the water phase, the compound partitions from the melted lipid droplet to the water phase. After homogenization, the oil in water emulsion is cooled, the lipid core starts crystallising with still a relatively high amount of active compound in the water phase. Further cooling leads to supersaturation of the compound in the water phase, the compounds tries to partition back into the lipid phase; a solid core has already started forming leaving only the liquid outer shell for compound accumulation. However, the improvement of controlled release profile can be obtained by alteration of the types of lipids and surfactants, the concentration of material used, and production temperature.

2.5 Occlusion effect and skin hydration

Occlusion effect is the property required in cosmeceutical products which prevents the loss of moisture caused by evaporation from the skin. Wissing and Muller (2002) found that the small particle size prevented moisture loss more than the large particle size. The high surface area of small particles could form a monolayer film on the skin layer and showed adhesiveness with the surfaces. Hence, skin layer had small dimensions of air channels to expose with outside environment and decreased in hydrodynamic evaporation of water. When applied SLNs onto the skin, the pressure created particle fusion and formed a dense film. This fusion is accelerated by capillary forced involved during water evaporation.

Jenning et al. (2000) studied the occlusion effect of SLNs containing retinol in o/w cream by hematoxylin/eosin staining of vertical skin slices after 24 hours incubation. They found the stratum corneum looked swollen and total thickness had augmented while untreated skin demonstrated a dense stratum corneum with corneocytes layers intimately conjugated. This might be due to the water loss prevention and disruption the lipid arrangement in lamellar layer of SLNs cream. Wissing and Muller (2003) tested the effect of SLNs on skin hydration *in vivo* study. The skin hydration was evaluated by corneometer (skin capacitance meter) and the result displayed that cream containing SLNs led to a significant enlarge in skin hydration more than conventional cream. This effect might be due to the highly crystalline property of cetyl palmitate in SLNs. Moreover, small particle size effect made capillary forces and formed a highly packed film of round SLNs with greatly fine pores. Because of that result, the hydrodynamic conditions for evaporation of water were undesirable, leading to increase skin hydration effect.

2.6 Skin elasticity

Skin elasticity is the property in cosmeceutical development for skin smoothness. The particles must be spherical-like shape. The increase of lipid concentration is the crucial factor that affects the augmentation of viscosity. The viscoelastic properties can be evaluated by suction and relaxation mode of skin elasticity meter (cutometer). Effat et al. (2011) found that SLNs containing coenzyme Q10 in cream increased the skin elasticity more than simple cream in 25 female volunteers, 20-24 years old, applying cream on the face before bedtime for 60 days.

2.7 Skin penetration

Skin local effect is the general performance of topically applied cosmetic compounds for prevention some side effects from active ingredients and only acting at the stratum corneum. Those actives are not purposed to penetrate into the deeper skin. SLNs can be incorporated into topical dosage forms (eg. ointments, gels, emulsions, creams) for increasing the penetration rate of active ingredient into certain layers of the skin by modulation drug molecule in supersaturated systems. The augmentation of saturation solubility leads to an increased diffusion pressure of drug into skin layer (Muller et al., 2002).

Dingler (1998) reported that SLNs could deliver coenzyme Q10 through skin more than solutions because lipid and surfactant in the formulation reacted with skin lipid and increased coenzyme Q10 penetration. Jenning et al. (2000) also found that retinol-SLNs dispersing in hydrogels penetrated into pig skin and accumulated in stratum corneum more than other skin layers. This phenomenon could also prevent the side effect of retinol in the deeper skin. Stecova et al. (2007) discovered that cyproterone acetate (CPA) 0.05% in SLNs penetrated into skin more than nanostructured lipid carriers (NLC), nanoemulsions (NE), and microspheres (MS). Tape stripping technique was used to detect CPA level in skin and also found that the most CPA distributed in stratum corneum and showed a little amount in dermis. Thus, the side effects of oral CPA such as loss of libido, decreasing of bone density, gynecomastia, etc. were minimized by SLNs formulation.

2.8 UV-blocking potential

SLNs structure has an unique characteristic for prevention ultraviolet (UV) radiation by film forming cover the skin and present UV scattering effect (physical/inorganic sunscreens). A great number of researchers tried to add the chemical substances such as oxybenzone (Wissing and Muller, 2003), trimethoxybenzoylchitin (Song and Liu, 2005), tocopherol acetate (Song and Liu, 2005), etc. into SLNs for UV absorption effect (chemical/molecular/organic sunscreens). Gulbake et al. (2010) tested UV-blocking potential of oxybenzone in the different formulations and also found that the incorporation of molecular sunscreen into SLNs led to a synergistic UV protective effect (UV scattering and UV

absorption). This indicated the quantity of molecular sunscreen could be minimized and reduced the side effects.

2.9 Skin irritation

Skin irritation is decreased by incorporation of active ingredient in SLNs because controlled release effect minimized side effects of active compound. Shah et al. (2007) developed SLNs containing tretinoin 0.05% w/w in gels and applied into the hair removal rabbit skin compared to Retino-A® cream. The result found that the rabbit skin became red (erythema score = 3) in Retino-A® cream whereas skin irritation could not be detected in SLNs formulation. Thus, SLNs protected skin from the side effect of isotretinoin (erythema) since SLNs decreased contact of carboxylic group with the skin.

CHAPTER III

MATERIALS AND METHODS

Materials

1. Absolute ethanol, AR grade (Lab Scan Co., Ltd., Thailand)
2. Acetone, AR grade (Lab Scan Co., Ltd., Thailand)
3. Acetonitrile, HPLC grade (Lab Scan Co., Ltd., Thailand)
4. Apocarotenal (Roche Diagnostics Thailand, Lot no. UE00809011)
5. Astaxanthin standard, purified from *H. pluvialis*, with courtesy of Associate Professor Artiwan Shotipruk, Ph.D.
6. Benzene (Merck, Germany)
7. Benzyl alcohol, AR grade (Lab Scan Co., Ltd., Thailand)
8. 1,1-diphenyl-2-picryl-hydrazyl radical (DPPH) (Sigma-Aldrich, Inc., USA, Lot no. 51K1419)
9. Dichloromethane, HPLC grade (Lab Scan Co., Ltd., Thailand)
10. Diethyl ether, AR grade (Lab Scan Co., Ltd., Thailand)
11. Disodium hydrogen phosphate (Asia Pacific Chemicals Limited, Lot no. F2F136)
12. Ethyl acetate, AR grade (Fisher scientific, UK)
13. Glyceryl behenate (Compritol$^®$ATO88) (Gattefosse', France, Lot no. 103100)
14. Glyceryl monostearate (Nikkol$^®$) (S. Tong Chemicals Co., Ltd., Thailand, Lot no. 2/2144744)
15. Glyceryl tristearate (Dynasan$^®$118) (Lonza Inc., Lot no. N5477395)
16. Hexane, AR grade (J.T.Baker, USA)
17. Isopropanol, AR grade (Lab Scan Co., Ltd., Thailand)
18. Methanol, AR grade (Lab Scan Co., Ltd., Thailand)
19. Methanol, HPLC grade (Lab Scan Co., Ltd., Thailand)
20. Poloxamer$^®$188 (Lutrol$^®$F-68) (BASF, Germany, Lot no. WPAB524C)
21. Polyoxyethylene 40 castor oil (Cremophor$^®$RH40) (Namsiang Group, Thailand, Lot no.0020010)

22. Polyoxyethylene fatty alcohol ether (Brij$^®$ S721) (Generous gift from CRODA, Thailand, Lot no. 61135)

23. Polyoxyethylene 20 sorbitan monooleate (Tween$^®$80) (Srichand United Dispensary Co., Ltd., Thailand, Lot no. 005858)

24. Polyoxyethylene 40 stearate (Myrj$^®$52) (Sigma-Aldrich, Inc., USA, Lot no. 82H0303)

25. Potassium dihydrogen phosphate (Merck, Germany, Lot no. 1102146)

26. Propylene glycol, USP grade (Srichand United Dispensary Co., Ltd., Thailand, Lot no. 10215)

27. Shrimp shell (Ratchathewee market, Bangkok, Thailand)

28. Siliga gel 60 (0.063-0.200 mm) (Merck, Germany, Lot no. TA1699334)

29. Sodium chloride (Merck, Germany, Lot no. K41653304049)

30. Sodium hydroxide (Merck, Germany, Lot no. B0119798)

Apparatus

1. Analytical balance (Model AX105, Mettler Toledo, Switzerland)

2. Centrifuge (Model Universal 320R, Hettich, Germany)

3. Conductivity meter (Model C535, Consort, Belgium)

4. Differential scanning calorimeter (DSC 6200, Seiko Instruments Inc., Japan)

5. Dry cabinet (Model GH-197, Ampore House, Taiwan)

6. Electronic balance (Precision Plus TP 2000, Mettler-toledo, Switzerland)

7. Freeze dryer (Model FD-6-850MPO, Dura-Dry^{TM}, FTS System Inc., USA)

8. High performance liquid chromatography system

   - Automatic sample injector (SIL-20AC, Shimadzu, Japan)

   - Column (Luna Phenomenex$^®$ C18 (2), 5 μm, 250 x 4.6 mm, USA, Lot no. 5291-75)

   - Communications bus module (SPD-M20A, Shimadzu, Japan)

   - PDA detector (SPD-M20A, Shimadzu, Japan)

9. High speed stirrer (WiggenHouser, Germany)

10. Magnetic stirrer (CAT, Germany)

11. Micropipette (Pipetman, Gilson, Inc., France)

12. Modified Franz Diffusion cells (Crown Glass Company, USA)

13. pH meter (Orion model 420A, Orion Research Inc., USA)

14. Photon correlation spectrometer (Zetasizer Nano ZS, Malvern Instruments, UK)

15. Powder X-ray diffractometer (MiniFlexII, Rigaku, Japan)

16. Rotary evaporator (Buchi heating bath B-490, Switzerland)

17. Scanning electron microscope (JSM-6510A, Jeol, Japan)

18. Sonicator (Model TP680DH, Elma, Germany)

19. Stability cabinet (Eurotherm Axyos, Germany)

20. Stopwatch (Heuer, Switzerland)

21. Ultracentrifuge (Model L80, Beckman, USA)

22. Ultrasonicator (Crest Ultrasonics, Model 275DAE, Malaysia)

23. Vacuum pump (CB 169 Vacuum System, Buchi, Switzerland)

24. Vortex mixer (Vortex Ginies-2, Scientific Industries, USA)

25. Water bath (Model WB22, Becthai Co., Ltd., Thailand)

Accessories

1. Centrifugal Filter Units, MWCO = 100 K (Amicon$^®$ Ultra-4, Millipore Ltd., Ireland, Lot no. R2BA90230)

2. Dialysis membrane (Regenerated cellulose membrane, MWCO 12,000-14,000, Membrane Filtration Product, Inc., USA)

3. Disposable syringe filter nylon 13 mm, 0.45 µm (Chrom Tech, USA)

4. Parafilm (American National Can TM, USA)

5. Polycarbonate centrifuge bottles (Beckman, USA, Lot no. A60519)

6. Pig skin (donated by Suntorn farm, Nakornpathom, Thailand)

7. TLC Alumina sheet silica gel 60F 254 20x20 cm (E. Merck, Germany)

8. Whatman filter paper No.1, 150 mm (Whatman International Ltd., England)

9. 96-well plates (Costar$^®$3912, Corning, Inc., USA)

Methods

1. Astaxanthin extraction from shrimp shell

1.1 Preparation of shrimp shell crude extract, hydrolysis reaction, and qualitative analysis of astaxanthin

1.1.1 Preparation of shrimp shell crude extract

Fresh shrimp shell was removed from the shrimp and was then heated by hot air oven at 70°C for 24 hours. Dried shrimp shell was ground into fine powders by food processor. A crude extract was obtained by passive extraction using isopropanol as an organic solvent in 1:2 dried weight of homogenized powders (g) per volume (mL) ratio for 30 minutes under mechanical stirring. The crude extract was filtered and evaporated using a rotary evaporator at 35°C for 30 minutes.

Column chromatography was subsequently used to separate astaxanthin (free and ester forms) from the crude extract. In this study, the mobile phase was modified from สกุลคุณ มากคุณ, 2546 to reduce the separation time. The stationary phase or adsorbent was silica gel whereas the mobile phase or eluent was the mixture of dichloromethane and methanol (4:1 v/v). Three fractions of eluate were collected (30 mL of each fraction) and categorized into astaxanthin diesters, astaxanthin monosters, and free astaxanthin, respectively. The solvent was removed by rotary evaporator, freeze dried at -91°C under 293 mmHg vacuum for 30 hours, and stored in the freezer at -21°C. All of these fractions were called as the non-hydrolyzed extracts.

1.1.2 Hydrolysis reaction

The hydrolysis reaction was performed to increase the free astaxanthin content. For hydrolysis, sodium hydroxide (NaOH) in methanol solution at different concentrations (0.01N, 0.03N, 0.05N) was prepared. The saponification was performed under nitrogen in darkness with continuous mixing by magnetic stirrer at 40°C for 5 hours to convert all ester forms of astaxanthin into free form (Yuan and Chen, 1999). The initial crude extract was weighed and blended with different concentrations of NaOH solutions at a ratio of 1:15 (w/v). At the end of 5 hours, only free astaxanthin fraction was separated by similar column chromatography, removed the solvent by rotary evaporator, and freeze dried at -91°C. This fraction was called as

the hydrolyzed extract. The extraction process and hydrolysis reaction were performed according to the diagram shown in Figure 8. The percentage yield of free astaxanthin (after hydrolysis and separation by column chromatography) for each NaOH concentration was calculated according to the following equation:

$$\text{ercentage ield of free astaxanthin fraction} \quad \frac{\text{eight}_{final}}{\text{eight}_{initial}} \qquad \text{uation}$$

Where, Weight_{final} is the weight of free astaxanthin fraction obtained after hydrolysis and separation by column chromatography (g), $\text{Weight}_{initial}$ is the weight of crude extract (g)
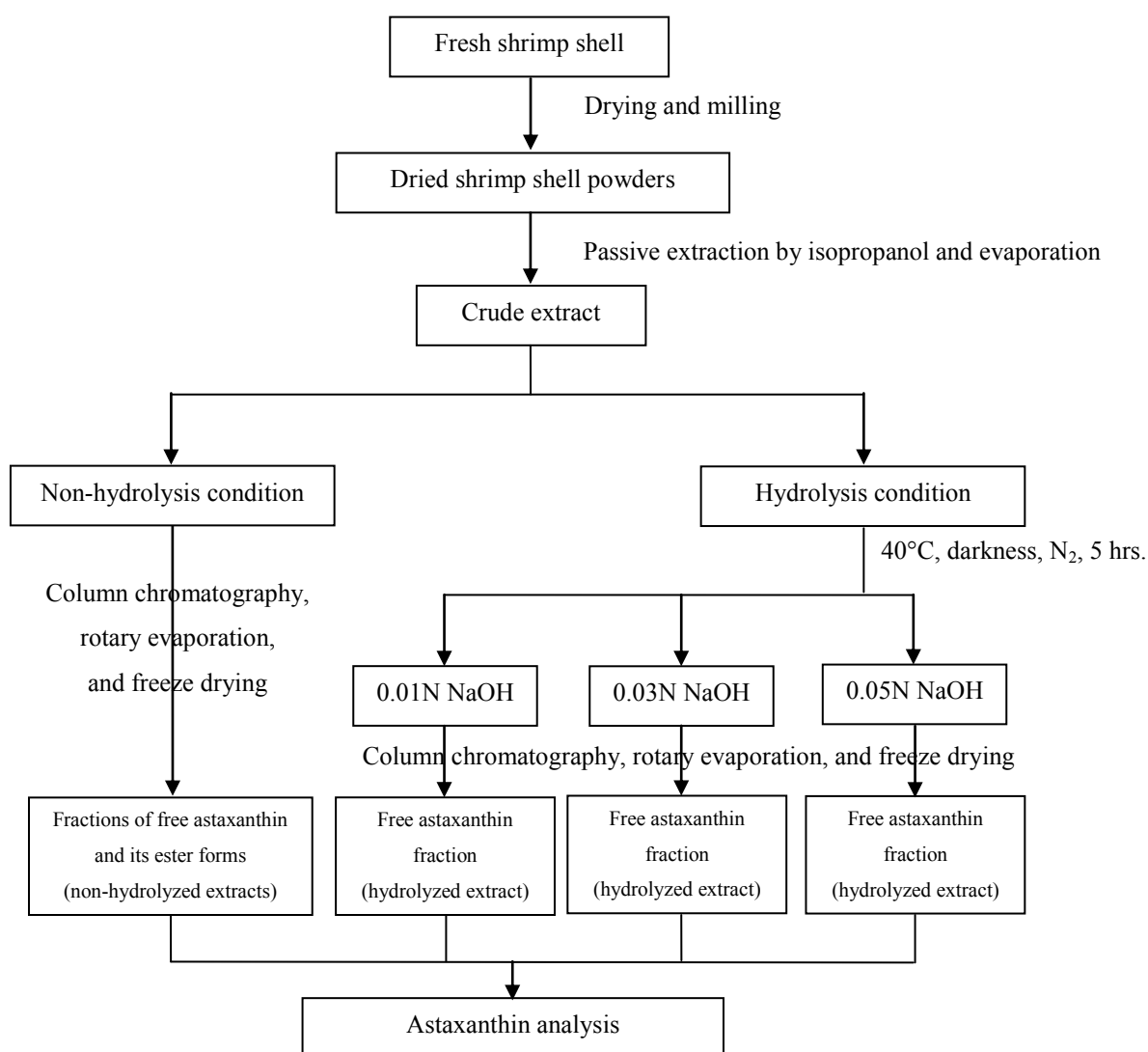
Figure 8 Diagram of shrimp shell extraction process and hydrolysis reaction.

1.1.3 Qualitative analysis of astaxanthin

The non-hydrolyzed fractions were confirmed the astaxanthin forms (free and ester forms) compared to the initial crude extract, whereas the hydrolyzed extract (only free form fraction) was identified for observing the degradation product during different hydrolysis conditions (in comparison to free astaxanthin reference standard). The qualitative analysis was performed using Thin-Layer Chromatography and High Performance Liquid Chromatography for reliability.

1.1.3.1 Thin-Layer Chromatography (TLC)

TLC was performed on the 2×5 cm plate precoated with silica gel 60 F254 on which the origin line was marked about 1 cm above the lower edge of the plate. All samples of the non-hydrolyzed and hydrolyzed extracts were dissolved in methanol and dichloromethane (1:1 v/v) (50 mg of dried extract/1 mL of mixed solvents) and spotted onto the plate paralleled with free astaxanthin standard solution. The analytical TLC plate was performed using ethyl acetate and benzene (2:3 v/v) as a mobile phase. The located bands were viewed by naked eye. The distance of each spot was measured and calculated for the R_f value in comparison to the reference standard according to the following equation:

$$R_f = \frac{\text{Migration distance of the compound from the origin (cm)}}{\text{Migration distance of the solvent from the origin (cm)}} \qquad \text{Equation}$$

1.1.3.2 High Performance Liquid Chromatography (HPLC)

HPLC method was used to confirm the identification of non-hydrolyzed and hydrolyzed extracts. The HPLC consisted of SIL-20AC series (Shimadzu, Japan) with photodiode array detector. A 250x4.6 mm Luna Phenomenex® analytical column with 5 μm C_{18} reversed-phase packing materials was used as the stationary phase. Two systems of mobile phase were developed for qualitative analysis as follows:

a) For non-hydrolysis condition

The mobile phase was methanol/acetonitrile/ dichloromethane/water (28:46:22:4 v/v) run under isocratic condition with a flow rate of 1.0 mL/min for 90 minutes (Yuan and Chen, 1999). The injection volume was 20

µL. The column effluent was observed continuously at 474 nm to detect free astaxanthin and its ester forms.

b) For hydrolysis condition (Anajarn et al., 2010)

The methanol/dichloromethane/acetonitrile/water (85:5:5:5 v/v) with a flow rate of 1.0 mL/min for 20 minutes was used to detect free astaxanthin and its degradation products. The injection volume was 20 µL and the column effluent was observed continuously at 474 nm.

The hydrolysis condition that gave the highest percentage yield of free astaxanthin and lowest degradation product was selected to quantify the real content of free astaxanthin and load into SLNs formulation. This sample was called as "the h drol zed extract".

1.2 Quantitative analysis of astaxanthin by HPLC method

HPLC technique was used to confirm the percentage purity of hydrolyzed extract from Section 1.1. Each concentration of hydrolyzed extract was determined in triplicate. HPLC method was validated using the guideline in the USP35/NF30 (United States Pharmacopeia, 2012). The analytical parameters used in the assay validation for HPLC method were specificity, linearity, accuracy, and precision as described in Appendix B.

1.2.1 HPLC condition

The chromatographic condition was modified from Anajarn et al. (2010) as follows:

Column	:	Luna Phenomenex® C18 (5 µm, 250 x 4.6 mm)
Mobile phase	:	Methanol/dichloromethane/acetonitrile/water (85:5:5:5)
Injection volume	:	20 µL
Flow rate	:	Isocratic, 0.8 mL/min
Detector	:	PDA detector at 474 nm
Temperature	:	25°C
Run time	:	20 minutes

The mobile phase was prepared by using methanol/dichloromethane/ acetonitrile/water (85:5:5:5 v/v). The solution was mixed together, filtered through 0.45 µm membrane filter and then degassed by sonication for 30 minutes prior to use.

The hydrolyzed extract was analyzed and compared with the free astaxanthin reference standard.

1.2.2 Preparation of standard solutions

A stock solution of free astaxanthin standard was prepared by accurately weighing 2.5 mg of free astaxanthin into a 100 mL volumetric flask. Methanol and dichloromethane (1:1 v/v) were added to dissolve and adjust to the final volume. This stock solution had a concentration of 0.025 mg/mL. Working standard solutions of free astaxanthin were prepared by pipeting 5, 25, 50, 100, 250, 500, and 1000 μL of the stock solution into a respective 10 mL volumetric flask. The solutions were adjusted to volume with methanol and dichloromethane (1:1 v/v) so that the concentrations of free astaxanthin were 0.0125, 0.0625, 0.125, 0.25, 0.625, 1.25, and 2.5 μg/mL, respectively. Three replications were injected to HPLC for each concentration. Peak areas were reported for all solutions. The equation was calculated from the relationship between peak area responses of free astaxanthin and their concentrations.

1.2.3 Preparation of samples

Briefly, three different concentrations (1, 5, and 10 μg/mL) of hydrolyzed extract in methanol and dichloromethane (1:1 v/v) were accurately prepared, filtered through 0.45 μm membrane filter and analyzed by HPLC method as described above. Each concentration was measured in triplicate. Amount of free astaxanthin in the sample was computed from the calibration curve and expressed as μg/mL. The percentage purity of free astaxanthin in the hydrolyzed extract was calculated according to the following equation:

$$\text{ercentage purit} \quad \frac{\text{oncentration of free astaxanthin (g m)}}{\text{oncentration of dried extract (g m)}} \qquad \text{uation}$$

1.3 Antioxidant activity testing

Hydrogen-donating activity of hydrolyzed extract was determined using the free radical generator 1,1-diphenyl-2-picryl-hydrazyl (DPPH). In this study, the method was slightly modified from Ponsuk Jithavech (2005).

1.3.1 Preparation of 0.1 mM DPPH radical solution

One milligram of DPPH was accurately weighed and dissolved in 25 mL of absolute ethanol.

1.3.2 Preparation of test samples

The test samples were prepared as stock solution with initial concentration of 2-3 mg/mL. The stock solution was diluted with absolute ethanol until a suitable range of concentration (mg/mL) was obtained.

1.3.3 Measurement of antioxidant activity

The DPPH solution (100 μL) and test sample solution (100 μL) were mixed together in 96-well microplate and incubated at 37°C for 30 minutes in the darkness. The absorbance of the mixture was determined by a microplate reader at 517 nm. Astaxanthin standard, apocarotenal, and ascorbic acid were used as the positive control for antioxidant activity testing.

The ability to scavenge the DPPH radical was calculated as percent inhibition using the following equation:

$$\text{nhibition} \quad \cdot \quad \frac{\text{Abs}_{\text{control}} \quad \text{Abs}_{\text{sample}}}{\text{Abs}_{\text{control}}} \qquad \text{uation}$$

Where,

Abs $_{\text{control}}$ is the absorbance of the control (100 μL of DPPH solution and 100 μL of absolute ethanol)

Abs $_{\text{sample}}$ is the absorbance of the test sample (100 μL of DPPH solution and 100 μL of test sample)

Graph showing concentrations of test sample versus % inhibition was plotted. The concentration at 50% inhibition (IC_{50}) of each test sample was computed from the polynomial equation of the initial linear portion of the graph. The mean±SD of IC_{50} values were obtained from triplicate experiments in all test samples.

2. Development of SLNs containing astaxanthin from shrimp shell extract (ASX-SLNs)

The production of SLNs can be carried out to obtain stable particles, with suitable characteristics, such as particle size and size distribution. These properties are

essential in SLNs preparation. The selection of SLNs ingredients (solid lipid, surfactant, and co-surfactant) is of utmost importance in the optimization of any nanoparticle formulations. These components contribute not only to control the particle size and stability of SLNs, but also to control the crystallization behaviour (Vitorino et al., 2011). Before the ASX-SLNs formulations were prepared, preliminary formulation studies included the selection of the appropriate solid lipid, surfactant, and co-surfactant type are described as follows.

2.1 Screening the types of solid lipids, surfactants, and co-surfactants

Each lipid was selected from the representative of triglycerides group (Dynasan®118), partial glycerides group (GMS and Compritol®ATO888), and waxes group (cetyl palmitate). The non-ionic surfactant with high HLB value was used in this study because it tended to generate o/w microemulsion and incorporate the astaxanthin within oil phase. These surfactants included polyoxyethylene 20 sorbitan monooleate (Tween®80), polyethylene-polypropylene glycol (Poloxamer®188), polyoxyethylene fatty alcohol ether (Brij®S721), PEG 40 hydrogenated castor oil (Cremophor®RH40), and polyethylene glycol monostearate (Myrj®52). Moreover, the selected co-surfactants were in the alcohol group which were isopropanol, ethanol, benzyl alcohol, and propylene glycol.

Miscibility test between the hydrolyzed extract from Section 1.1 and SLNs components was observed at temperature 70°C by mixing the individual solid lipid with the extract at a weight ratio of 1:1, whereas the surfactant and co-surfactant were pre-mixed at a weight ratio of 1:1 before blending with the extract at the same ratio. The components that were found to be miscible with the extract without separation and precipitation were then chosen for further study. In addition, the miscibility among solid lipid, surfactant, and co-surfactant was screened by the blending of each lipid with the mixed surfactants at a weight ratio of 1:1 at 70°C. Groups of components which showed homogeneous appearences were also chosen for Section 2.2.

2.2 Preparation of blank-SLNs by microemulsion method

The microemulsion method was selected to prepare SLNs. This technique is

suitable for lipophilic substances, which does not use the organic solvent, and can be prepared by the conventional equipment. Moreover, it also generates smaller particles than other methods (Bunjes and Siekmann, 2006).

2.2.1 Construction of pseudoternary phase diagrams

The pseudoternary phase diagrams were constructed using solid lipid, mixed surfactants (1:1 w/w) and water at 70°C by water titration method (modified from Ma et al., 2007; Morel et al., 1996). Briefly, the solid lipid and mixed surfactants were blended at the weight ratios of 1:6, 1:3, 1:1, 3:1, and 6:1 and then melted at 70°C. Water was added dropwise into the lipid-surfactant mixture under continuous mixing at the same temperature until the mixtures became turbid liquid or gel formation. The samples were classified as microemulsions when they appeared as clear liquids. To construct phase diagram, all data were analyzed by using Sigmaplot Program Version 12.0. The diagrams that gave the high area of isotropic zone were chosen for subsequent study.

2.2.2 Confirmation and identification of microemulsion type

After the region of microemulsion and the boundary line had been identified from Section 2.2.1, a new set of solid lipid, mixed surfactants, and water ratios was specified within the microemulsion region of each phase diagram. The microemulsion formulations within isotropic zone that have a quantity of solid lipid less than water phase were again prepared at these ratios and same temperature (70°C) as in topic 2.2.1 to identify the type of microemulsion.

To identify the microemulsion type, the selected microemulsions were dispersed into water or their respective lipids at the same temperature. If microemulsion was easily dispersed in the water, the microemulsion was defined as o/w. On the other hand, if microemulsion was easily dispersed in the lipid, the microemulsion was defined as w/o. Only the o/w microemulsions were selected for the next step.

2.2.3 Preparation of blank-SLNs and selection of the appropriate formulations

All SLNs formulations were prepared by the method of Anurak et al. (2011) with slight modification. Blank-SLNs formulations were prepared by using the appropriate ratios of solid lipids, mixed surfactants, and water in isotropic zone. The

selected o/w microemulsions from Section 2.2.2 were prepared at 70°C. An optically transparent system was formed. This hot o/w microemulsion was then dispersed in cold water (4°C) at a ratio of 1:20 (w/v) under mild mechanical stirring at 1,400 rpm for 15 minutes to obtain blank-SLNs.

The physical stability of SLNs was studied according to the study of Suratchawadee Amorndechawat (2008). All blank-SLNs formulations were kept at ambient temperature for 4 weeks to evaluate their initial particle size, size distribution, zeta potential, and appearances. The desirable formulations needed to maintain a good appearance throughout the storage period. Physical appearance of SLNs was evaluated by visual observation whereas the particle size and size distribution were determined by photon correlation spectroscopy at 0, 2, and 4 weeks. They must not be phase separation or gel formation. Moreover, formulation must become homogenous when redispersed and average particle sizes must be less than 500 nm with uniform size distribution (measured by polydispersity index). The stable blank-SLNs formulations were then selected for Section 2.3.

2.3 Loading of astaxanthin from shrimp shell extract to SLNs (ASX-SLNs)

Types of solid lipids, which generated the stable blank-SLNs from Section 2.2, were selected to quantify the solubility of hydrolyzed extract in each lipid. This value was used to determine the loading amount of hydrolyzed extract in SLNs. The method followed Shah et al. (2007) since the equilibrium solubility could not be performed in this case. Briefly, 0.5 g of the hydrolyzed extract was taken in test tube and the solid lipid was separately heated at 70°C. This molten lipid was gradually added in portions to the extract with continuous stirring by vortex. The amount of molten lipid required to solubilize the extract was noted by visual observation and performed in triplicate. The end point of the solubility study was the clear formation, homogeneous dispersion of extract, and orange color solution. The solubility of hydrolyzed extract in each solid lipid was calculated by the following equations:

$$\text{olubilit of h drol zed extract (mg mg of lipid)} \quad \frac{\text{n itial amount of extract added (mg)}}{\text{Amount of lipid used (mg)}} \quad \text{uation}$$

After the selection of appropriate blank-SLNs formulations, one gram of the microemulsion (solid lipid, surfactant, co-surfactant, and water) within isotropic zone

was prepared again. Then, 0.5 g of the hydrolyzed extract (from Section 1.1) was added to the mixture, melted at 70°C, and mixed together. ASX-SLNs were obtained by dispersing this mixture into cold water (20 mL) under mild mechanical stirring at 1,400 rpm for 15 minutes (Anurak et al., 2011). The final concentration of hydrolyzed extract in ASX-SLNs was 25 mg/mL. The ASX-SLNs formulations were characterized and stability study was evaluated in the next part.

3.   Physicochemical characterization of ASX-SLNs

The characteristics of freshly prepared blank-SLNs and ASX-SLNs were evaluated. The physical appearances, morphology, particle size, size distribution, and zeta potential were the parameters representing the quality of SLNs. Solid state characterization was also performed to investigate the degree of crystallinity and the modification of lipid in SLNs. Furthermore, these parameters are strongly associated with the drug incorporation in SLNs. The following topics were used for screening the formulation.

3.1 Physical appearances

The physical appearances such as color, gel formation, and phase separation were visually observed.

3.2 Morphology

The morphological feature was investigated using scanning electron microscope (SEM). The ASX-SLNs formulations were lyophilized using Dura-Dry^{TM} lyophilizer. Five milliliters of each sample was rapidly precooled at -40°C, lyophilized for 14 hours at a temperature range -10°C to 20°C, and a vacuum of 500 mmHg. After the elimination of excess water in SLNs sample by freeze-dryer, a few amounts of the sample were placed on a slab. A sputter coater was used to coat the dried samples with gold, fixing them onto stubs. Ultimately, the samples were examined under a JSM-6510A$^{®}$ SEM (JEOL, Tokyo, Japan).

3.3 Particle size analysis

The mean particle size (z-value), particle size distribution (polydispersity index, PDI), and zeta potential were measured by photon correlation spectroscopy, PCS (Zetasizer Nano ZS, Malvern Instruments, Malvern, UK). A sample was dispersed in distilled water before being used. The SLNs dispersion was put in a

quartz cuvette. The sample was then placed inside the instrument chamber and allowed to be temperature equilibrium between sample and sample holder at 30°C. The obtained value from each formulation was the average of 3 measurements.

3.4 The percentage of entrapment efficiency

To quantify the entrapment efficiency, 0.5 g of ASX-SLNs formulations was carried out by ultrafiltration method (Schwarz and Mehnert, 1999; Hsu et al., 2003) using centrifugal filter device (Amicon® with cellulose membrane MWCO = 100 K, equivalent to 30-90 nm), at 12,000 rpm, 25°C, for 30 minutes per cycle. The filtrates (free) were collected and the precipitated pellets containing hydrolyzed extract (entrapped) were lyzed by adding methanol. Both of the obtained solutions were analyzed for content of free and entrapped astaxanthin using HPLC as described in Section 1.2.1. The triplicate observations were measured. The percentages of entrapment efficiency and recovery were calculated by the following equations:

$$\text{ntrapment efficienc ( )} \quad \frac{\text{Amount of entrapped astaxanthin}}{\text{Amount of initial astaxanthin added}} \qquad \text{uation}$$

$$\text{ecover ( )} \quad \frac{\text{Amount of entrapped astaxanthin} \quad \text{Amount of free astaxanthin}}{\text{Amount of initial astaxanthin added}} \qquad \text{uation}$$

3.5 Thermal analysis by differential scanning calorimetry (DSC)

The DSC thermogram was obtained using differential scanning calorimeter (DSC6200, Seiko Instruments Inc., Japan) (Jingfei et al., 2010). Standard aluminium sample pans (40 µL) were used. Blank-SLNs and ASX-SLNs formulations were transformed into lyophilized form. Approximately 5 mg sample was correctly weighed into crimped aluminum pans and then sealed for analysis. An empty pan was used as reference. The DSC runs were conducted over a temperature range 15-250ºC at rate of 10ºC/min. Ultra high pure nitrogen was used at a flow rate of 2 mL/min. The percentage of crystallization index (%CI) was calculated as follows:

$$\text{r stallization index ( )} \quad \frac{\text{nthalp} \qquad \text{g}}{\text{nthalp}_{\text{bulk material}} (\text{ g}) \quad \text{oncentration of lipid}} \qquad \text{uation}$$

3.6 Powder X-ray diffractometry (PXRD) analysis

PXRD patterns were recorded to evaluate the physical nature of the formulations and the change of crystallinity of excipients, drug, drug and excipients after preparation process. Blank-SLNs and ASX-SLNs formulations were freeze dried so as to keep the formulation in powdered form. To prepare the mixture of SLNs ingredients for PXRD analysis, hydrolyzed extract, solid lipid, surfactant, co-surfactant, and water were ground together in the mortar. The ratios of each component were same to that of weight ratios in each SLNs formulation. The proper amount of the sample was placed onto the glass plate containing rectangular window. After firmly pressed it down by using another piece of glass plate, any surplus of sample was removed. The sample plate stuffed with the sample was mounted onto the sample holder. PXRD patterns were reported on a MiniFlexII, Rigaku, Powder X-ray diffractometer at a scanning rate of 0.02°min⁻ between 3° and 40° 2θ range (Jingfei et al., 2010).

4. Physical and chemical stability of ASX-SLNs

The samples of ASX-SLNs were divided and kept in tightly closed glass bottles (tubular glass vial for antibiotics 10 mL). The samples were stored at room temperature and protected from light for 3 months. The control solution contained the same amount of astaxanthin from hydrolyzed extract dissolved in propylene glycol and ethanol (1:1 v/v). The samples were withdrawn and investigated at 0, 1, 2, and 3 months in three batches (n=3). Physical and chemical stability of the samples were evaluated as follows:

4.1 Physical appearances

The physical appearances were evaluated as described in Section 3.1.

4.2 Particle size analysis

The particle size, size distribution, and zeta potential were measured using the same procedure as in Section 3.3.

4.3 The percentages of recovery and entrapment efficiency

The percentages of recovery and entrapment efficiency were determined as same as in Section 3.4.

4.4 Thermal analysis by differential scanning calorimetry (DSC)

The DSC thermogram was evaluated as described in Section 3.5.

ASX-SLNs formulations were determined all of above topics whereas control solution was only investigated physical appearances and recovery. The stable ASX-SLNs formulations were then selected for the next part.

5.   Evaluation of *in vitro* release and pig skin permeation of ASX-SLNs

5.1 *In vitro* release study

The stable ASX-SLNs from Section 4 were selected to study the release profile. The release study was operated by using vertical Franz diffusion cell, which consisted of donor and receiver compartments (Wissing and Muller, 2002). The dialysis membrane was placed between two compartments. The type of membrane was regenerated cellulose tubular membrane with molecular weight cut-off 12,000-14,000 (Cellu-Sep®). The membrane was hydrated in purified water for 24 hours, then washed by hot water and soaked in receiver medium for 1 hour before use. The receiving compartment contained 13 mL of phosphate buffer saline pH 7.4 and ethanol (7:3 v/v) which was set at 37±0.5°C by a circulating water jacket.

The membrane (diameter 1.7 cm) and the receptor compartment were carefully fitted with the donor compartment. One milliliter of SLNs formulation was dropped into the donor chamber, then covered with parafilm to prevent evaporation. One milliliter of the solution with the concentration 1 mg/mL of the hydrolyzed extract was used as a control (the solution of astaxanthin from hydrolyzed extract in Tween®80 2%w/v, isopropanol 2%w/v, and water 96% w/v). The receptor fluid was continuously mixed by magnetic stirring bar throughout the time of study. A volume of 0.5 mL was withdrawn from the receiver medium at certain time intervals of 0.5, 1, 1.5, 2, 4, 6, 8, 12, 16, 20, and 24 hours. The receptor compartment was replaced with the same volume of receptor solution to keep the constant volume during the experiment and to maintain sink conditions. The receptor fluid was diluted at appropriate concentration and measured by HPLC method as in Section 1.2.1. The triplicate observations were measured (n=3). The cumulative amount of free astaxanthin release was calculated by the following equation:

umulative amount of free astaxanthin release (   ) $\dfrac{A_t}{A}$ uation

Where, A_t is the cumulative amount of free astaxanthin released at a particular time.

A_0 is the initial amount of free astaxanthin loaded to the donor compartment.

5.2 *In vitro* permeation study

5.2.1 Preparation of newborn pig skin membrane

Permeation study was evaluated utilizing modified Franz diffusion cell. The abdominal skin of newborn pig was used in this experiment (Cilurzo et al., 2007). After removal of subcutaneous fat and extraneous tissue, the obtained skin was cleaned in purified water, wrapped in aluminium foil, and kept in a freezer (-21°C) until being used. The frozen skin was thawed by immersing in phosphate buffer saline pH 7.4 for 1 hour before being used.

5.2.2 Permeation study

The step of permeation study was the same as release study from Section 5.1 except that the membrane used in this study was newborn pig skin. The newborn pig skin was sandwiched firmly between the donor and receptor compartments with stratum corneum side facing the donor compartment. Phosphate buffer saline (pH 7.4) containing 30% ethanol (Fang et al., 2008; Gulbake et al., 2010; Wang et al., 2009) was used as receptor medium for astaxanthin. The skin and receptor medium were equilibrated to 32°C and 37°C, respectively, for 30 minutes. After equilibration, 1 mL of SLNs formulation or control solution (containing 1 mg/mL of the hydrolyzed extract) was added onto donor compartment of each Franz diffusion cell. All formulations were freshly prepared before being used. A volume of 0.5 mL of receptor medium was withdrawn at time interval of 2, 4, 6, 8, 12, 16, 20, and 24 hours and was substituted with fresh receptor solution to keep the constant volume during experiment.

5.2.3 Skin retention of free astaxanthin

At the end of study (24 hours), the skin surface and the donor cap of each cell were washed 3 times with ethanol and analyzed the content of free astaxanthin by HPLC with same condition of Section 1.2.1. The pig skin was then removed, cut into small pieces and extracted with ethanol by vortexing for 5 minutes,

sonicating for 5 minutes, and shaking overnight at ambient temperature. Each skin sample was then centrifuged and the supernatant was analyzed for the free astaxanthin accumulation in the skin. Each set of experiment was performed in six replicates (n=6). The cumulative amount of permeated free astaxanthin per unit area was constructed versus time. The flux was calculated from the slope. The percentage of free astaxanthin permeated, the percentage of free astaxanthin accumulated in the skin, and the steady state flux were determined and compared among the SLNs formulation and control solution.

6.   Statistical analysis

The data were statistically analyzed by using student's t-test, one-way analysis of variance (ANOVA). When a significant difference ($p<0.05$) was indicated, the data were subjected to multiple comparison by Tukey or Dunnett test to campare the difference. The licensed statistical package for social sciences (SPSS) software for windows version 17.0 was used in this study.

CHAPTER IV

RESULTS AND DISCUSSION

1. Astaxanthin extraction from shrimp shell

1.1 Preparation of shrimp shell crude extract, hydrolysis reaction, and qualitative analysis of astaxanthin

Although the isopropanol was selected to extract the active compound from the homogenized shrimp powder, various organic solvents were used to find the extraction yield of crude extract. The data in Appendix A also confirmed the high extraction efficiency of isopropanol. After passive extraction process by isopropanol, the crude extract from dried shrimp shell was obtained and further separated by column chromatography into different forms of astaxanthin. The order of eluated fractions was astaxanthin diesters, monoesters, and free form, respectively (as shown in Figure 9). These ingredients were then isolated into three spots by TLC. From the data of สกุลคุณ มากคุณ (2546), the shrimp shell crude extract is composed of free astaxanthin (R_f = 0.35-0.45), astaxanthin monoesters (R_f = 0.75-0.80), and astaxanthin diesters (R_f = 0.90-0.96) when using isopropyl acetate and benzene (1:3 v/v) as a mobile phase. In this experiment, ethyl acetate and benzene (2:3 v/v) was employed as a mobile phase. The result of TLC was similar to the previous results (สกุลคุณ มากคุณ, 2546) as shown in Figure 10. HPLC method was also used to confirm the identity of astaxanthin and its esters.
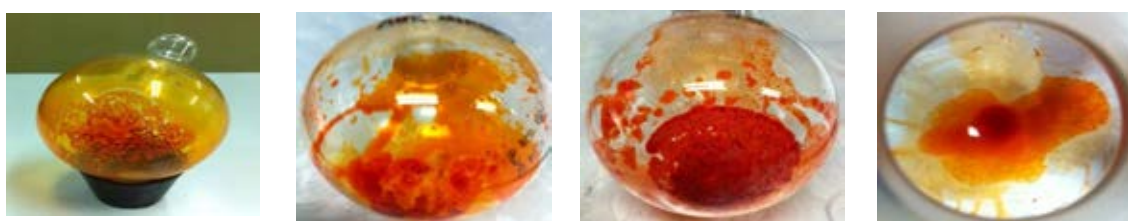
(A) Crude extract   (B) Astaxanthin   (C) Astaxanthin   (D) Free astaxanthin
                        diesters fraction   monoesters fraction   fraction

Figure 9 Fraction appearances of the extracts after separation by column chromatography (non-hydrolyzed extracts).

(A)   (B)   (C)
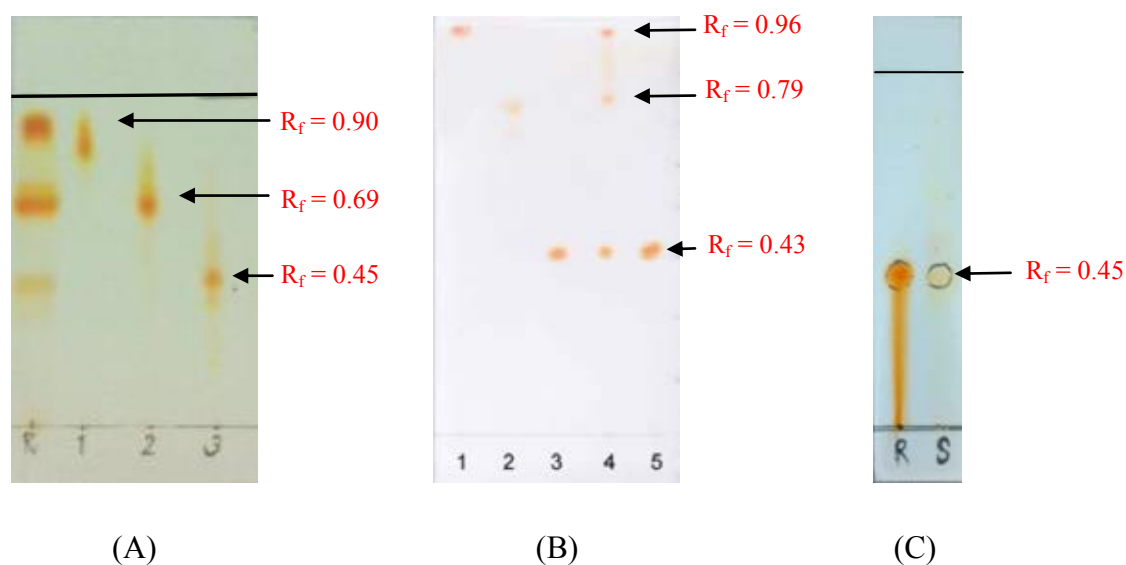
Figure 10 TLC chromatogram of non-hydrolyzed extracts:

        (A) Mobile phase was ethyl acetate and benzene (2:3 v/v). From left to right: crude extract (R), astaxanthin diesters fraction (1), astaxanthin monoesters fraction (2), and free astaxanthin fraction (3).

        (B) Mobile phase was isopropyl acetate and benzene (1:3 v/v). From left to right: astaxanthin diesters fraction (1), astaxanthin monoesters fraction (2), free astaxanthin fraction (3), crude extract (4), and astaxanthin standard (5) (สกุลคุณ มากคุณ, 2546).

        (C) Mobile phase was ethyl acetate and benzene (2:3 v/v). Comparison of R_f values between astaxanthin standard (R) and free astaxanthin fraction (S).

        From HPLC chromatogram as shown in Figure 11, the peak of astaxanthin standard and free astaxanthin fraction showed the same retention time (approximately 4.0 minutes) when using methanol/acetonitrile/dichloromethane/water (28:46:22:4 v/v) as a mobile phase. Therefore, this system could separate three components of the crude extract. The untreated crude extract gave very low peak of free astaxanthin with the presence of two more lipophilic peaks at 10-20 and 35-75 minutes, attributed to be monoesters and diesters of astaxanthin, respectively. Astaxanthin diesters have much lower polarity than other forms because their two hydroxyls on the terminal rings have been absolutely esterified with fatty acids (Figure 12). It had been demonstrated that free astaxanthin was eluted before monoesters and diesters form, respectively. Due to

the various fatty acids of astaxanthin esters, the chromatogram exhibited many peaks of astaxanthin ester forms and it was also difficult to separate all astaxanthin esters (Johnson and An, 1991; Hinostroza and Bjerkeng, 2002). According to a little content of free astaxanthin in the crude extract, the hydrolysis of astaxanthin ester forms was necessary to increase the amount of free astaxanthin.

Hydrolysis reaction of shrimp shell crude extract could be made from sodium hydroxide in methanol solution at different concentrations. When hydrolysis condition was performed within the first few hours, some conversion of astaxanthin ester forms into free form was observed from TLC (as shown in Figure 13A). At the end of the five hours reaction, the remaining astaxanthin ester forms were discarded and only free astaxanthin was collected by column chromatography. The appearance of astaxanthin product is shown in Figure 13B. The percentage yields of free astaxanthin after saponification and separation by column chromatography at different NaOH concentrations were 21.12, 52.34, and 32.14%w/w when using 0.01N, 0.03N, and 0.05N NaOH, respectively. The peak of free astaxanthin was also analyzed by HPLC as shown in Figure 14.

From the HPLC data, the main peak of free astaxanthin was eluted at 7.30 minutes and similar to the free astaxanthin standard. The result was found to be in accordance with the findings from Armenta and Guerrero (2009) who reported astaxanthin is the one component isolated from fermented shrimp by-products (*Litopenaeus vannamei*). Moreover, Chen and Meyers (1983) also revealed the presence of astaxanthin in the samples of crawfish (*Procambarus clarkii*) from the heat-processed exoskeleton. In addition, Ogawa et al. (2007) examined the main pigments in shrimp waste and summarized that astaxanthin was the most plentiful carotenoids. From the HPLC chromatogram, 0.03N NaOH was the optimal condition to hydrolyze the crude extract that gave the highest percentage yield of free astaxanthin fraction with the least amount of degradation peaks. This result also showed that a higher methanolic NaOH concentration should be avoided to reduce the astaxanthin degradation. Consequently, the hydrolyzed extract (0.03N NaOH) was selected for further quantitative analysis, antioxidant activity study, and formulation of SLNs.
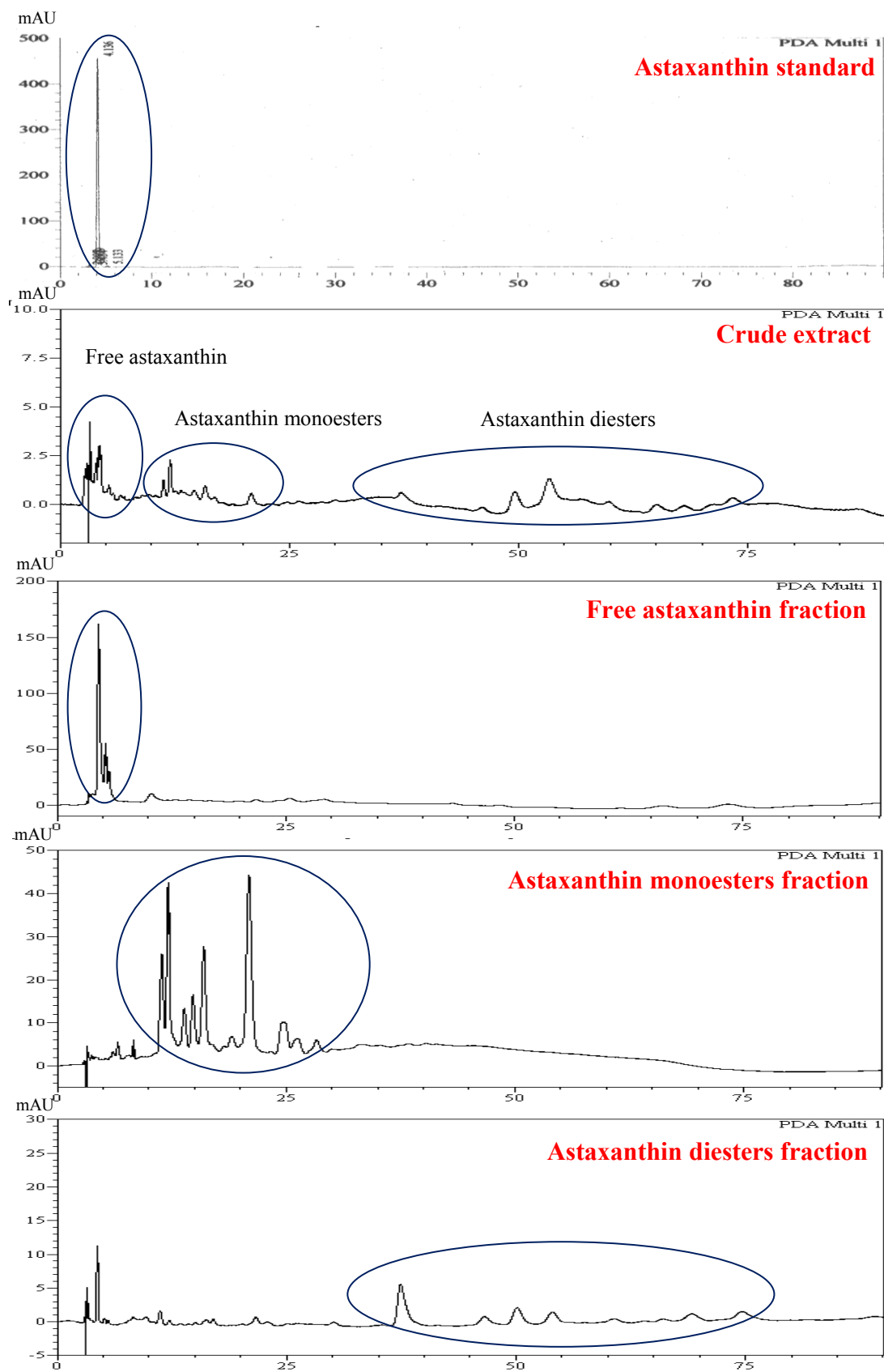
Figure 11 HPLC chromatogram using methanol/acetonitrile/dichloromethane/water (28:46:22:4 v/v) as a mobile phase for separation of free astaxanthin and its esters forms (HPLC for non-hydrolysis condition).

(A) Free astaxanthin

(B) Astaxanthin monoesters (R_1 = fatty acid)

(C) Astaxanthin diesters (R_1, R_2 = fatty acid)
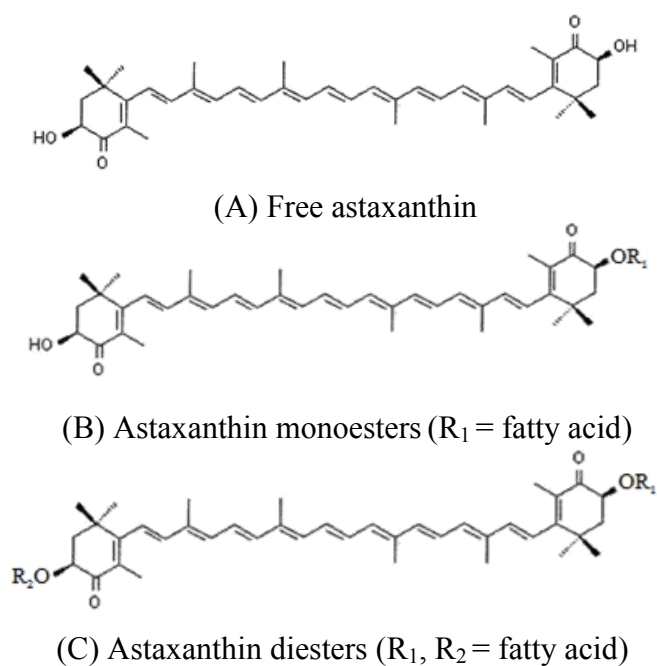
Figure 12 The structure of three astaxanthin forms.

(A)

(B)
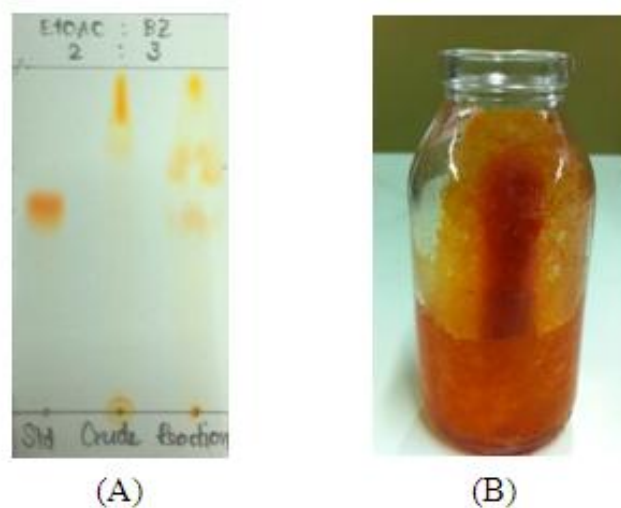
Figure 13 TLC chromatogram observed during hydrolysis reaction (A) and the appearance of hydrolyzed extract at 0.03N NaOH after separation by column chromatography (B).
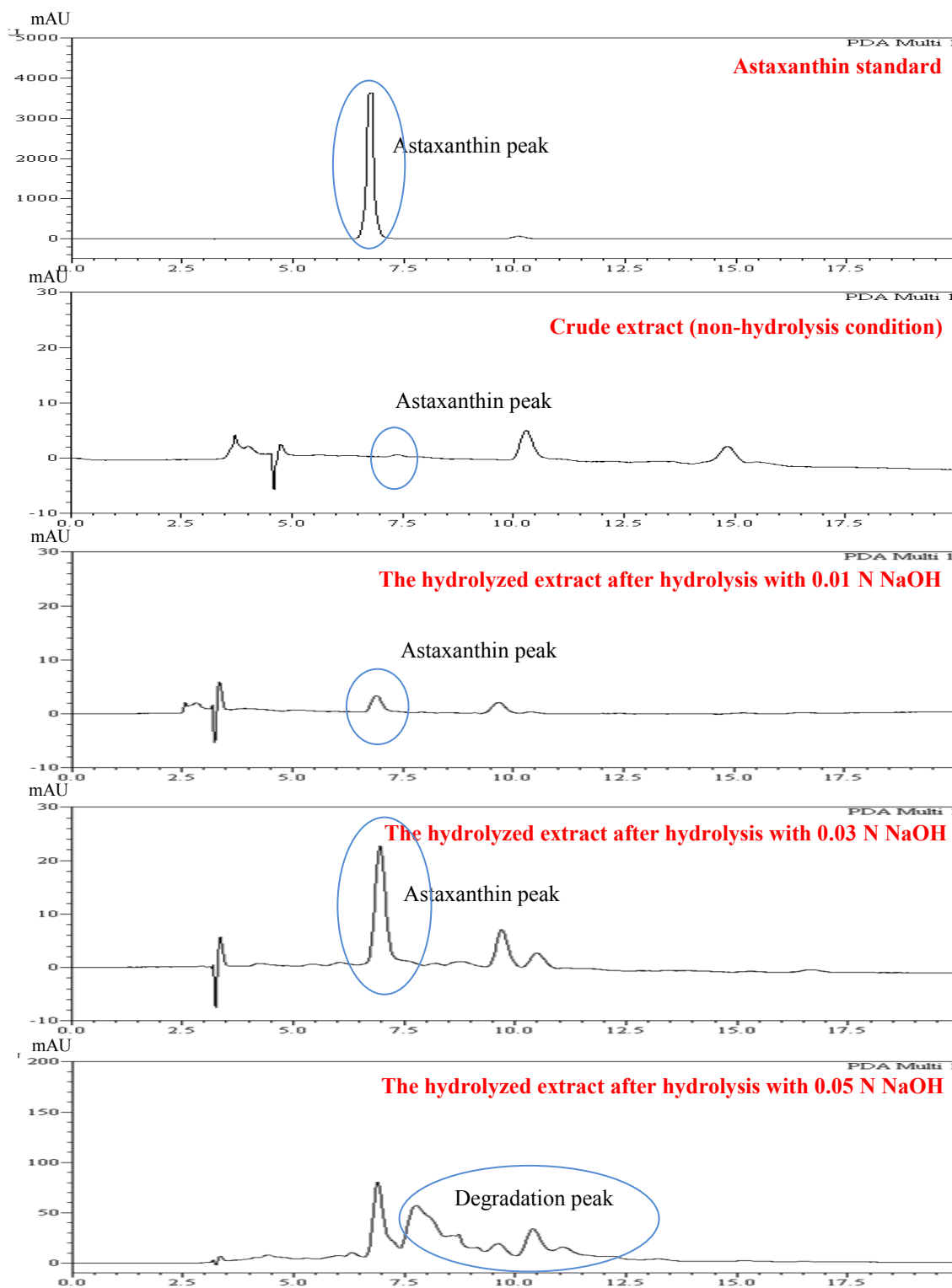
Figure 14 HPLC chromatogram using methanol/acetonitrile/dichloromethane/water (85:5:5:5 v/v) as a mobile phase for separation of free astaxanthin and degradation products (HPLC for hydrolysis condition).

1.2 Quantitative analysis of astaxanthin by HPLC method

Three concentrations of hydrolyzed extract (0.03N NaOH) were prepared and analyzed for free astaxanthin content by HPLC method (the data are shown in Table 1). When the extract concentration increased, the free astaxanthin concentration was also detected proportionally. The result showed that the hydrolyzed extract contained the equivalent amount of free astaxanthin as 21.66±0.75%w/w. When the amount of free astaxanthin was calculated on the basis of the percentage yield of free astaxanthin after saponification with 0.03N NaOH (52.34%w/w) from Section 1.1, the real content of free astaxanthin was 11.34 mg in 100 mg of crude extract.

Sowmya and Sachindra (2012) extracted astaxanthin from shrimp waste by solvent extraction (acetone) at a ratio of 1:1 (g/mL) and also found that crude extract from shrimp processing by-products was composed of free astaxanthin 29.21%w/w without hydrolysis condition. This might be due to the different types of organic solvent used in the study. Since the higher polarity index of acetone (5.1) than isopropanol (3.9), the capacity of solvent to extract free astaxanthin might increase and affected the higher content of free astaxanthin in crude extract. Moreover, the extraction by acetone was performed until the filtrate was colorless which resulted in the higher astaxanthin content. Calo et al. (1995) also reported that the astaxanthin content varies depending on the strain and the culture method used. However, this hydrolyzed extract was used to study the antioxidant activity in the next step.

Table 1 The percentage purity of free astaxanthin from hydrolyzed extract (the free astaxanthin concentration in the extract was calculated from the calibration curve).

Actual concentration of extract (µg/mL)	Peak area			Mean	Calculated concentration of astaxanthin (µg/mL)	%Purity of astaxanthin in extract (w/w)	Mean±SD
	Set 1	Set 2	Set 3				
1.00	70674	69543	73674	70109	0.2231	22.31	
5.00	329854	324712	324912	327283	1.0416	20.83	21.66±0.75
10.00	677986	696010	670324	686998	2.1820	21.82	

1.3 Antioxidant activity testing

DPPH radical scavenging assay was selected to determine the antioxidant activity of active compound because this technique is easy, effective, highly reproducible, and is a rapid way to study (Gulcin, 2006). DPPH radical is reduced by donating hydrogen atom of the antioxidant molecule and resulting in the absorbance decreases. In this study, astaxanthin standard, apocarotenal, and ascorbic acid were used as a positive control. The IC_{50} of each test sample was calculated from the equation of linear regression analysis and the data are shown in Figure 15. The IC_{50} in mg/mL ranking is as follows: ascorbic acid < astaxanthin standard < apocarotenal < astaxanthin from hydrolyzed extract (0.03N NaOH). The highest activity in ascorbic acid resulted in the different characteristic in terms of water-soluble compound. Thus, three lipophilic compounds (in carotenoid group) were compared the antioxidant activity. By comparing the IC_{50} value, astaxanthin standard showed highest activity whereas the DPPH radical scavenging activity of astaxanthin from hydrolyzed extract was lower than astaxanthin standard ($p<0.05$).

Chen et al. (2011) also studied the antioxidant activity on DPPH radical of astaxanthin extract from discharged wastewater during the production of chitin. The results found that the IC_{50} value was 0.84 mg/mL. Moreover, the scavenging effect of the obtained extract increased proportionally with the increase of concentration. The quantity of free astaxanthin in the obtained pigment analyzed by HPLC was 30.02%. This implied that the result was attributed to the low quantity of astaxanthin in the shrimp shell extract and the radical scavenging activity of extract was correlated with astaxanthin content. If the purity of astaxanthin from shrimp shell extract increased, the stronger activity from DPPH assay should be obtained. According to the determination of astaxanthin from hydrolyzed extract, the IC_{50} in mg/mL unit was converted into μmole/mL on the basis of molecular weight and actual astaxanthin content (21.66%w/w) as shown in Figure 16. This conversion also found that astaxanthin from hydrolyzed extract presented the highest antioxidant activity ($p<0.05$). In the future, the solvent extraction process should be improved so as to increase free astaxanthin content in the extract and present the high antioxidant activity. Astaxanthin extraction can be carried out by other methods such as microbial

extraction (Khanafari et al., 2007) and supercritical fluid extraction (Machmudah et al., 2006).
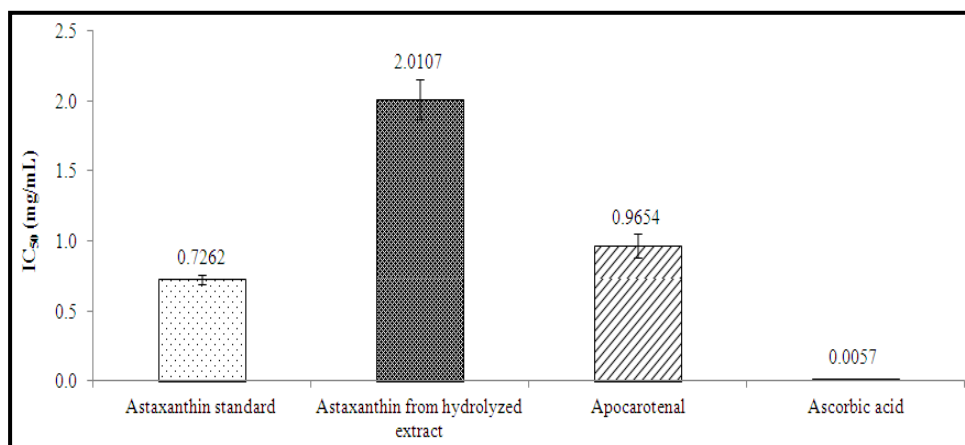
Figure 15 IC_{50} (mg/mL) of astaxanthin standard, astaxanthin from hydrolyzed extract (0.03N NaOH), apocarotenal, and ascorbic acid in DPPH assay (significantly different among three test samples, $p<0.05$).
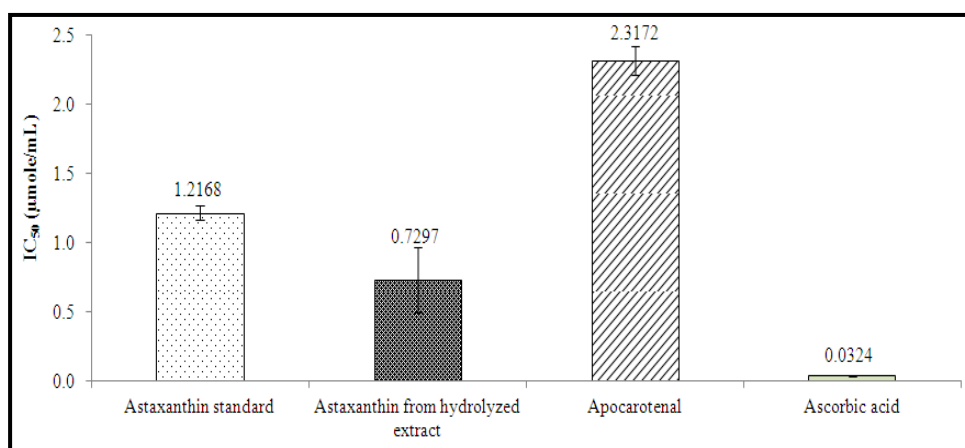
Figure 16 IC_{50} (µmole/mL) of astaxanthin standard, astaxanthin from hydrolyzed extract (0.03N NaOH), apocarotenal, and ascorbic acid in DPPH assay (significantly different among three test samples, $p<0.05$).

2. Development of SLNs containing astaxanthin from shrimp shell extract (ASX-SLNs)

2.1 Screening the types of solid lipids, surfactants, and co-surfactants

Various solid lipids were used to study the miscibility test: Dynasan[®]118 (triglycerides group), GMS (partial glycerides group), Compritol[®]ATO888 (partial glycerides group), and cetyl palmitate (waxes group). A great number of literatures used these lipids to prepare SLNs formulation and its property could be miscible with a lipophilic compound (Silva et al., 2011; Luo et al., 2006; Pathak and Nagarsenker, 2009; Effat et al., 2011). All types of solid lipids were able to mix with the extract at a weight ratio of 1:1. The characteristics of extract in different lipids at molten state (70°C) and solidified state (room temperature) are displayed in Figure 17. It was found that all types of lipids demonstrated the effective solubilizing potential for the extract among 2 states and homogeneous matrices were obtained in solidified lipids. In addition, as reported by Muller et al. (2002), the selected lipids possessed biocompatibility and acceptability for topical use.

Five surfactants used in this study were the non-ionic surfactants with high HLB values and tended to form o/w microemulsion which included Tween[®]80 (HLB 15), Poloxamer[®]188 (HLB 29), Brij[®]S721 (HLB 15.5), Cremophor[®]RH40 (HLB 14-16), and Myrj[®]52 (HLB 16.9). Isopropanol, ethanol, benzyl alcohol, and propylene glycol were selected as co-surfactant. Twenty types of mixed surfactants (1:1 combination of surfactant and co-surfactant) were able to mix with the extract at the same ratio. In order to screen the miscibility of three main components (solid lipid, surfactant, co-surfactant), each lipid was blended together with the mixed surfactants at a weight ratio of 1:1 at 70°C. Total 80 formulations were monitored for the miscibility and it was also found that Dynasan[®]118 and GMS could mix together with other ingredients whereas Compritol[®]ATO888 could not or displayed turbid appearance. Moreover, propylene glycol with chosen solid lipid and mixed surfactants was not compatible at all. Thus, Compritol[®]ATO888 and propylene glycol were excluded from further study. In the case of cetyl palmitate, it was able to mix only with isopropanol and all surfactants. In conclusion, the two solid lipids (Dynasan[®]118 and GMS), three co-surfactants (isopropanol, ethanol, benzyl alcohol) and all types of

surfactants were used in the further experiment, whereas cetyl palmitate was only investigated with all surfactants and isopropanol.

| (A) | (B) | (C) | (D) | (E) | (F) | (G) | (H) |
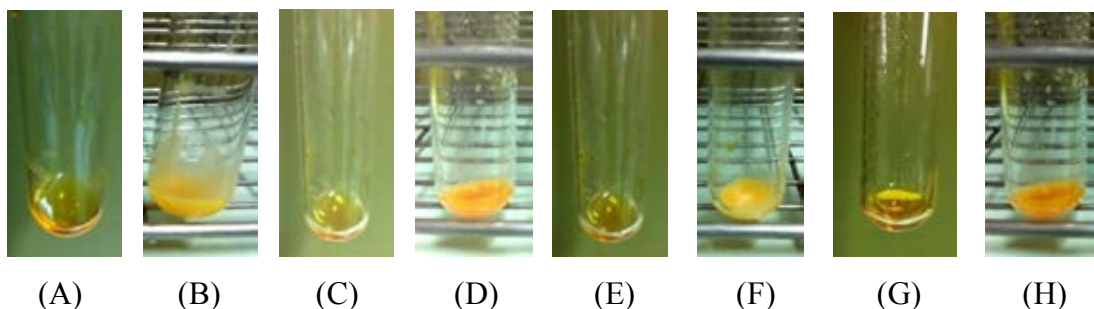
Figure 17 Photographs of hydrolyzed extract in different solid lipids at molten state (70°C) and solidified state at room temperature (RT): (A) Dynasan®118 (70°C), (B) Dynasan®118 (RT), (C) GMS (70°C), (D) GMS (RT), (E) Compritol®ATO888 (70°C), (F) Compritol®ATO888 (RT), (G) Cetyl palmitate (70°C), and (H) Cetyl palmitate (RT)

2.2 Preparation of blank-SLNs by microemulsion method

2.2.1 Construction of pseudoternary phase diagrams

The 35 pseudoternary phase diagrams were built using three different types of lipids, i.e., Dynasan®118, GMS, and cetyl palmitate by water titration method at 70°C. Water was gradually added to the mixtures of lipid and mixed surfactants at various ratios under continuous stirring until the mixture became turbid liquid or gel formation. To find the boundary line of microemulsion region, the ratios of lipid, mixed surfactants, and water were calculated. The data were plotted and the phase diagrams were constructed as shown in Figures 18-24. Detail of titration results and amount of water added to form microemulsion boundary within each phase diagram is provided in Appendix C.

From the pseudoternary phase diagram, the area in isotropic zone showed a little area when using cetyl palmitate as a solid lipid, Poloxamer®188 as a surfactant, and benzyl alcohol as a co-surfactant. The microemulsion formulas within this zone were thus excluded from further study because it tended to present w/o microemulsion.

Considering Figures 18-24, it was found that the area in isotropic region appeared to decrease when using Poloxamer[®]188 as a surfactant for all lipids. This could be due to the higher HLB value of Poloxamer[®]188 (HLB 29) than Tween[®]80 (HLB 15), Brij[®]S721 (HLB 15.5), Cremophor[®]RH40 (HLB 14-16), and Myrj[®]52 (HLB 16.9) (Rowe et al., 2006). Poloxamer[®]188 may facilitate the formation of o/w microemulsion lower than other surfactants. Therefore, formulations that generated the large region of o/w microemulsion, containing Tween[®]80, Brij[®]S721, Cremophor[®]RH40, and Myrj[®]52 as surfactants, were selected to further prepare SLNs. Moreover, the microemulsion formulations within isotropic zone that had a quantity of solid lipid less than water phase were selected and prepared again at these ratios to confirm the formation of microemulsion as well as to identify the type of microemulsion. Therefore, sixteen diagrams contained the large area of isotropic zone were chosen to further study.

2.2.2 Confirmation and identification of microemulsion type

Sixteen pseudoternary phase diagrams were selected to confirm and identify the microemulsion type. Various ratios of solid lipid, mixed surfactants, and water within the area of isotropic zone were specified and re-prepared. In case of lipophilic compound, the o/w microemulsion is necessary to form and incorporate the astaxanthin in lipid phase. The samples were identified as o/w microemulsion by miscibility test as shown in Figures 25-26. The numbers in isotropic zone of each phase diagram were classified as o/w microemulsion. The formulas of solid lipid, mixed surfactants, and water that formed o/w microemulsion in isotropic zone are summarized in Table 2.

Surfactant = Tween®80:IPA (1:1), at 70°C
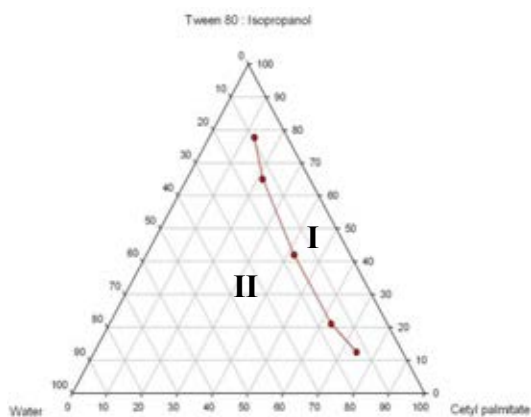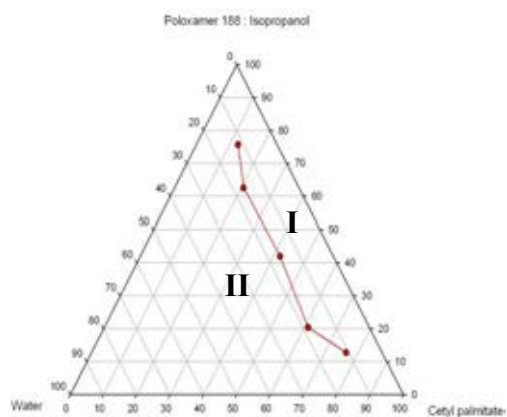
Surfactant = Poloxamer®188:IPA (1:1), at 70°C

Surfactant = Brij®S721:IPA (1:1), at 70°C

Surfactant = Cremophor®RH40:IPA (1:1), at 70°C

Surfactant = Myrj®52:IPA (1:1), at 70°C

IPA = isopropyl alcohol

I: flowable microemulsion region
(liquid clear zone)

II: viscous or non-microemulsion
region

Figure 18   The pseudoternary phase diagrams of cetyl palmitate, various surfactants, isopropyl alcohol, and water at 70°C.

Surfactant = Tween®80:IPA (1:1), at 70°C   Surfactant = Poloxamer®188:IPA (1:1), at 70°C
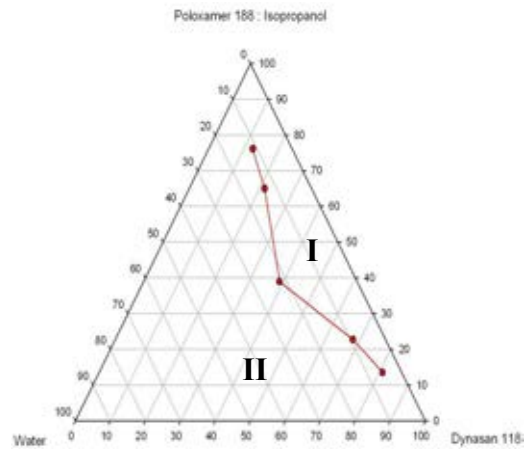
Surfactant = Brij®S721:IPA (1:1), at 70°C   Surfactant = Cremophor®RH40:IPA (1:1), at 70°C

Surfactant = Myrj®52:IPA (1:1), at 70°C
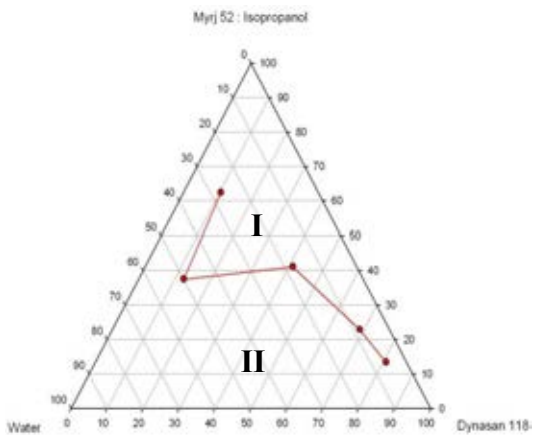
IPA = isopropyl alcohol

I: flowable microemulsion region
      (liquid clear zone)

II: viscous or non-microemulsion
      region

Figure 19   The pseudoternary phase diagrams of Dynasan®118, various surfactants,
isopropyl alcohol, and water at 70°C.

Surfactant = Tween®80:BA (1:1), at 70°C   Surfactant = Poloxamer®188:BA (1:1), at 70°C
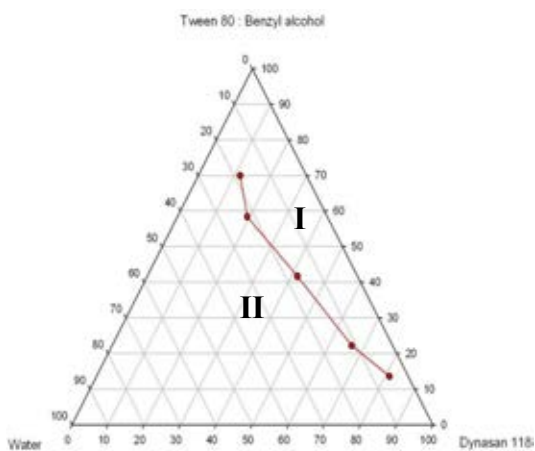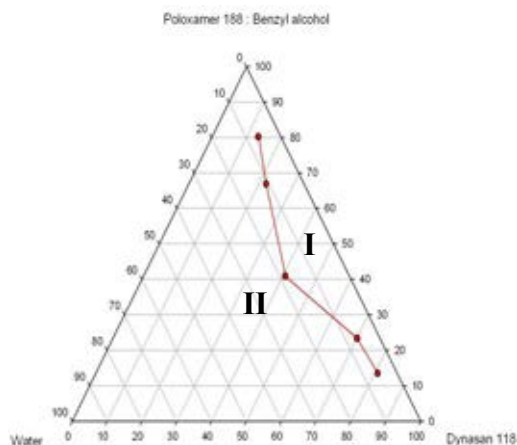
Surfactant = Brij®S721:BA (1:1), at 70°C   Surfactant = Cremophor®RH40:BA (1:1), at 70°C
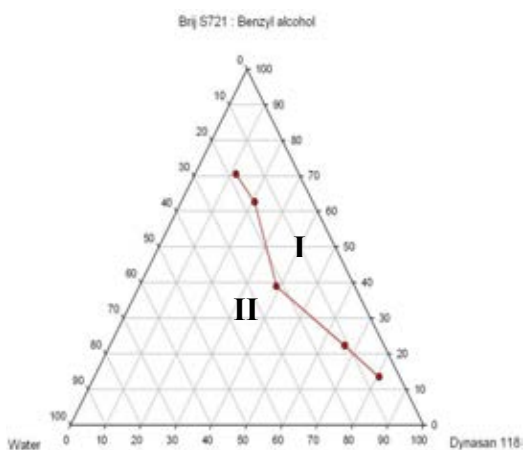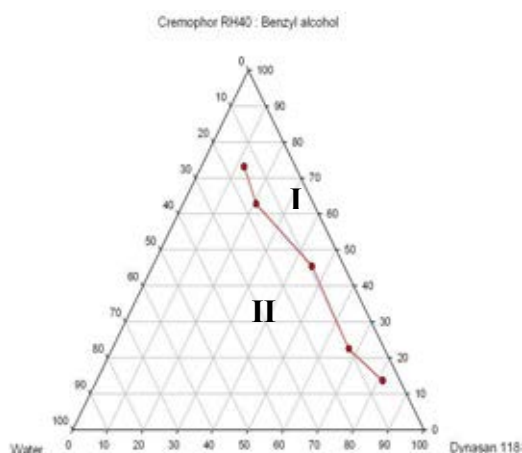
Surfactant = Myrj®52:BA (1:1), at 70°C
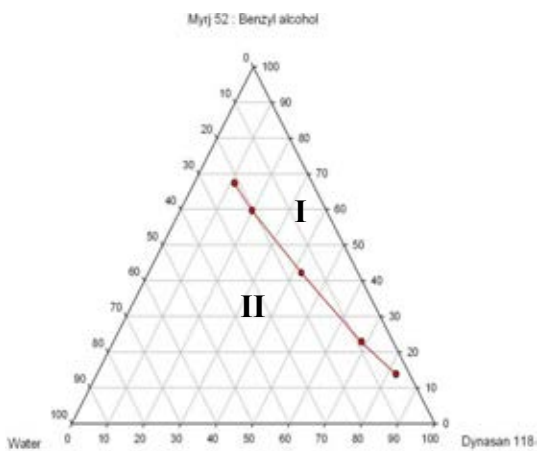
BA = benzyl alcohol

I: flowable microemulsion region
     (liquid clear zone)

II: viscous or non-microemulsion
     region

Figure 20   The pseudoternary phase diagrams of Dynasan®118, various surfactants,
benzyl alcohol, and water at 70°C.

Surfactant = Tween®80:EA (1:1), at 70°C
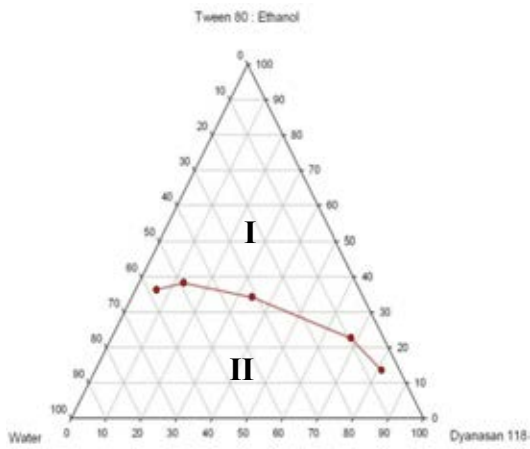
Surfactant = Poloxamer®188:EA (1:1), at 70°C
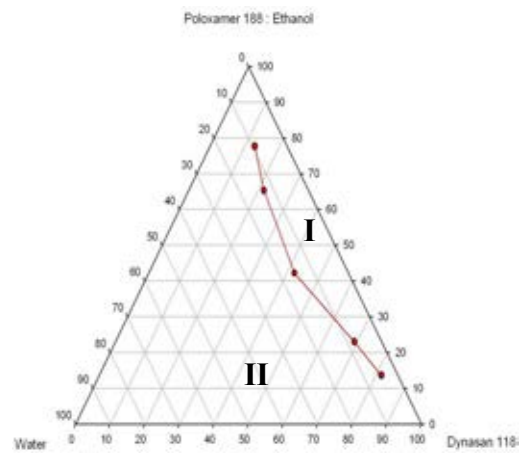
Surfactant = Brij®S721:EA (1:1), at 70°C
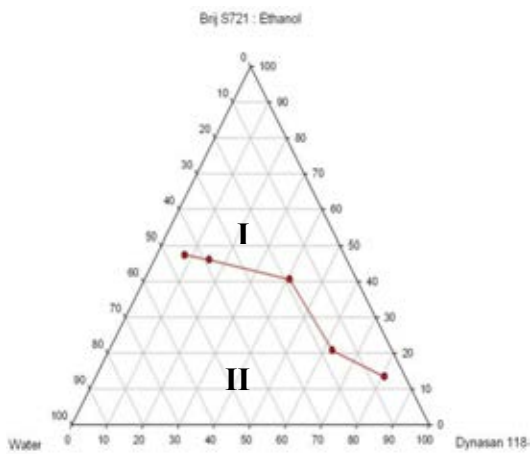
Surfactant = Cremophor®RH40:EA (1:1), at 70°C
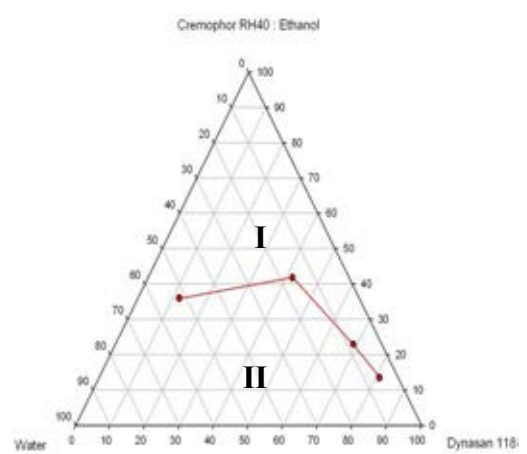
Surfactant = Myrj®52:EA (1:1), at 70°C
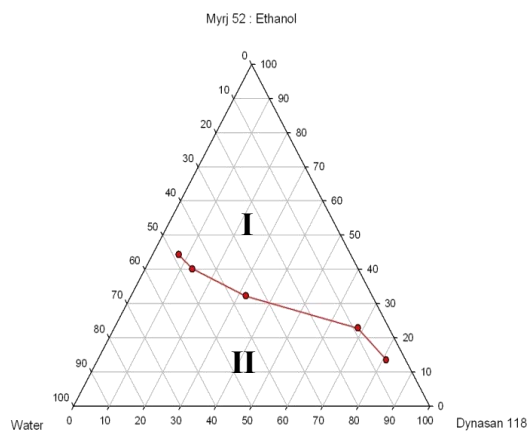
EA = ethyl alcohol

I: flowable microemulsion region
    (liquid clear zone)

II: viscous or non-microemulsion
    region

Figure 21   The pseudoternary phase diagrams of Dynasan®118, various surfactants,
ethyl alcohol, and water at 70°C.

Surfactant = Tween®80:IPA (1:1), at 70°C
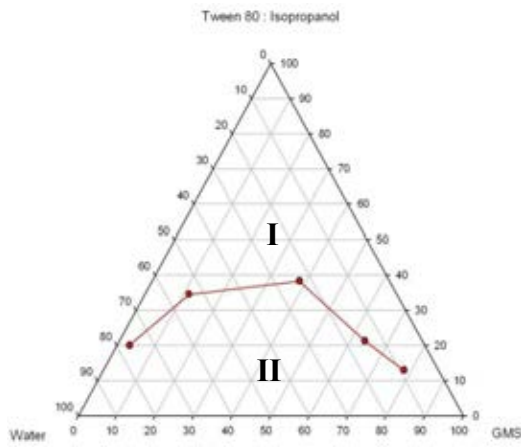
Surfactant = Poloxamer®188:IPA (1:1), at 70°C
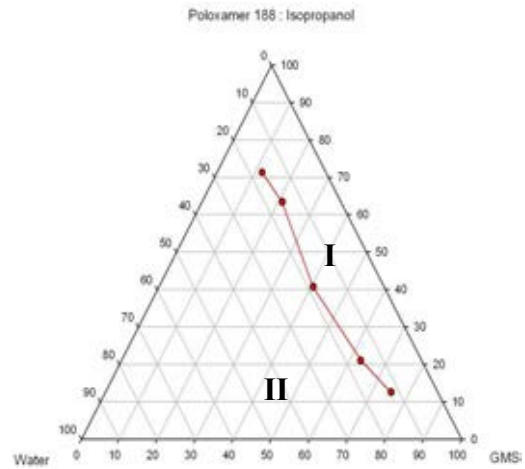
Surfactant = Brij®S721:IPA (1:1), at 70°C
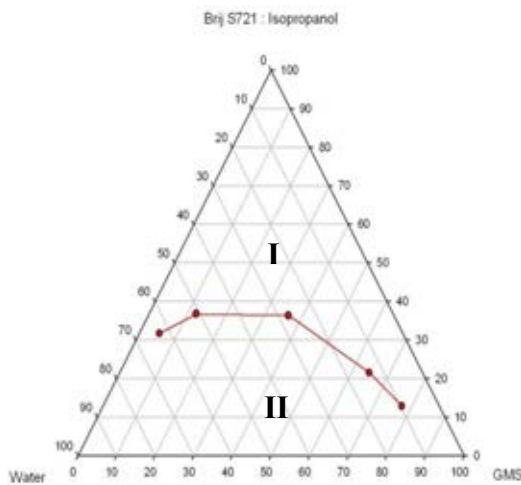
Surfactant = Cremophor®RH40:IPA (1:1), at 70°C
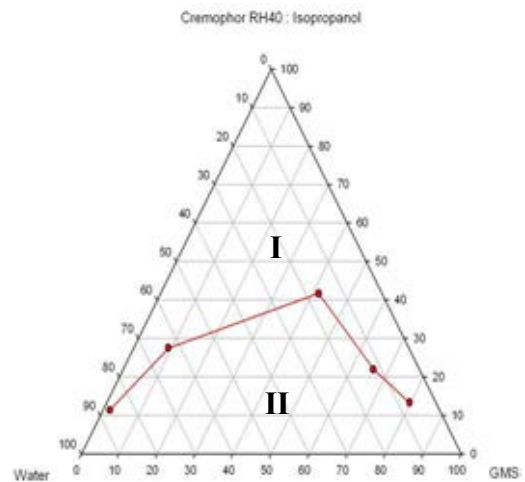
Surfactant = Myrj®52:IPA (1:1), at 70°C
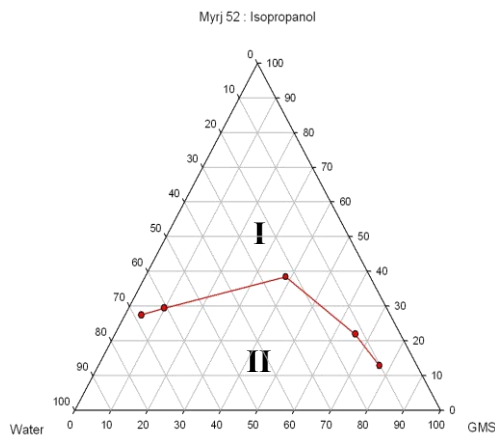
IPA = isopropyl alcohol

I: flowable microemulsion region
      (liquid clear zone)

II: viscous or non-microemulsion
      region

Figure 22   The pseudoternary phase diagrams of GMS, various surfactants, isopropyl alcohol, and water at 70°C.

Surfactant = Tween®80:BA (1:1), at 70°C
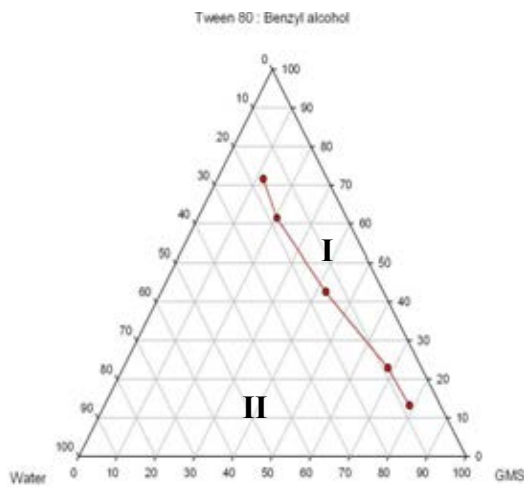
Surfactant = Poloxamer®188:BA (1:1), at 70°C
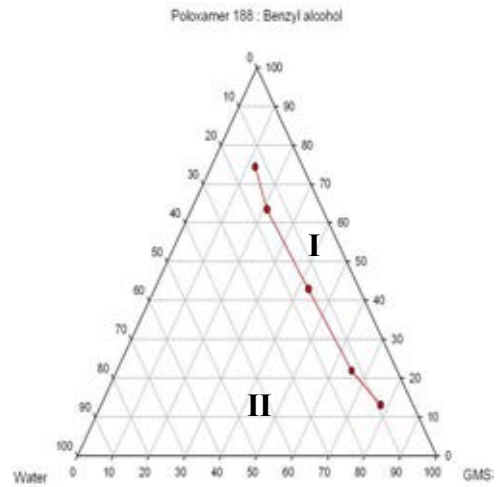
Surfactant = Brij®S721:BA (1:1), at 70°C
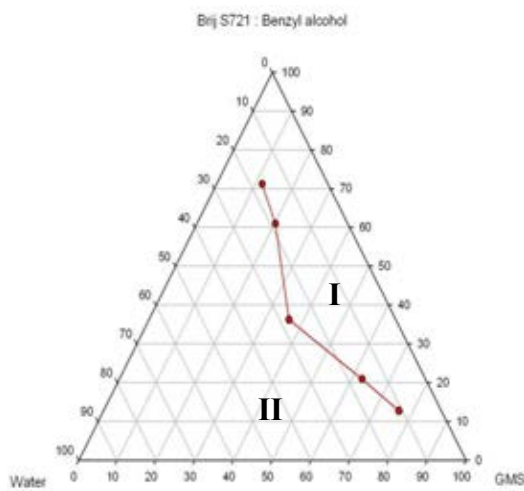
Surfactant = Cremophor®RH40:BA (1:1), at 70°C
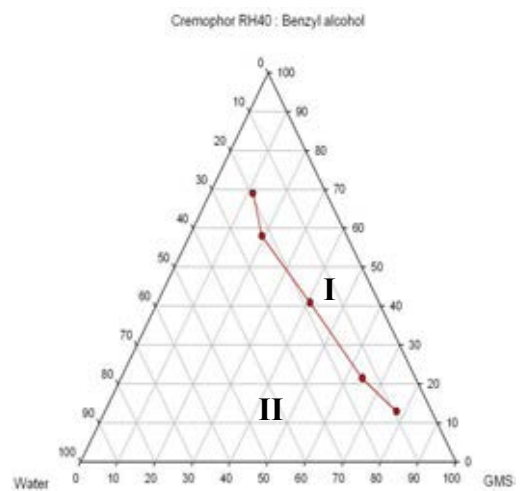
Surfactant = Myrj®52:BA (1:1), at 70°C
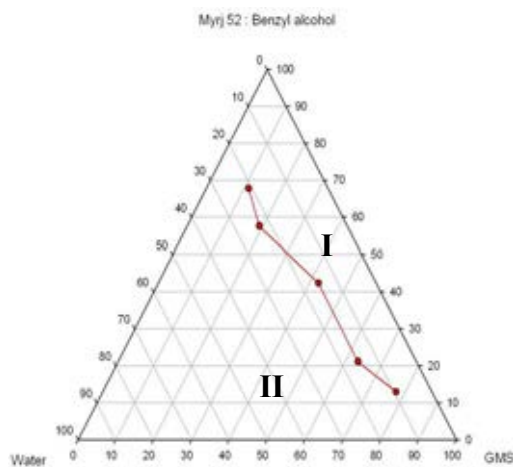
BA = benzyl alcohol

I: flowable microemulsion region
    (liquid clear zone)

II: viscous or non-microemulsion
    region

Figure 23   The pseudoternary phase diagrams of GMS, various surfactants, benzyl
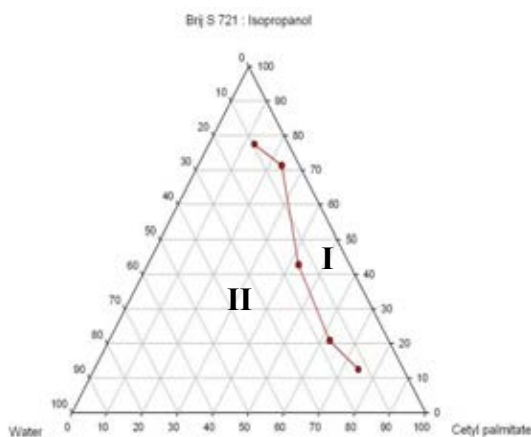alcohol, and water at 70°C.

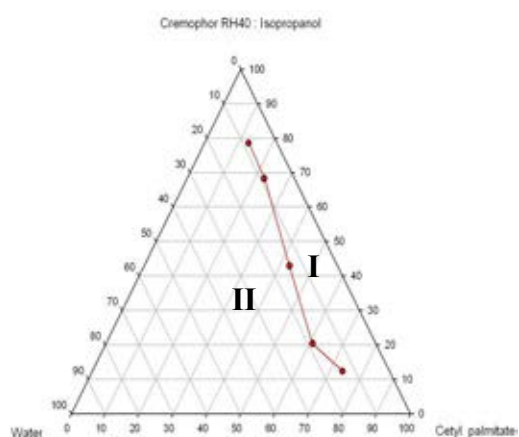Surfactant = Tween®80:EA (1:1), at 70°C   Surfactant = Poloxamer®188:EA (1:1), at 70°C
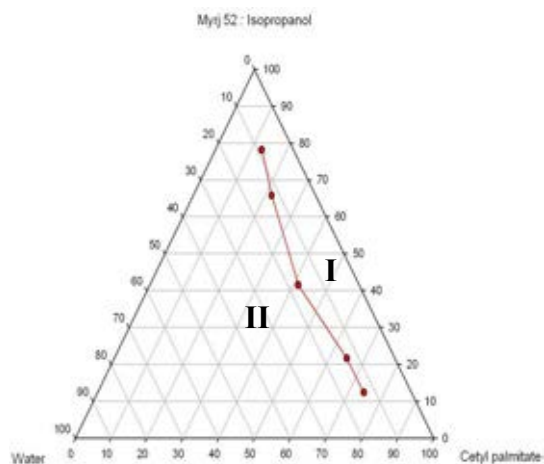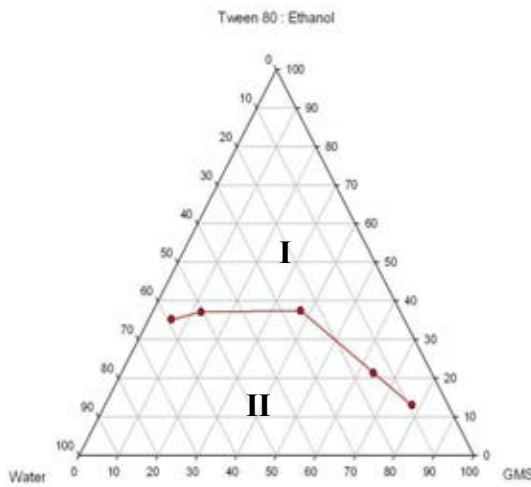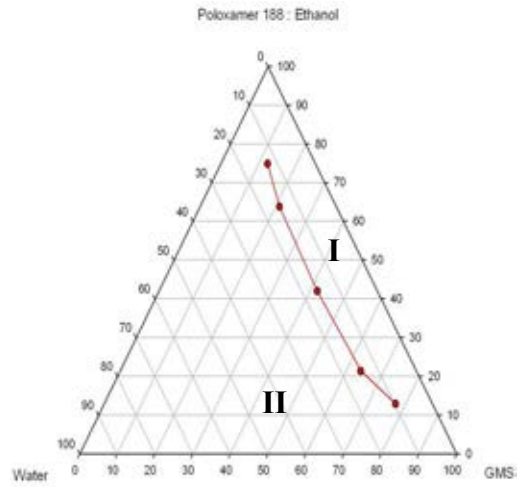

Surfactant = Brij®S721:EA (1:1), at 70°C   Surfactant = Cremophor®RH40:EA (1:1), at 70°C
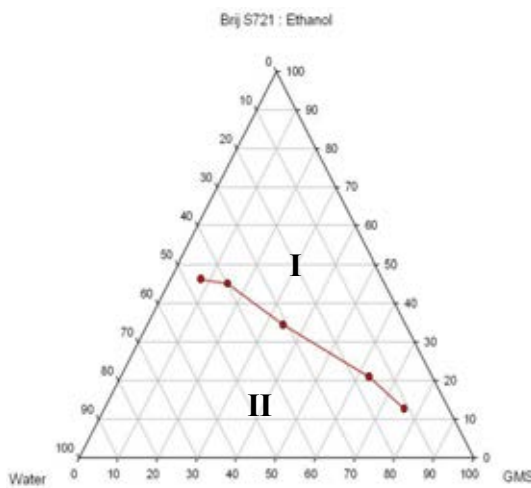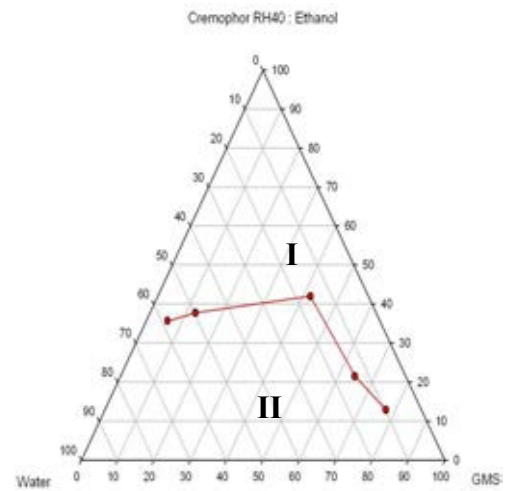
Surfactant = Myrj®52:EA (1:1), at 70°C
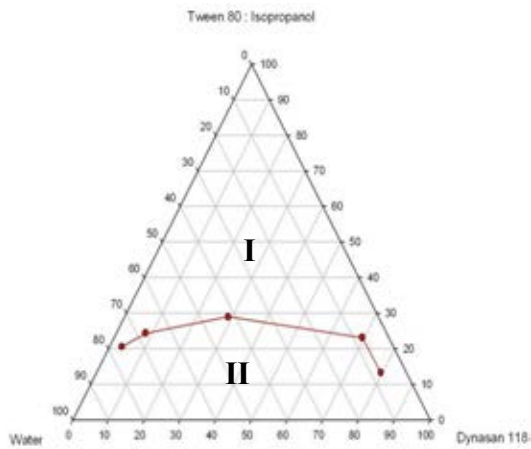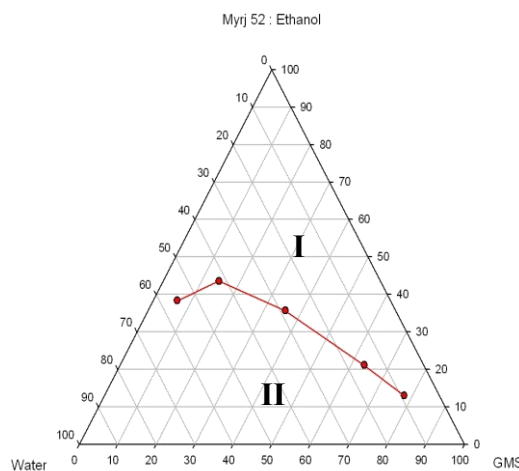

EA = ethyl alcohol

I: flowable microemulsion region
    (liquid clear zone)

II: viscous or non-microemulsion
    region

Figure 24 The pseudo-ternary phase diagrams of GMS, various surfactants, ethyl alcohol, and water at 70°C.

Surfactant = Tween®80:IPA (1:1), at 70°C
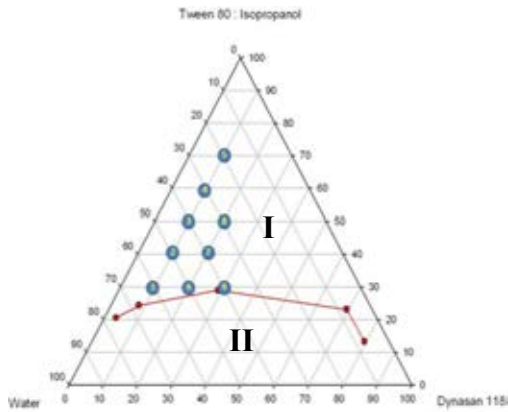
Surfactant = Cremophor®RH40:IPA (1:1), at 70°C
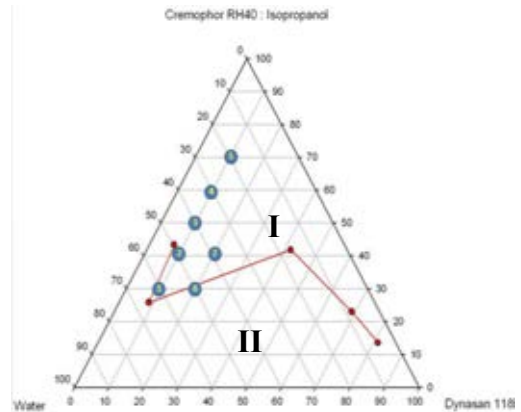
Surfactant = Brij®S721:IPA (1:1), at 70°C
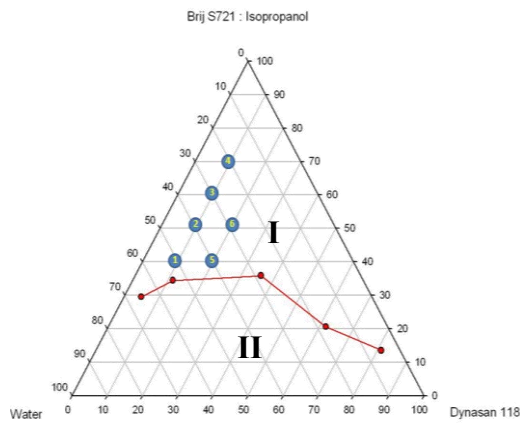
Surfactant = Myrj®52:IPA (1:1), at 70°C
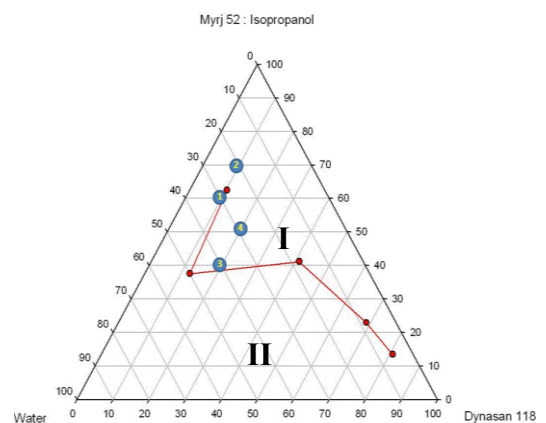
Surfactant= Tween®80:EA (1:1), at 70°C
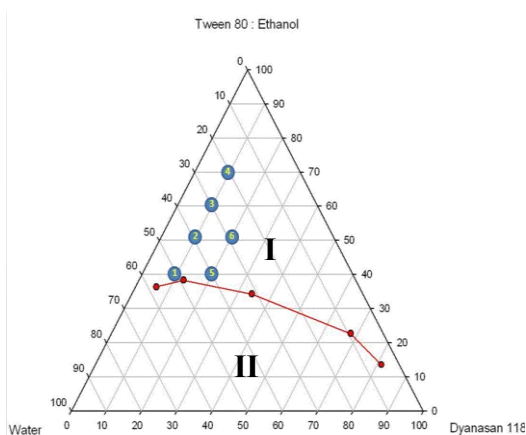
Surfactant = Cremophor®RH40:EA (1:1), at 70°C
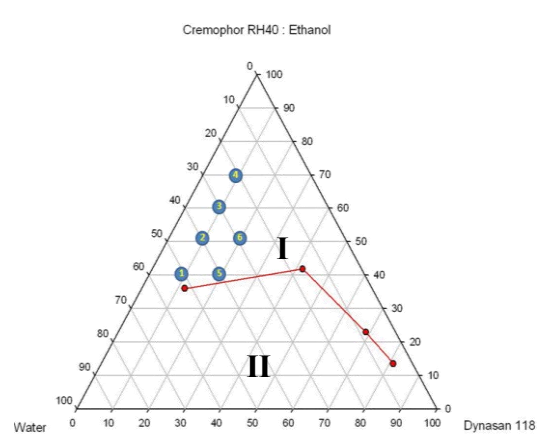
Figure 25 Confirmation of o/w microemulsion in the isotropic zone of pseudoternary phase diagrams containing Dynasan®118 at 70°C (I = flowable microemulsion region (liquid clear zone), II = viscous or non-microemulsion region).
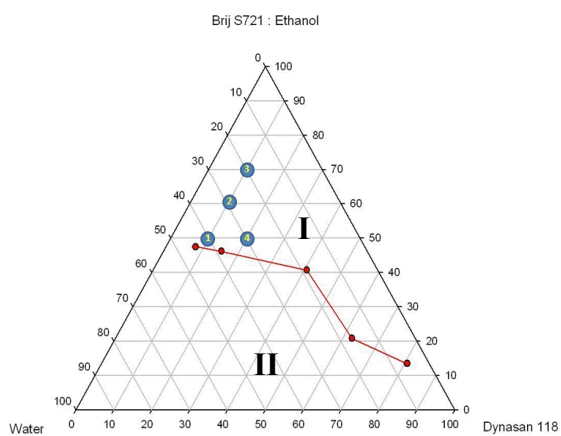
Surfactant = Brij®S721:EA (1:1), at 70°C   Surfactant = Myrj®52:EA (1:1), at 70°C
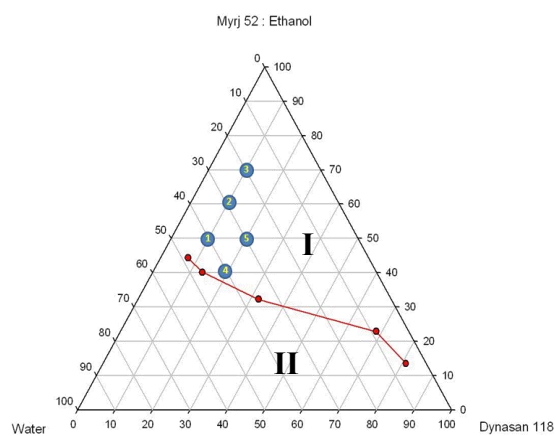
Figure 25 (Cont.) Confirmation of o/w microemulsion in the isotropic zone of pseudoternary phase diagrams containing Dynasan®118 at 70°C (I = flowable microemulsion region (liquid clear zone), II = viscous or non-microemulsion region).
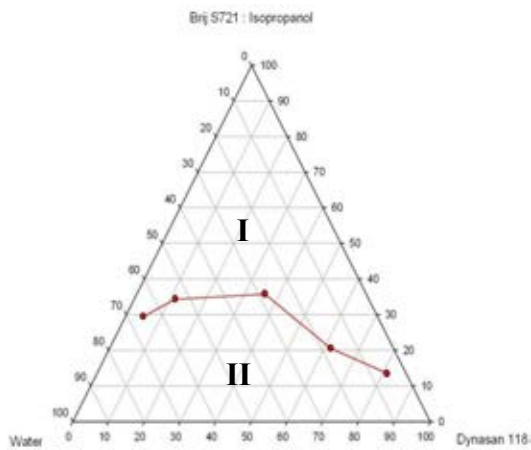
Surfactant = Tween®80:IPA (1:1), at 70°C
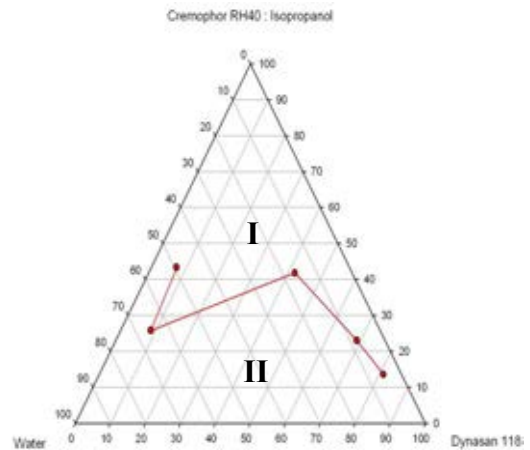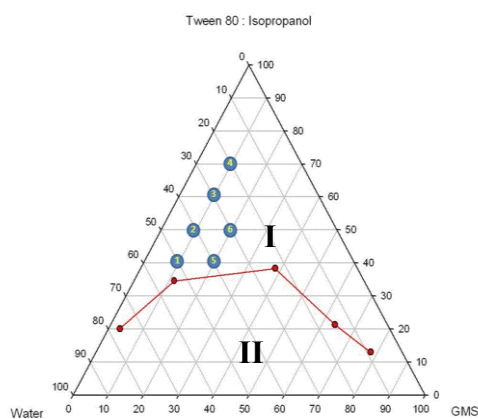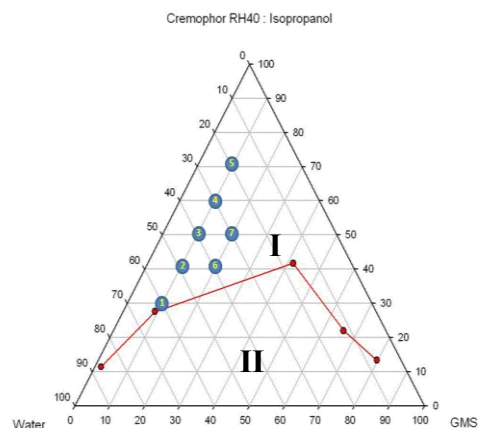
Surfactant = Cremophor®RH40:IPA (1:1), at 70°C

Surfactant = Brij®S721:IPA (1:1), at 70°C
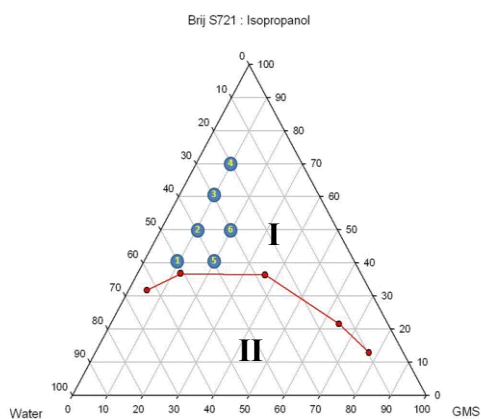
Surfactant = Myrj®52:IPA (1:1), at 70°C
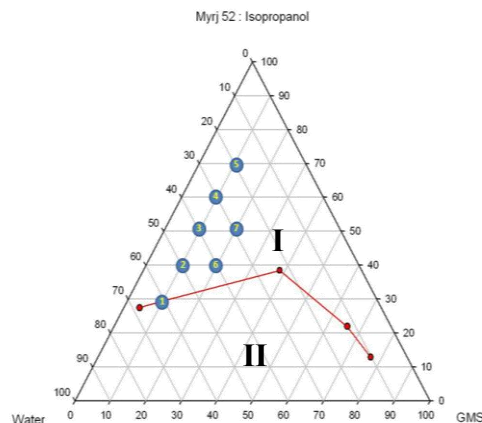
Surfactant = Tween®80:EA (1:1), at 70°C
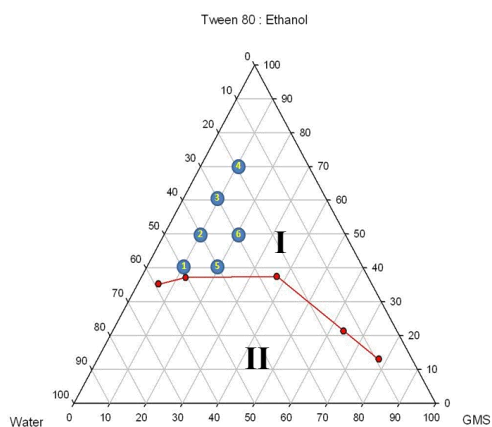
Surfactant = Cremophor®RH40:EA (1:1), at 70°C
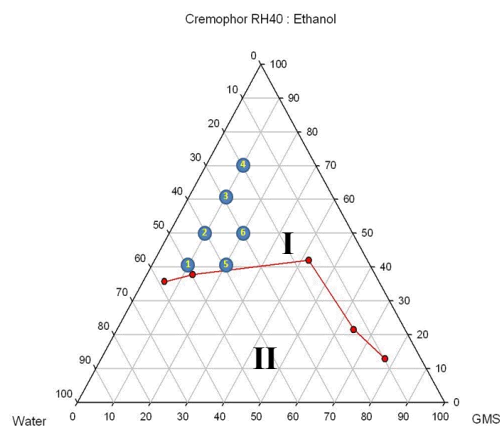
Figure 26 Confirmation of o/w microemulsion in the isotropic zone of pseudoternary phase diagrams containing GMS at 70°C (I = flowable microemulsion region (liquid clear zone), II = viscous or non-microemulsion region).
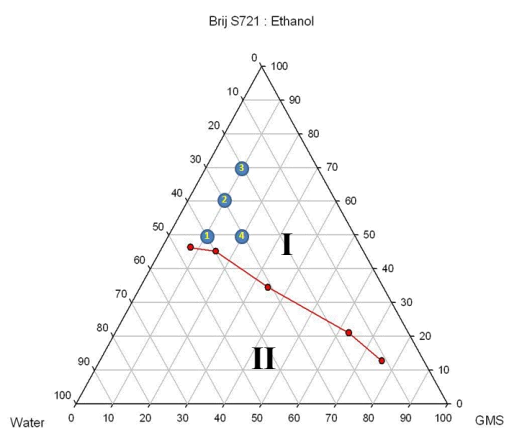
Surfactant = Brij®S721:EA (1:1), at 70°C   Surfactant = Myrj®52:EA (1:1), at 70°C
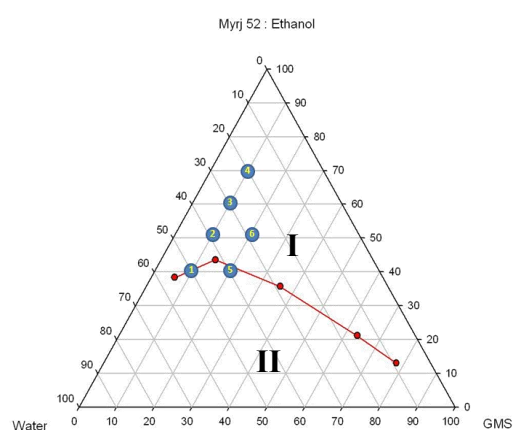
Figure 26 (Cont.) Confirmation of o/w microemulsion in the isotropic zone of pseudoternary phase diagrams containing GMS at 70°C (I = flowable microemulsion region (liquid clear zone), II = viscous or non-microemulsion region).

2.2.3 Preparation of blank-SLNs and selection of the appropriate formulations

The hot o/w microemulsions were prepared again according to the formula in Table 2 and transformed into SLNs by dispersing them into cold water (4°C) at a ratio of 1:20 (w/v) under mild mechanical stirring to obtain blank-SLNs. Then, they were kept for 4 weeks at ambient room temperature to select formulations that showed good physical stability. To understand easily, the identification codes were created as follows:

-The first letter of the formula coding represents types of solid lipids (D = Dynasan[®]118, G = GMS).

-The adjacent number represents percentages of solid lipid in o/w microemulsion region.

-The second letter represents types of surfactants (T = Tween[®]80, C = Cremophor[®]RH40, B = Brij[®]S721, M = Myrj[®]52).

-The third letter represents types of co-surfactants (I = Isopropanol, E = Ethanol).

-The last number represents percentages of surfactant and co-surfactant in o/w microemulsion region.

For example, D10TI30 means that the formulation was prepared by using 10%w/w of Dynasan[®]118 as solid lipid, 30%w/w of mixed surfactants (Tween[®]80 15%w/w and Isopropanol 15%w/w) and water 60%w/w to make the hot o/w microemulsion. To study physical stability of various blank-SLNs formulations, the following definitions were used:

Stable (S)	:	Good stability, no sedimentation, and no gelation
Phase separation (PS)	:	Sedimentation with clear supernatant. Sediment was easily redispersible
Gel formation (GF)	:	Extensive gelation with SLNs unable to flow

Table 2 shows the physical stability of blank-SLNs formulations including size, size distribution of freshly prepared blank-SLNs and appearance modification for 4 weeks. Bar graph in Figure 27 exhibits the particle size of freshly prepared blank-SLNs dispersions containing Dynasan[®]118 or GMS as solid lipid with various types and amounts of mixed surfactants.

Table 2   Size, polydispersity index (PDI), zeta potential, and physical stability during storage at ambient room temperature of various blank-SLNs formulations.

No.	Code	Freshly prepared SLNs (Week 0)			Appearance (Week)		
		Size (nm)	PDI	Zeta potential (mV)	0	2	4
1	D10TI30	132.8±1.4	0.305±0.039	-47.4±8.58	S	S	S
2	D10TI40	141.6±1.3	0.329±0.038	-37.7±8.35	S	PS	-
3	D10TI50	145.1±3.0	0.285±0.028	-35.0±2.80	S	PS	-
4	D10TI60	250.3±4.5	0.499±0.036	-32.7±5.38	S	PS	-
5	D10TI70	272.2±9.2	0.499±0.038	-31.5±8.87	S	PS	-
6	D20TI30	257.1±8.3	0.382±0.051	-38.9±4.47	S	S	PS
7	D20TI40	271.3±11.0	0.386±0.085	-29.3±7.88	S	S	PS
8	D20TI50	296.2±9.3	0.246±0.041	-28.4±2.91	S	PS	-
9	D30TI30	276.6±8.6	0.297±0.038	-27.2±1.32	PS	-	-
1	D10CI30	73.1±8.2	0.600±0.230	-44.7±7.33	S	S	S
2	D10CI40	90.2±0.2	0.498±0.062	-35.0±1.30	S	S	S
3	D10CI50	192.4±6.2	0.308±0.030	-32.2±1.03	S	S	S
4	D10CI60	459.6±93.5	0.563±0.011	-29.3±0.53	S	S	PS
5	D10CI70	538.0±10.4	0.541±0.010	-23.6±2.59	S	S	PS
6	D20CI40	200.5±6.6	0.283±0.055	-25.8±3.86	S	S	PS
7	D20CI50	251.9±2.9	0.307±0.022	-22.6±1.34	S	S	PS
1	D10BI40	467.6±38.0	0.612±0.118	-25.8±1.28	S	PS	-
2	D10BI50	607.6±58.0	0.771±0.145	-23.2±5.58	S	PS	-
3	D10BI60	1268.0±342.3	0.822±0.090	-22.6±9.62	PS	-	-
4	D10BI70	1480.0±941.8	0.835±0.143	-21.9±0.79	PS	-	-
5	D20BI40	1221.0±224.3	0.785±0.162	-20.5±2.16	PS	-	-
6	D20BI50	1771.0±257.2	0.922±0.083	-19.3±0.20	PS	-	-
1	D10MI60	824.7±268.8	0.756±0.193	-23.7±3.16	S	S	S
2	D10MI70	890.5±316.9	0.789±0.159	-23.6±3.37	S	S	S
3	D20MI40	271.4±8.0	0.381±0.061	-29.3±4.65	S	S	S
4	D20MI50	304.2±7.6	0.478±0.093	-24.7±1.08	S	S	S
1	D10TE40	94.3±2.5	0.307±0.041	-30.8±3.09	S	S	S
2	D10TE50	124.3±3.4	0.365±0.055	-30.5±1.73	S	PS	-
3	D10TE60	148.3±0.6	0.640±0.117	-23.9±2.64	S	PS	-
4	D10TE70	154.1±14.7	0.576±0.190	-20.3±5.51	S	PS	-
5	D20TE40	218.3±4.5	0.261±0.048	-22.4±3.29	S	S	PS
6	D20TE50	231.0±6.6	0.212±0.027	-21.8±3.52	S	PS	-
1	D10CE40	142.1±46.7	0.517±0.220	-22.4±2.95	S	S	S
2	D10CE50	194.2±36.3	0.604±0.010	-22.1±6.07	S	S	S
3	D10CE60	208.9±115.7	0.749±0.175	-17.8±8.36	S	S	PS
4	D10CE70	323.4±39.7	1.000±0.000	-15.1±3.32	S	S	PS
5	D20CE40	204.6±1.7	0.282±0.062	-21.8±2.91	S	S	PS
6	D20CE50	235.6±2.8	0.305±0.008	-19.8±4.24	S	S	PS
1	D10BE50	618.9±49.2	0.700±0.070	-23.9±8.44	S	PS	-
2	D10BE60	1230.0±39.2	0.948±0.057	-20.3±4.65	PS	-	-
3	D10BE70	1383.0±404.4	0.894±0.137	-19.8±3.32	PS	-	-
4	D20BE50	780.7±0.42	0.647±0.204	-22.4±6.80	PS	-	-
1	D10ME50	202.7±32.4	0.377±0.149	-30.8±2.64	S	PS	-
2	D10ME60	325.4±45.6	0.463±0.124	-30.5±5.51	S	S	S
3	D10ME70	538.1±19.5	0.698±0.121	-22.1±3.29	S	S	S
4	D20ME40	181.3±13.8	0.483±0.167	-17.8±3.52	S	S	PS
5	D20ME50	246.8±7.9	0.479±0.050	-15.1±2.95	S	S	PS

Note: S = stable, PS = phase separation, - = could not be determined

Table 2 (Cont.) Size, polydispersity index (PDI), zeta potential, and physical stability during storage at ambient room temperature of various blank-SLNs formulations.

No.	Code	Freshly prepared SLNs (Week 0)			Appearance (Week)		
		Size (nm)	PDI	Zeta potential (mV)	0	2	4
1	G10TI40	155.2±3.7	0.426±0.059	-30.8±3.65	S	S	PS
2	G10TI50	173.7±6.8	0.521±0.140	-30.5±4.79	S	PS	-
3	G10TI60	269.0±7.0	0.494±0.098	-23.9±0.74	S	PS	-
4	G10TI70	286.1±6.2	0.735±0.267	-22.4±0.42	S	PS	-
5	G20TI40	273.1±6.4	0.487±0.058	-22.1±5.95	PS	-	-
6	G20TI50	764.9±88.8	0.613±0.297	-19.2±6.93	PS	-	-
1	G10CI30	137.0±3.9	0.486±0.018	-30.8±2.71	S	S	S
2	G10CI40	152.5±4.2	0.495±0.099	-28.4±4.81	S	S	PS
3	G10CI50	283.0±10.9	0.527±0.021	-25.4±5.38	S	PS	-
4	G10CI60	489.5±221.0	0.646±0.242	-21.2±8.87	S	PS	-
5	G10CI70	591.8±162.4	0.770±0.101	-19.1±4.47	S	PS	-
6	G20CI40	357.9±181.4	0.685±0.286	-15.1±7.88	PS	-	-
7	G20CI50	786.0±234.0	0.684±0.277	-14.9±2.91	PS	-	-
1	G10BI40	678.1±28.7	0.605±0.033	-23.9±7.33	S	PS	-
2	G10BI50	813.0±182.1	0.703±0.016	-22.4±2.30	S	PS	-
3	G10BI60	1312.7±603.6	0.575±0.198	-21.8±1.03	PS	-	-
4	G10BI70	1672.1±241.5	0.860±0.070	-20.3±0.53	PS	-	-
5	G20BI40	1410.1±79.0	0.727±0.054	-19.2±2.59	PS	-	-
6	G20BI50	1932.5±121.7	0.894±0.121	-17.8±3.86	PS	-	-
1	G10MI30	299.3±212.9	0.589±0.100	-21.8±2.54	S	S	PS
2	G10MI40	323.4±53.8	0.595±0.052	-19.8±4.25	S	S	PS
3	G10MI50	342.4±18.0	0.588±0.063	-17.8±3.45	S	S	PS
4	G10MI60	972.3±321.6	0.597±0.185	-15.1±6.26	S	S	S
5	G10MI70	1087.4±46.2	0.379±0.069	-14.9±3.05	S	S	S
6	G20MI40	468.1±237.3	0.475±0.151	-17.8±4.12	S	S	PS
7	G20MI50	811.0±9.9	0.793±0.021	-13.0±7.39	S	S	PS
1	G10TE40	105.7±0.9	0.400±0.026	-28.5±2.38	S	S	PS
2	G10TE50	195.9±7.3	0.104±0.016	-27.0±8.03	S	PS	-
3	G10TE60	211.6±32.4	0.666±0.104	-23.4±9.44	S	PS	-
4	G10TE70	325.9±159.1	0.513±0.020	-21.2±0.50	S	PS	-
5	G20TE40	382.8±110.2	0.488±0.440	-20.1±0.61	PS	-	-
6	G20TE50	569.5±108.0	0.640±0.085	-19.5±9.44	PS	-	-
1	G10CE40	150.4±4.6	0.828±0.025	-20.2±8.27	S	S	S
2	G10CE50	207.7±7.3	0.536±0.041	-19.4±4.40	S	S	S
3	G10CE60	220.3±43.1	0.422±0.213	-17.5±3.72	S	PS	-
4	G10CE70	361.1±17.5	0.688±0.023	-15.3±2.78	S	PS	-
5	G20CE40	407.5±105.6	0.470±0.034	-20.1±2.86	PS	-	-
6	G20CE50	537.0±145.8	0.617±0.086	-18.4±4.72	PS	-	-
1	G10BE50	673.1±324.5	0.726±0.146	-20.6±3.15	S	PS	-
2	G10BE60	1634.0±335.9	0.828±0.171	-19.5±7.74	PS	-	-
3	G10BE70	1968.0±531.0	0.916±0.199	-18.4±3.23	PS	-	-
4	G20BE50	810.2±205.9	0.660±0.203	-15.4±1.07	PS	-	-
1	G10ME40	153.3±15.2	0.333±0.029	-35.0±6.43	S	S	PS
2	G10ME50	236.9±26.9	0.539±0.009	-31.5±4.97	S	S	PS
3	G10ME60	387.2±9.9	0.332±0.034	-31.1±7.05	S	S	PS
4	G10ME70	642.7±29.9	0.484±0.128	-24.5±8.89	S	S	PS
5	G20ME40	498.0±6.0	0.421±0.038	-28.4±7.39	S	S	S
6	G20ME50	581.9±130.1	0.632±0.189	-23.7±2.38	S	S	S

Note: S = stable, PS = phase separation, - = could not be determined

Figure 27 Comparison of particle size of freshly prepared blank-SLNs formulations.
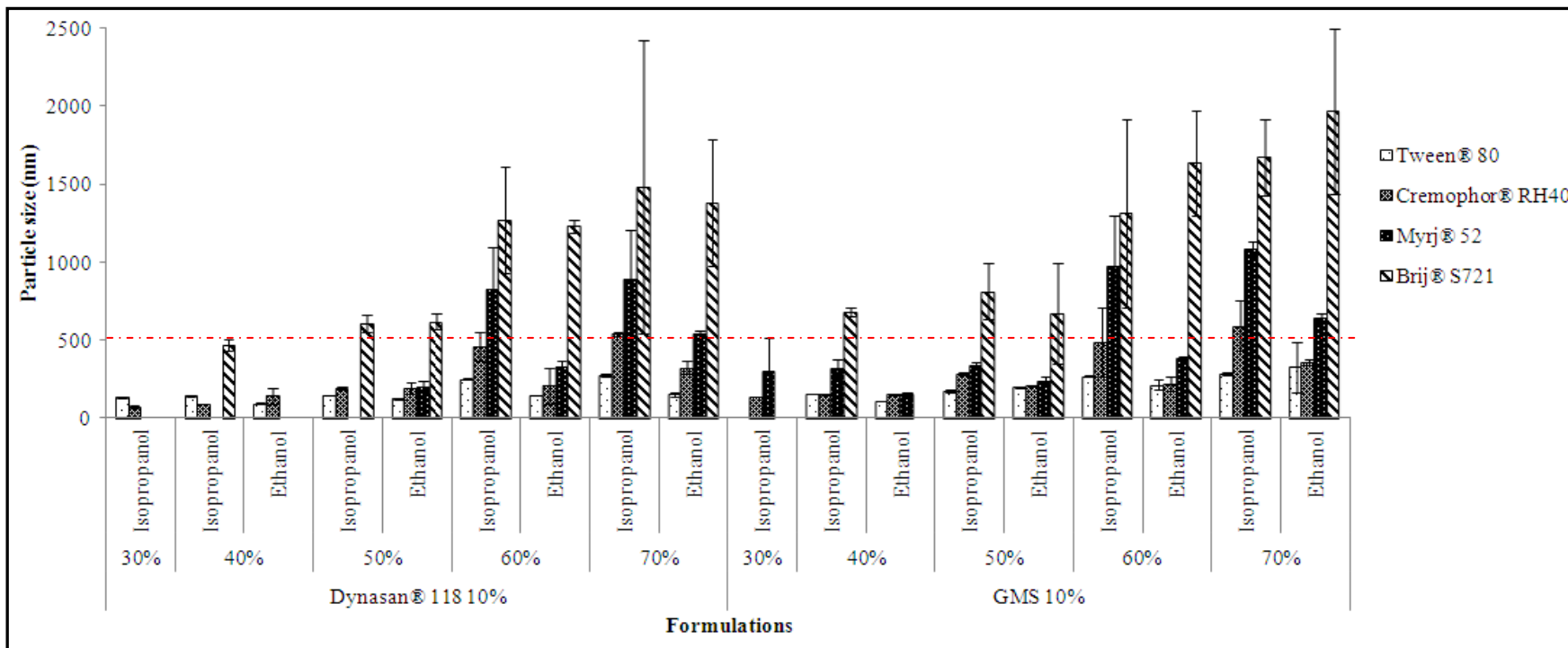
Figure 27 (Cont.) Comparison of particle size of freshly prepared blank-SLNs formulations.
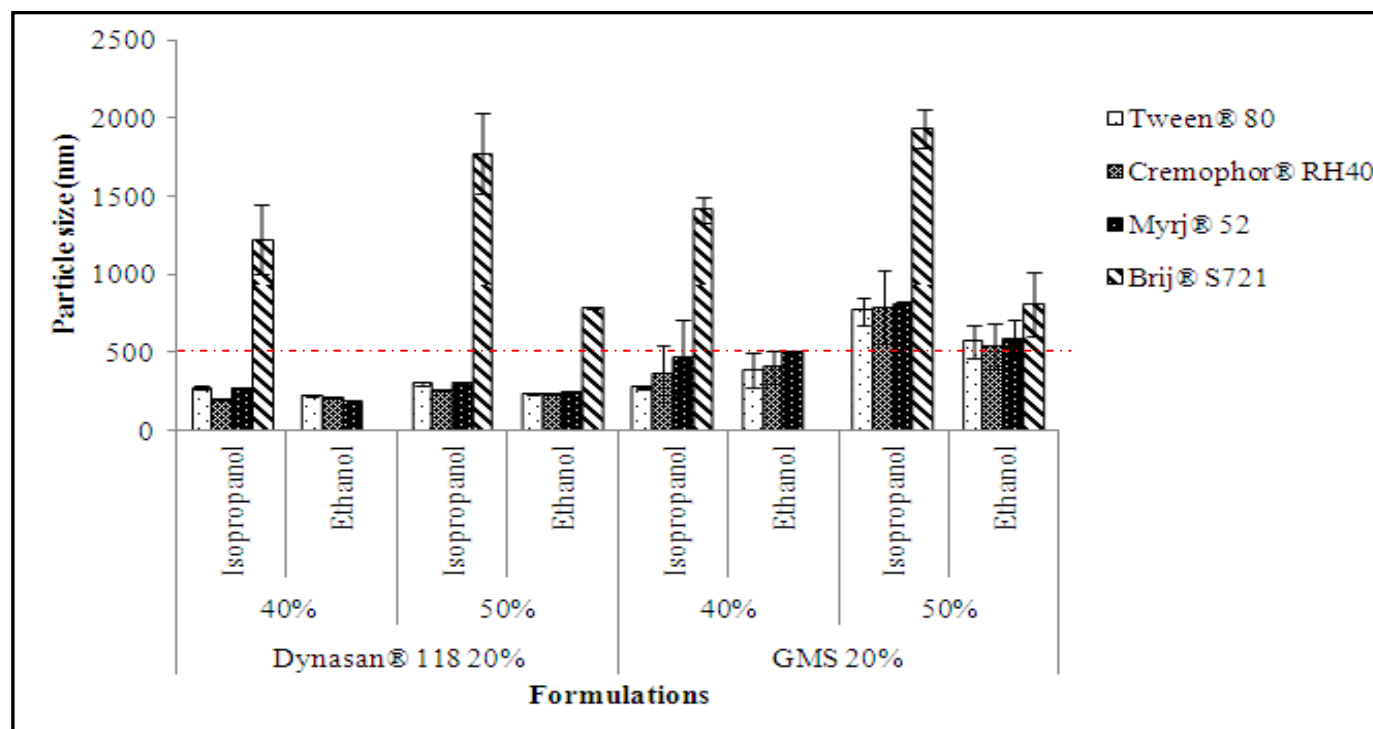
Size determination was generally used as a characterization tool. When the composition was modified in an attempt to optimize the formulations, particle size was chosen as a quality response parameter (Heurtault et al., 2003). The effects of types and amounts of solid lipids, surfactants, and co-surfactants on the particle size of freshly prepared blank-SLNs were investigated. The studied solid lipids were Dynasan118[®] and GMS. The studied surfactants were Tween[®]80, Cremophor[®]RH40, Myrj[®]52, and Brij[®]S721 whereas the co-surfactants were isopropanol and ethanol. Concentrations of solid lipids and mixed-surfactants were varied within the pseudoternary phase diagram of o/w microemulsion region.

2.2.3.1 Effect of solid lipid types

The appearance of Dynasan-SLNs was translucent than that from GMS-SLNs indicating the smaller average particle size of the Dynasan-SLNs. This might be due to the higher melting point of GMS which could promote rapid lipid recrystallization (Ekambaram and Abdul, 2011). Thus, the formulation consisting of GMS (m.p. 63.1°C) might exhibit more tendency to form globular structure than that consisting of Dynasan[®]118 (m.p. 60.8°C).

2.2.3.2 Effect of surfactant and co-surfactant types

Among four non-ionic surfactants tested, blank-SLNs prepared using Tween[®]80 demonstrated the lowest size, whereas SLNs prepared using Brij[®]S721 showed the largest size. In general, trend of particle size was: Tween[®]80 < Cremophor[®]RH40 < Myrj[®]52 < Brij[®]S721. The solid surfactants (Myrj[®]52 and Brij[®]S721) could generate larger SLNs than the liquid surfactants (Tween[®]80 and Cremophor[®]RH40). For this reason, the liquid state of surfactant might be able to form a more flexible film at the o/w interface than those of solid surfactants. Friberg and Kayali (1991) reported that the low HLB of surfactant preferred to be adsorbed toward the oil/water rather than oil/air interface. Thus, the formulation consisting of Tween[®]80 and Cremophor[®]RH40 might exhibit more tendency to form a smaller particle size than other surfactants. Following this assumption, the trend of particle size should be: Tween[®]80 (HLB 15) ~ Cremophor[®]RH40 (HLB 14-16) < Brij[®]S721 (HLB 15.5) < Myrj[®]52 (HLB 16.9). Ekambaram and Abdul (2011) prepared ramipril-SLNs by hot homogenization followed by the ultrasonication method. They revealed that the low HLB value affected the decrease of particles size in the order of Span[®]20

(HLB 8.6) < Tween®80 (HLB 15) < Poloxamer®188 (HLB 29). On the contrary, the result from this study showed the different trends, this might be associated with the structure of surfactant and lipid-surfactant interaction. However, the reasons for such observations were still unclear. For the result of different types of co-surfactants (isopropanol and ethanol) on the particle sizes could not be concluded from this experiment because of variation in size between the same formulation.

2.2.3.3 Effect of amounts of solid lipids, surfactants, and co-surfactants

The results showed that the larger mean particle size and broader size distribution caused by the increasing lipid concentration from 10% to 20% (within isotropic zone) in all formulations. In addition, the collision and aggregation of nanoparticles, which were facilitated by a high lipid concentration, led to the formation of larger particles (Zhang et al., 2009).

Normally, surfactant played an important role to reduce the size of droplets as described in terms of nature and structure of surfactant. The concentration of surfactant in the formulation could influence the particle size. The particle size and PDI were decreased with the increase of surfactant concentration. High concentrations of surfactant could reduce the surface tension and facilitate the particle partition during the size reduction process resulting in smaller particle size (Shah et al., 2007). Other researchers also observed the particle size reduction at higher surfactant concentration (Hu et al. 2004; Liu et al., 2007). Conversely, when the quantity of mixed surfactants increased, the mean particle size also increased in this study. The aggregation phenomenon of nanoparticles might be associated with an intrinsic thermodynamic instability of the surfactant molecules in lipid matrix. This resulted in the adsorption of surfactant around SLNs structure. At very low concentration, the surfactant molecule is directly adsorbed onto the particle surface. Nevertheless, at the higher surfactant concentration, compression of the surfactant molecules at the particles surface with construction of loops and tails comes to be dominant and ultimately caused the bridging between primary structure of nanoparticles (Frietas and Muller, 1999; Goppert and Muller, 2005). Moreover, the interfacial fluidity and low interfacial tension can be achieved by using a proper amount of co-surfactant. However, the droplet size increased with an increase of co-

surfactant concentration. This may be due to the interfacial film extension by co-surfactant effect. (Gao et al., 1998; Zhao et al., 2010; Negi et al., 2012).

The zeta potential is a measure of the electrostatic or charge repulsion or attraction between particles, and is one of the fundamental parameters known to affect stability. Its measurement brings detailed insight into the causes of dispersion, aggregation or flocculation, and can be applied to improve the formulation of dispersions, emulsions, and suspensions. The different blank-SLNs formulations were respectively measured for zeta potential by PCS. The zeta potentials of blank-SLNs were negative. This negative charge was likely caused by the ionization of fatty acids from GMS and Dynasan$^{®}$118 used (Huang et al., 2008). When the amount of mixed surfactants increased, the zeta potential also showed the less negative value. It was possible that the adsorption of non-ionic surfactant onto the particles might occur and reduce the negative charge. The less negative zeta potential related to the aggregation or flocculation of dispersion system (James et al., 1992). These results were in agreement with the larger particle size when increasing the mixed surfactants concentration.

In conclusion, the content of solid lipid, surfactant, and co-surfactant in SLNs formulations thus influenced the mean particle sizes and showed the same general trend for all solid lipids, surfactants, and co-surfactants used in this study. To select the formulations that showed appropriate appearance, particle size, and good physical stability, all formulations were visually observed immediately after preparation and during storage at ambient room temperature for 4 weeks. The stable fourteen formulations of blank-SLNs which had an average particle size less than 500 nm would be selected for subsequent loading of the hydrolyzed extract. The photo of selected blank-SLNs is shown in Figure 28.
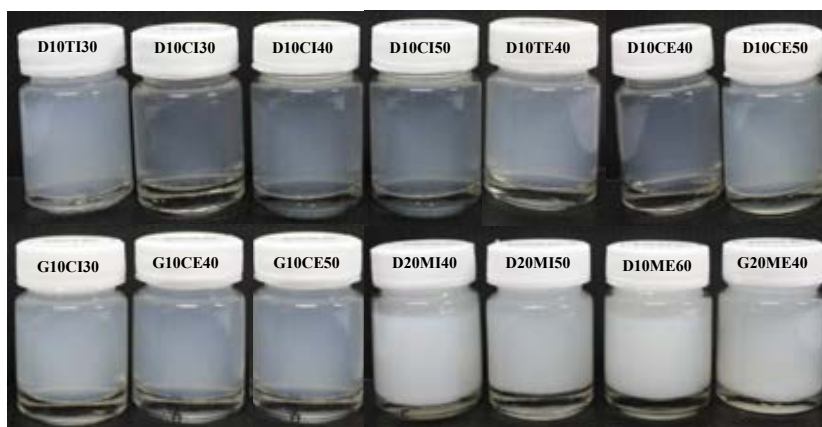
Figure 28 The appearances of freshly prepared blank-SLNs containing Dynasan®118 and GMS as solid lipid.

2.3 Loading of astaxanthin from shrimp shell extract to SLNs (ASX-SLNs)

Concentration of the hydrolyzed extract in the preparation was calculated based on solubility in solid lipid and IC_{50} value regarding free radical scavenging activity (DPPH assay). The most essential factor that determines the loading capacity of active compound in the solid lipid is the drug solubility in melted lipid (Shah et al., 2007). Thereby, so as to acheive adequate entrapment efficiency, the drug solubility in the molten lipid must be high (Lee et al., 2007). From the solubility potential in two lipids found that 5.7781±0.0028 mg and 5.3763±0.0066 mg of the hydrolyzed extract could be solubilized in one milligram of Dynasan®118 and GMS, respectively. In addition, the theoretical final lipid concentration in all blank-SLNs was 5-10 mg/mL (after water dilution). It meant that 28.89 mg and 26.88 mg of the hydrolyzed extract would be solubilized in 5 mg of Dynasan®118 and GMS, respectively.

Moreover, IC_{50} value of the hydrolyzed extract from Section 1.3 was 2.0107 mg/mL. In order to achieve antioxidant effect of the extract, its concentration reached the active site should be adequate (Manosroi et al., 2011). The pre-determined concentration for topical application would be approximately 10 times of IC_{50} to account for the loss of active compound during application (Panida Borisut, 2011). Hence, the hydrolyzed extract would be further incorporated in SLNs at concentration of 25 mg/mL. At this concentration and the result of solubility in each lipid were

enough to load the hydrolyzed extract in lipid matrix. Therefore, the SLNs formulation was intended to contain around 25 mg/mL of the hydrolyzed extract. In other words, the formulation would contain 5.41 mg/mL of free astaxanthin in preparations.

Tominage et al. (2012) tested the cosmetic benefits of astaxanthin from *Haematococcus pluvialis* on 30 human subjects. Two dosage forms of astaxanthin were applied to healthy volunteers containing 6 mg per day of oral supplementation and 2 mL (78.9 µM or 0.047 mg/mL) per day of topical application for two months. They also found significant improvement in skin wrinkles, age spot, elasticity, skin texture, and corneocyte condition. In comparison to the loading dose of real astaxanthin in SLNs (5.41 mg/mL), this dose might be effective to present the anti-aging activity. To study the effect of extract loading on particle size and entrapment efficiency, the blank-SLNs formulations from topic 2.2 were selected to entrap the active compound. These 14 formulas were D10TI30, D10CI30, D10CI40, D10CI50, D10TE40, D10CE40, D10CE50, G10CI30, G10CE40, G10CE50, D20MI40, D20MI50, D10ME60, and G20ME40. ASX-SLNs formulations were prepared to final concentration of the hydrolyzed extract about 25 mg/mL. All formulations were prepared in 3 batches and characterized in the next part.

3. Physicochemical characterization of ASX-SLNs

3.1 Physical appearances

The physical appearances such as color, gel formation, and phase separation were visually observed. The photos of freshly prepared blank-SLNs and ASX-SLNs formulations are shown in Figure 29. All SLNs formulations showed good physical appearances. They were well dispersed with milky and orange color. No gel formation and phase separation occurred.
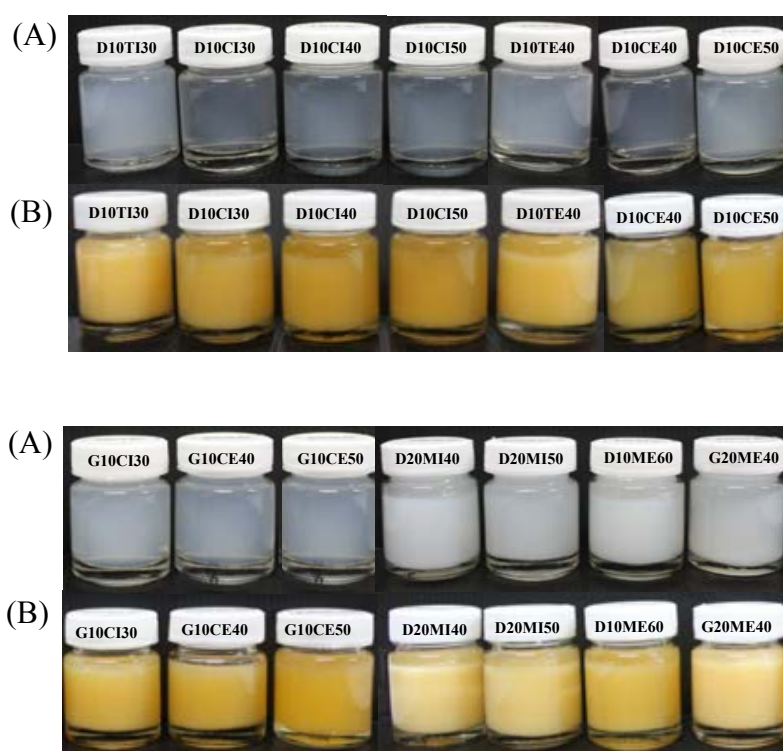
Figure 29 The appearances of freshly prepared SLNs formulations: (A) Blank-SLNs and (B) ASX-SLNs.

3.2 Morphology

The morphological feature of ASX-SLNs was investigated using scanning electron microscope (SEM). The observation of size, shape, and surface topography are shown in Figure 30. The particles of all formulations were difficult to conclude that the nanoparticles exhibited spherical shape and were homogenous in size distribution. In group of Myrj®52, the particles tended to aggregate and appeared an

irregular shape (bar = 50 µm) whereas the particles looked a spherical shape in group of Tween®80 and Cremophor®RH40 (bar ≤ .   m). However, the morphology should be investigated by the higher resolution microscopy such as field-electron scanning microscopy (FE-SEM).
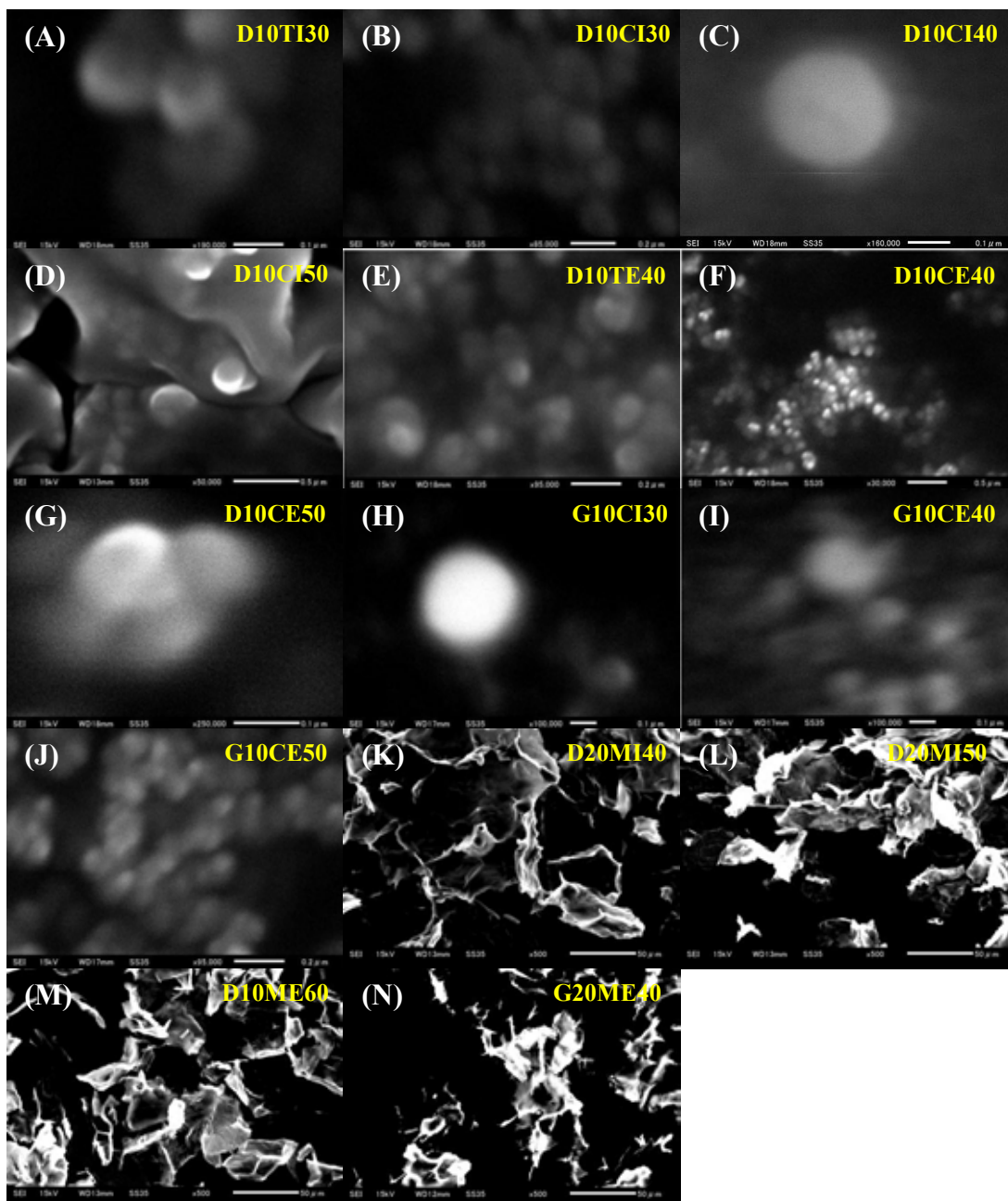
Figure 30 Scanning electron micrographs of freshly prepared ASX-SLNs formulations (A-J: bar ≤ 0.5µm, K-N: bar = 50 µm)

3.3 Particle size analysis

The different SLNs formulations were respectively measured by PCS. All data are shown as mean±SD (n=3). Figure 31 shows the particle size, polydispersity index, and zeta potential of freshly prepared SLNs formulations. The particles size of ASX-SLNs formulations were about 152-413 nm and were different from each other depending on formulations.
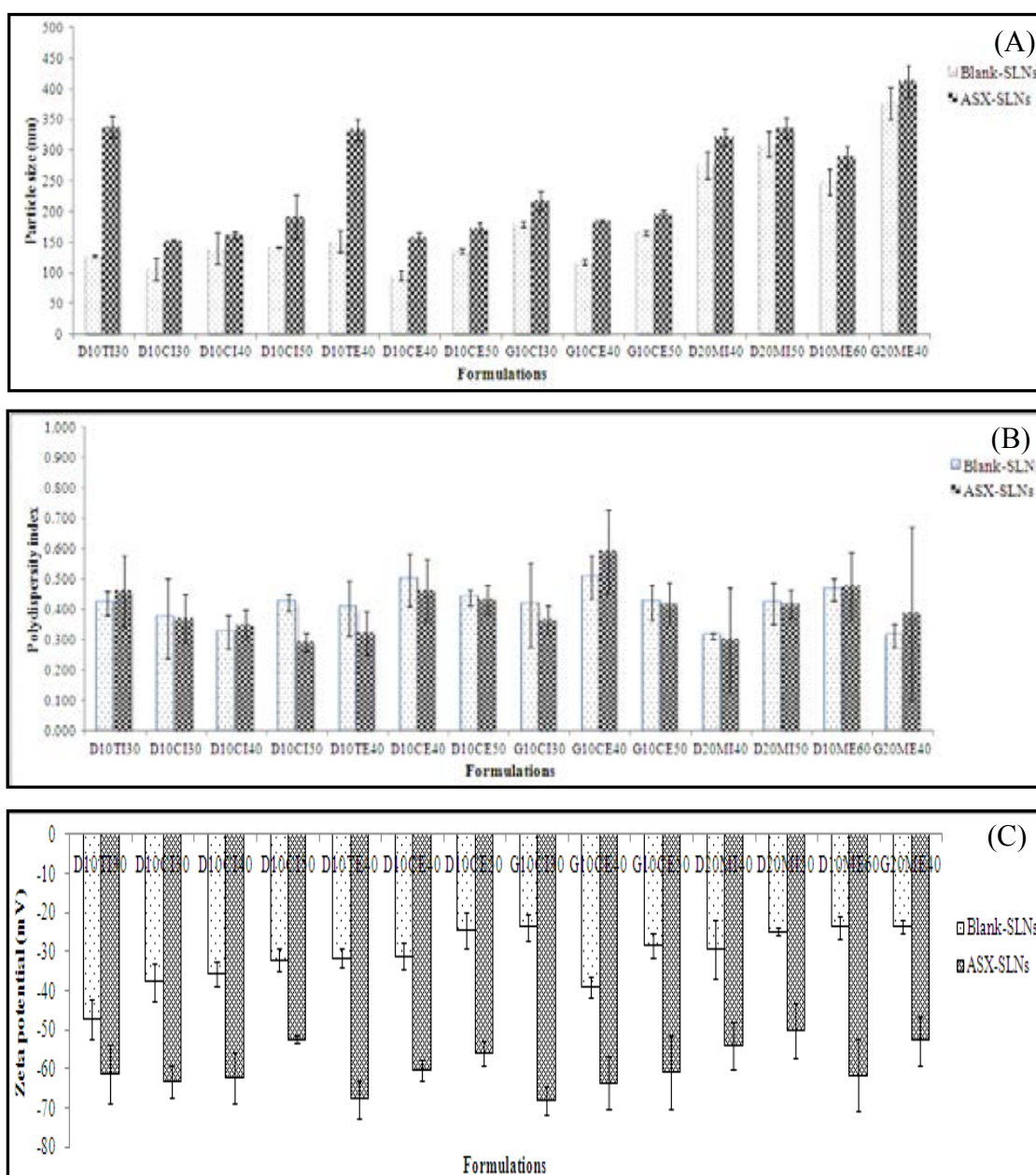
Figure 31 Histogram of particle size (A), polydispersity index (B), and zeta potential (C) of freshly prepared blank-SLNs and ASX-SLNs formulations.

An increase of particle size was observed for all ASX-SLNs as compared to blank-SLNs, suggesting the presence of astaxanthin from hydrolyzed extract in the matrix of nanoparticles. This result agreed with the previous study of Das et al. (2012) who developed clotrimazole-loaded SLNs. The mean diameters of all preparations were in nanometer range and polydispersity index of these particle were 0.3-0.6. According to Sanad et al. (2010), these values led to a relatively broad size distribution and were suitable for topical application. After loading the astaxanthin from hydrolyzed extract into the selected blank-SLNs, the zeta potential values of the prepared ASX-SLNs were above |-50| mV which were a prerequisite for the stability of SLNs.

The effect of solid lipid types and mixed surfactants concentrations on particle size of ASX-SLNs was investigated and the result showed the same trend with 14 formulations of blank-SLNs. Among the different solid lipids tested, ASX-SLNs formulations prepared using Dynasan[®]118 were smaller than GMS when compared to the same formulation such as D10CI30 (152.4±2.50 nm) and G10CI30 (217.5±15.09 nm), D10CE40 (158.7±6.66 nm) and G10CE40 (184.5±1.27 nm), D10CE50 (173.9±8.37 nm) and G10CE50 (196.1±6.53 nm). This phenomenon could be attributed to the melting point of lipid in which GMS (m.p. 63.1°C) has a higher melting point than Dynasan[®]118 (m.p. 60.8°C). The higher in melting point could promote rapid lipid crystallization resulting in the larger particle size of the former SLNs (Ekambaram and Abdul, 2011). Moreover, the use of higher melting point lipids tended to obtain the larger particle size, indicating the dispersed phase became higher viscosity (Siekmann and Westesen, 1992). However, no association between particle size and chemical structure of the lipids were investigated. This might be because of the complicated arrangement of these lipids.

Among the mixed surfactants concentration used, the lower concentration was found to result smaller particle size than the higher concentration, for example, D10CI30 (152.4±2.50 nm), D10CI40 (161.8±5.44 nm), and D10CI50 (192.2±35.42 nm), D10CE40 (158.7±6.66 nm) and D10CE50 (173.9±8.37 nm), G10CE40 (184.5±1.27 nm) and G10CE50 (196.1±6.53 nm), D20MI40 (321.1±13.95 nm) and D20MI50 (336.1±18.00 nm). This might be due to the increase of viscosity of the external aqueous phase or the accumulation of excess surfactant molecules at the

partilcles surface; loops and tails were formed, eventually causing an agglomeration of primary SLNs (Tiyaboonchai et al., 2007).

3.4 The percentage of entrapment efficiency

The entrapment efficiency of SLNs was examined using centrifugal filter device and HPLC technique. The triplicate observations were measured (n=3). Table 3 shows the percentage of entrapment efficiency of freshly prepared ASX-SLNs formulations and the percentage of recovery which included the combined content of entrapped and unentrapped free astaxanthin. The results revealed that types of solid lipids and amount of mixed surfactants affected entrapment efficiency. All formulations had moderate to high entrapment efficiency with high recovery. The values were different depending on formulations. The entrapment efficiency of ASX-SLNs formulations were about 46–91% with >97% of recovery. The high percentage of recovery indicated that only a little amount of astaxanthin was lost during preparation.

The entrapment efficiency was highest and lowest in the formulation of G10CI30 (90.84±0.84%) and D10ME60 (45.85±2.72%), respectively. In case of D10CI30 (88.08±0.37%) and G10CI30 (90.84±0.84%), D10CE40 (83.72±2.16%) and G10CE40 (90.58±0.77%), D10CE50 (67.99±2.82%) and G10CE50 (81.82±2.39%), the different types of solid lipids affected the dissimilar entrapment efficiency. Considering effect of lipid type, GMS was discovered to increase the entrapment efficiency compared to Dynasan[®]118. This could be due to different groups of solid lipid, GMS is partial glycerides and Dynasan[®]118 belongs to triglycerides group, which GMS might offer more room to accommodate the astaxanthin in lipid matrix (Wang et al., 2005)

When concerning the same formulation at different mixed-surfactants concentrations in case of D10CI30, D10CI40, and D10CI50, the entrapment efficiency of these formulations was 88.08±0.37%, 85.21±1.26%, and 76.87±0.71%, respectively. This result was similar to D10CE40 (83.72±2.16%) and D10CE50 (67.99±2.82%), G10CE40 (90.58±0.77%) and G10CE50 (81.82±2.39%), D20MI40 (63.86±1.00%) and D20MI50 (56.97±1.81%), slightly reduction in entrapment efficiency was noticed from these formulations. The entrapment efficiency of SLNs decreased when increasing mixed surfactants concentration with a constant amount of

lipid. This is reasonable as the lipid surface of SLNs formed was too tiny to absorb surfactant and co-surfactant molecules. This might affect the micellar solutions formation of free astaxanthin in the water phase. Hence, the astaxanthin solubility in the water phase would increase since it could diffuse from the SLNs into the micelles resulting in the reduction of final entrapment efficiency. This agreed with the finding of Paliwal et al. (2009) which stated that an increase in surfactant concentration decreased entrapment efficiency. The use of Myrj$^®$52 as a solid surfactant in SLNs showed less entrapment efficiency than the group of Tween$^®$80 and Cremophor$^®$RH40. This result referred to the low ability of astaxanthin accommodation in lipid matrices when using Myrj$^®$52 as a surfactant.

Some publications discovered that the entrapment efficiency of active drug usually increased as the particle size increased (Sanad et al., 2010; Yuan et al., 2008). As a result, the large particle size had greater accommodation for the hydrophobic drug than the small particles. Conversely, Tiyaboonchai et al. (2007) also reported that the higher surfactant concentration resulted in bridging and forming of larger particle sizes. Since their drug (curcuminoids) was mainly dissolved in the surfactant layer around SLNs surface, the entrapment efficiency was accordingly decreased when increasing the surfactant concentration due to smaller surface area of particles. Moreover, they found that at higher lipid concentration, more SLNs generated with inadequate quantities of surfactants to incorporate the total drug molecule at the SLNs surface leading to lower entrapment efficiency. To investigate this explanation, Pearson correlation was used to evaluate the data relationship and also found that the average size of ASX-SLNs formulations did not give good correlation ($p>0.01$) to entrapment efficiency (Figure 32). The explanation of the effect of solid lipid and surfactant concentration on particle size and entrapment efficiency therefore could be different depending on many factors such as the nature of the incorporated drug, the type of lipid and surfactant used.
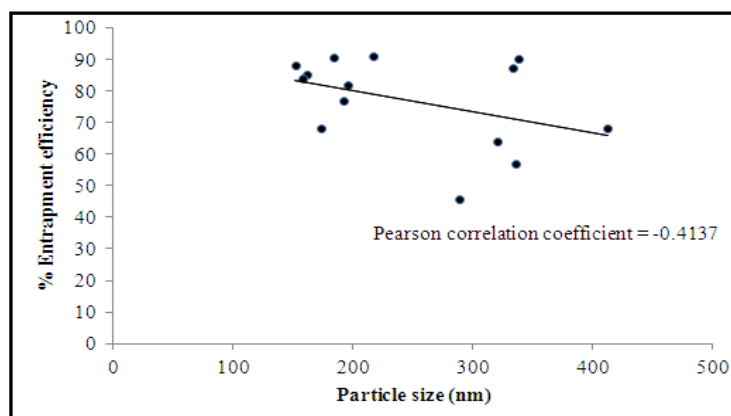
Figure 32 Relationship between entrapment efficiency and particle size of ASX-SLNs formulations.

Table 3 The percentages of recovery and entrapment efficiency of freshly prepared ASX-SLNs formulations.

Formulations	Recovery (%)	Entrapment efficiency (%)
D10TI30-ASX	98.41±2.26	90.18±1.19
D10CI30-ASX	99.78±1.23	88.08±0.37
D10CI40-ASX	98.29±1.07	85.21±1.26
D10CI50-ASX	99.93±1.24	76.87±0.71
D10TE40-ASX	98.94±0.84	87.32±2.14
D10CE40-ASX	100.04±0.44	83.72±2.16
D10CE50-ASX	99.85±0.90	67.99±2.82
G10CI30-ASX	99.42±0.58	90.84±0.84
G10CE40-ASX	98.21±0.85	90.58±0.77
G10CE50-ASX	99.93±0.81	81.82±2.39
D20MI40-ASX	97.38±1.08	63.86±1.00
D20MI50-ASX	97.90±0.75	56.97±1.81
D10ME60-ASX	98.03±0.96	45.85±2.72
G20ME40-ASX	99.84±1.53	68.01±2.66

3.5 Thermal analysis by differential scanning calorimetry (DSC)

Differential scanning calorimetry (DSC) is widely used to evaluate the status of the lipid in SLNs. The fundamental operation of DSC is to distinguish the lipid modification after preparation process on the basis of different melting points and enthalpies. In this study, DSC has been performed and thermograms of solid lipid, solid surfactant, and lyophilized SLNs formulations were presented in Appendix D. The onset, endset, melting temperature, melting enthalpy, and the percentage of crystallinity index (%CI) were calculated and recorded in Table 4. %CI can be used as a parameter in order to quantify the extent of crystallinity. The lipid polymorphism is monitored due to the organization of alkane chains into dissimilar packing patterns: α hexagonal , β′ (orthorhombic), and β (triclinic). Hexagonal packing is the most disordered form, orthorhombic packing is less disordered, and triclinic packing is the most organized form (Allais et al., 2003). The raw material of Dynasan®118, GMS, and Myrj®52 (solid surfactant) revealed a prominent endothermic peak at 60.8°C, 63.1°C, and 50.4°C, respectively with melting enthalpy 173.0, 162.0, and 159.0 J/g, respectively. This result indicated the crystalline nature of each material.

DSC graphs of blank-SLNs and ASX-SLNs were compared. The reduction in crystallinity of solid lipid after SLNs preparation process pointed by decreasing in melting point and onset temperature (Severino et al., 2011). For blank-SLNs and ASX-SLNs, one broad peak and nearly similar melting point peak of solid lipid (Dynasan®118 or GMS) were obtained while onset temperature was lower than pure solid lipid. This might be because of the smaller particle size of the SLNs, their higher surface area and the existence of surfactant (Venkateswarlu and Mannjunath, 2004). Moreover, this result indicated solid lipid became more amorphous after SLNs formation and lipid crystallinity was diminished after astaxanthin loading into SLNs. Furthermore, the enthalpies of all ASX-SLNs formulations were slightly more than their respective blank-SLNs. The presence of the astaxanthin prevented formation of unstable modification or accelerated the transformation to the more stable polymorph leading to higher enthalpy (Muhlen et al., 1998). As the crystal is more ordered, less space is accessible for guest molecules that serve to disturb the thermodynamically preferred crystal ordering.

Moreover, the crystallinity might be changed because of the interaction between matrix and surfactants (Helgason et al., 2009). The distribution of surfactant in the melted phase can change the lipid crystallization resulting in lower melting point. Kumar and Randhawa (2013) found that the choice of surfactant in the formulation could control the particle size, crystallization, and polymorphic transition of SLNs. In this case, the use of Myrj®52 as a solid surfactant in SLNs showed the %CI value more than the use of Tween®80 and Cremophor®RH40 (liquid surfactant). This resulted in the low ability of astaxanthin accommodation in lipid matrices when using Myrj®52 as a surfactant and was in accordance with lower value of entrapment efficiency. A negative correlation ($p<0.01$) was also found between the %CI and entrapment efficiency suggesting that it was more difficult to incorporate the astaxanthin in lipid matrix based on the increase of crystallinity (Figure 33). The SLNs formation induced the reduction of lipid crystallinity in both blank- and ASX-SLNs. Overall, it could summarize that lipid matrix became the less ordered form compared to the bulk solid lipid. The crystallinity reduction was further confirmed by PXRD as discussed in the next Section.

Table 4 DSC results of bulk materials, lyophilized blank-SLNs, and ASX-SLNs formulations.

Code	Endotherm				%CI
	Enthalpy (J/g)	Peak (°C)	Onset (°C)	Endset (°C)	
Bulk Dynasan[®]118	173.0	60.8	41.9	67.8	-
Bulk GMS	162.0	63.1	43.6	71.7	-
Myrj[®]52	159.0	50.4	34.6	58.2	-
D10TI30-Blank	26.5	50.1	33.2	62.3	30.64
D10TI30-ASX	27.5	43.4	28.1	55.3	31.79
D10CI30-Blank	22.4	50.5	32.7	57.2	25.90
D10CI30-ASX	23.6	40.1	28.1	51.7	27.28
D10CI40-Blank	18.7	48.2	32.3	58.4	21.62
D10CI40-ASX	19.8	39.9	27.2	50.2	22.89
D10CI50-Blank	13.2	47.1	31.7	55.6	15.26
D10CI50-ASX	14.5	41.2	27.2	47.7	16.76
D10TE40-Blank	15.4	48.6	28.3	60.8	17.80
D10TE40-ASX	15.9	40.9	25.0	53.6	18.38
D10CE40-Blank	7.2	48.1	34.2	57.6	8.35
D10CE40-ASX	8.7	40.9	27.0	53.5	10.02
D10CE50-Blank	10.1	50.8	32.3	62.7	11.72
D10CE50-ASX	11.3	42.0	26.3	54.2	13.09
G10CI30-Blank	24.5	54.5	35.1	62.2	30.23
G10CI30-ASX	25.7	40.5	24.5	50.3	31.73
G10CE40-Blank	18.3	55.0	33.5	63.8	22.62
G10CE40-ASX	19.3	38.7	25.1	52.4	23.83
G10CE50-Blank	18.1	52.5	34.6	59.6	22.38
G10CE50-ASX	19.2	39.9	28.2	46.3	23.70
D20MI40-Blank	74.1	43.7	30.6	60.3	42.85
D20MI40-ASX	78.2	40.8	27.2	55.2	45.20
D20MI50-Blank	68.3	43.2	30.0	57.7	39.49
D20MI50-ASX	72.4	40.9	27.2	58.9	41.85
D10ME60-Blank	53.0	58.8	37.6	75.2	61.27
D10ME60-ASX	55.5	43.9	26.9	47.4	64.16
G20ME40-Blank	60.4	43.2	30.7	58.4	37.28
G20ME40-ASX	63.2	44.1	34.3	67.4	39.01
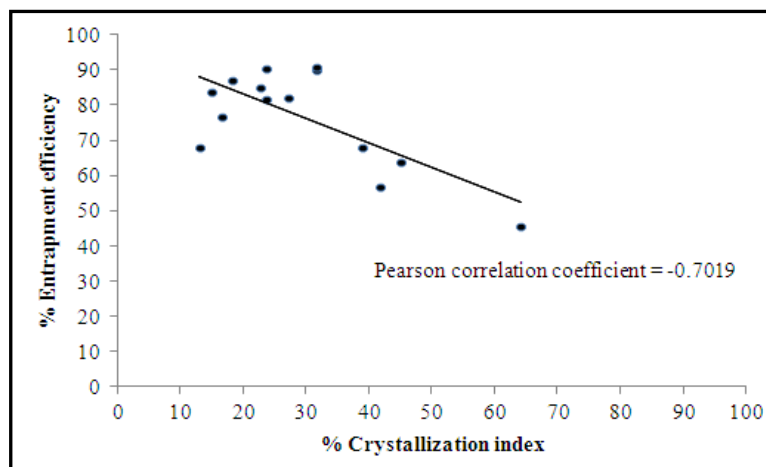
Figure 33 Relationship between entrapment efficiency and crystallization index of ASX-SLNs formulations.

3.5 Powder X-ray diffractometry (PXRD) analysis

The DSC data was confirmed by PXRD analysis of bulk materials, blank-physical mixture, ASX-physical mixture, lyophilized blank-SLNs, and ASX-SLNs. PXRD pattern strong peak at θ = 5.42°, 19.44°, and 23.40° clearly belonged to Dynasan®118 whereas GMS showed strong peak at θ . °, 19.36° and 23.08°. PXRD patterns for all formulations are presented in Figures 34-35. The pattern of the bulk solid lipid displayed noticeable difference from nanoparticles with comparative intense peak (y-axis) than the SLNs. It was explicit that in the blank-SLNs and ASX-SLNs, the reduction of lipid crystallinity was dominant phenomenon and became more amorphous form which could provide more space for higher astaxanthin incorporation. On the contrary, there was no strong peak corresponding to the crystallinity of bulk free astaxanthin (from the hydrolyzed extract). This can be understood that free astaxanthin from hydrolyzed extract appeared as the amorphous form. The reduction in astaxanthin crystallinity and more amorphous conversion after ASX-SLNs preparation could not observe from this study because the extract already existed in an amorphous state (Figure 34).

From the patterns presented a prominent peak of the more disordered form, meaning a shift to higher surface energy after SLNs preparation. The peak of the SLNs from the PXRD had a slight reduction of intensity. This indicated that the solid

lipid lost their crystal lattices and turned to the lower degree of crystallinity. From the PXRD patterns of physical mixture presented the strong peak of bulk solid lipid in all formulations including blank-physical mixture and ASX-physical mixture. This could be understood that bulk solid lipid did not change crystalline order after grinding in the mortar. The PXRD patterns of SLNs were usually broader than bulk lipid as a result of small particle size and the reduction in crystalline order. These results were in accordance with the development of SLNs containing clotrimazole (Das et al., 2012), raloxifene hydrochloride (Burra et al., 2013), lopinavir (Negi et al., 2012), and lidocaine (Pathak and Nagarsenker, 2009) which indicated the change in crystalline behavior of SLNs lipid matrix. Moreover, this result agreed with DSC data and proposed that SLNs made from microemulsion method caused the higher astaxanthin accommodation than physical mixture.

The loss of strong characteristic peaks of crystalline form of Dynasan[®]118 and GMS in SLNs containing Tween[®]80 and Cremophor[®]RH40 as a surfactant indicated solid lipid turned to amorphous form more than the formulation that used Myrj[®]52 as a surfactant. The more intensity of solid lipid peak in the latter SLNs formulation indicated that solid lipid still had more crystalline than the two former formulations. However, the solid lipid crystallinity decreased after SLNs preparation in all formulations. Comparison of diffractograms between the blank- and ASX-SLNs revealed not much difference in the figure in terms of peaks positioning and intensity, showing that the incorporation of astaxanthin did not change the property of SLNs.
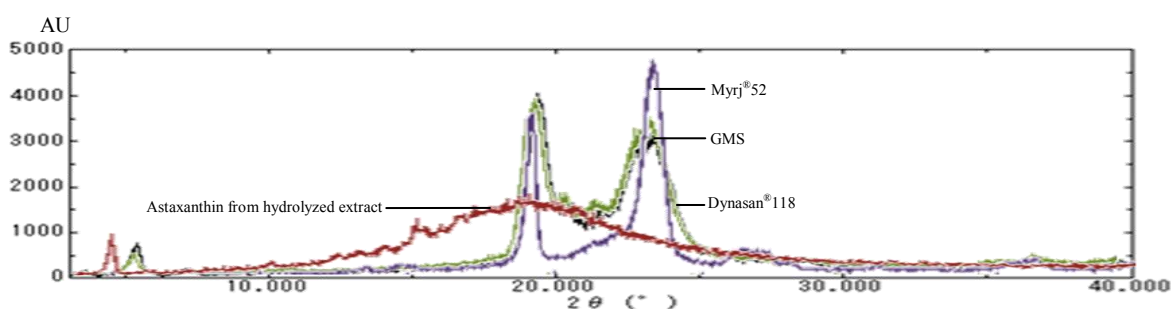
Figure 34 PXRD patterns of bulk materials: Dynasan[®]118 (green line), GMS (black line), Myrj[®]52 (purple line), and astaxanthin from hydrolyzed extract (red line).
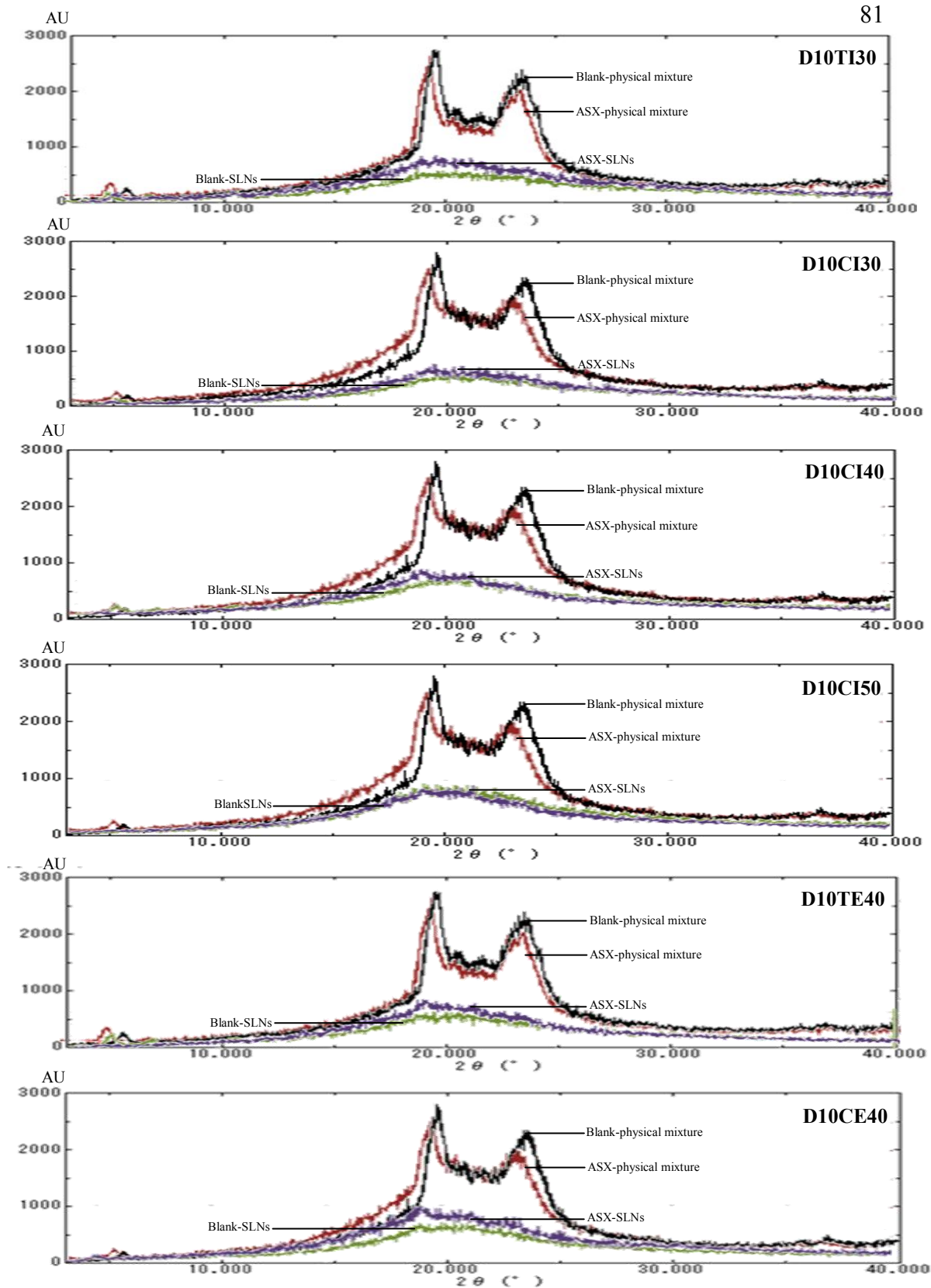
Figure 35 PXRD patterns of blank-physical mixture (black line), ASX-physical mixture (red line), lyophilized blank-SLNs (green line), and ASX-SLNs formulations (purple line).
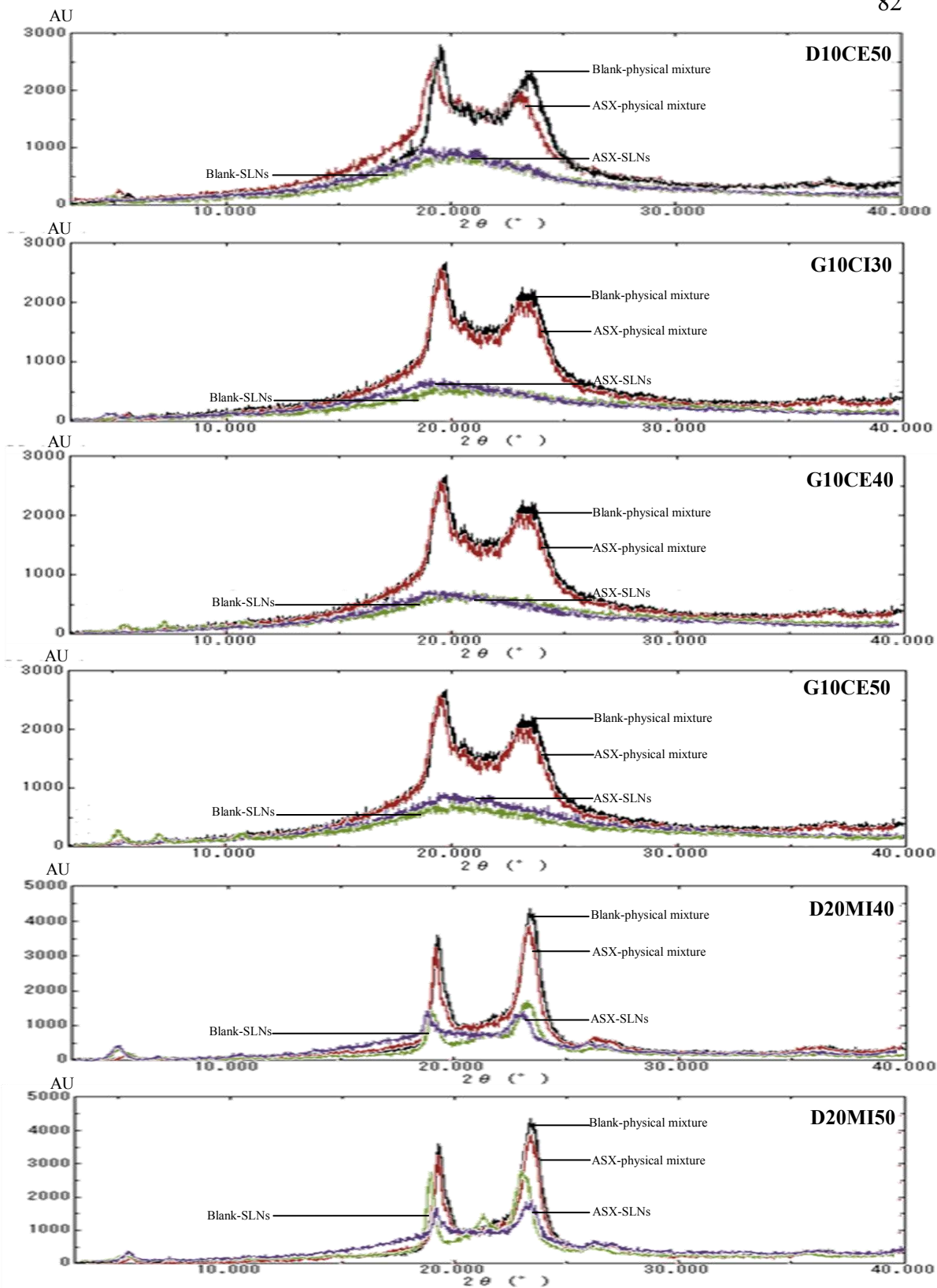
Figure 35 (Cont.) PXRD patterns of blank-physical mixture (black line), ASX-physical mixture (red line), lyophilized blank-SLNs (green line), and ASX-SLNs formulations (purple line).
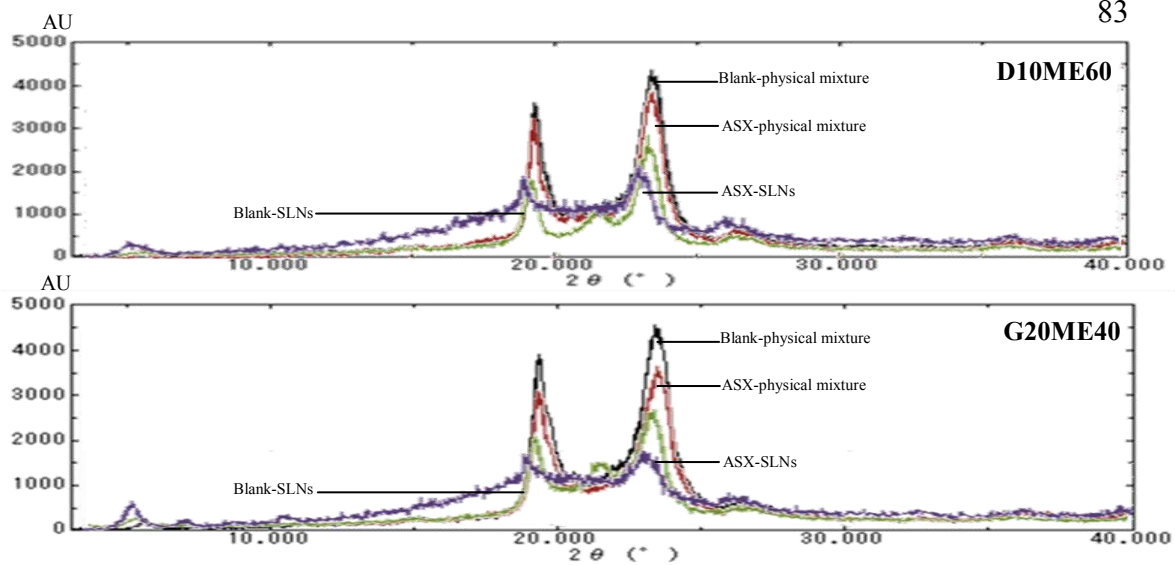
Figure 35 (Cont.) PXRD patterns of blank-physical mixture (black line), ASX-physical mixture (red line), lyophilized blank-SLNs (green line), and ASX-SLNs formulations (purple line).

4.   Physical and chemical stability of ASX-SLNs

One of the advantages of SLNs was to protect the astaxanthin from physical and chemical instability. In order to investigate this benefit, ASX-SLNs formulations were evaluated in comparison to the control solution which contained 25 mg/mL astaxanthin from hydrolyzed extract in propylene glycol and ethanol (1:1 v/v). The samples were withdrawn and examined at 0, 1, 2, and 3 months as shown in these following topics.

4.1 Physical appearances

The physical appearances of 14 ASX-SLNs formulations possessed good appearance (Figure 36). No phase separation occurred during storage. However, gel formation occurred in D10CE50, G10CI30, G10CE40, G10CE50, D20MI50, and G10ME40 formulations after storage for 3 months. The possible reason for gelation process was the structural changes during storage or recrystallization of lipid from spherical to platelet-like colloidal crystals form which favored sites of particle aggregation (Heurtault et al., 2003). For o/w microemulsion method, the samples were subjected to heat during the production process. High temperature could lead to change in the crystalline structure of lipids resulting in the subsequent and gradual gelation (Freitas and Muller, 1998). This observation indicated the need for alternative methods to store the nanoparticles. Therefore, transformation of SLNs dispersions into lyophilized powder may be able to prevent aggregation and gelation of nanoparticles and improve their physical stability (Mehnert and Mader, 2001). Moreover, the dilution by incorporation of SLNs into the cream base might reduce the probability of SLNs particles collision and increase further physical stability (Dingler et al., 1999).

Moreover, the change in orange color could be detected by visual observation. The physical instability of ASX-SLNs and control solution might associate with the astaxanthin content because the active compound presented the dominant orange color. To prove this assumption, the free astaxanthin content in formulation was investigated by HPLC technique and the percentage of recovery was calculated to represent the amount of free astaxanthin at any time periods (the data are shown in Section 4.3).
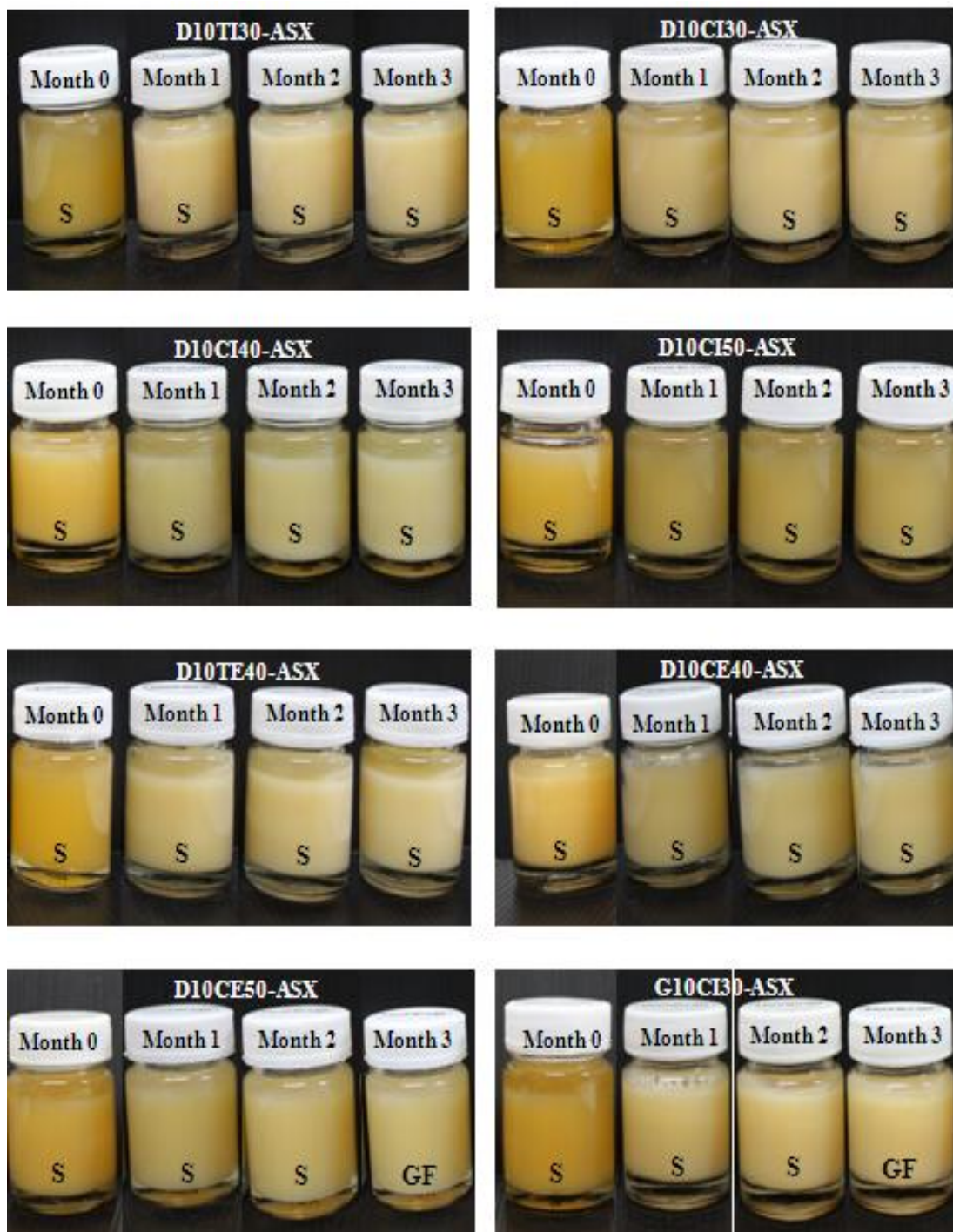
Figure 36 The appearances of 14 ASX-SLNs formulations and control solution during storage at room temperature and protected from light (S = stable, GF = gel formation).
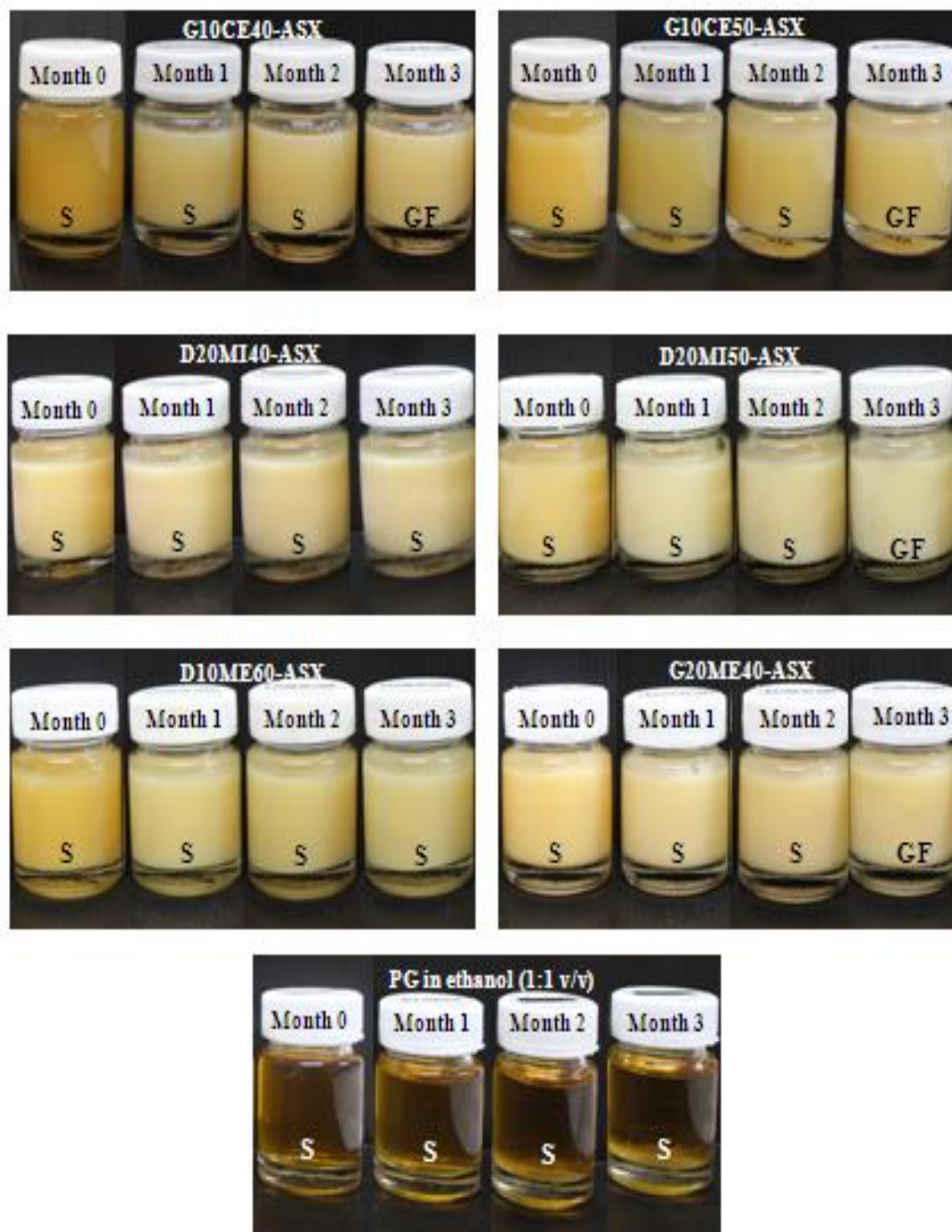
Figure 36 (Cont.) The appearances of 14 ASX-SLNs formulations and control solution during storage at room temperature and protected from light (S = stable, GF = gel formation).

4.2 Particle size analysis

Particle size, size distribution, and zeta potential of ASX-SLNs at each month are shown in Figure 37. The mean diameters of all formulations were in nanometer range and polydispersity index of these particles demonstrated broad size distribution. The particle size of all formulations slightly increased during the study period. The mean particle size of ASX-SLNs formulations, D10CI40, D10CE50, G10CI30, G10CE40, G10CE50, D20MI50, and G10ME40 after preparation for 3 months, exhibited a significant increase in size ($p<0.05$) whereas other formulations were found to be stable. This is in accordance with the gelling phenomena which referred to a major increase of particle size. Han et al. (2008) reported that the surfactant and the character of lipid matrix have been discovered to be major factors affecting the stability of SLNs under the storage condition. Zeta potential of all ASX-SLNs changed into the less negative charge after storage for 3 months. This result referred to the loss of electrostatic stabilization which supported the aggregation of nanoparticles. From the physical stability result obtained, the stable ASX-SLNs formulations during storage at room temperature were selected to further study. These 7 formulations were D10TI30, D10CI30, D10CI50, D10TE40, D10CE40, D20MI40, and D10ME60.

4.3 The percentages of recovery and entrapment efficiency

The percentage recovery of all formulations gradually decreased within 3 months especially in the control solution (Table 5). The free astaxanthin remaining at 3 months was more than 51.19% in all ASX-SLNs formulations. While the control solution showed a significant decrease in free astaxanthin content from 100.99% (month 0) to 33.12% (month 3). Free astaxanthin concentrations were significantly associated with the studied delivery system (SLNs and control solution) ($p<0.05$), displaying consistently lower values in the control solution. It was summarized that free astaxanthin was more labile to degradation in the control solution than in the SLNs. This result displayed the ability of SLNs to prevent pigment degradation over control solution and the storage time was the main factor affecting the degradation of the extracted pigment.

The entrapment efficiency of ASX-SLNs formulations tended to decrease during storage. This might be due to the free astaxanthin was expelled from lipid

matrix into the external aqueous phase resulting in the diminution of the entrapment efficiency. Solid lipid that formed highly crystalline particles with a perfect lattice in lipid matrix over time promoted the migration of astaxanthin towards SLNs surface (could be confirmed by the increase of %CI value in the next part). Jenning et al. (2000) also explained that polymorphism affected the drug content in nanoparticles and drug expulsion during polymorph transition to more stable form (β form). Astaxanthin expulsion from the lipid matrix was common problem during storage of SLNs as well as the aggregation, phase separation, and gelation. The perfect lattice caused the expulsion of incorporated astaxanthin from lipid matrix led to lower entrapment efficiency. The unentrapped astaxanthin of all formulations decreased with time (Figure 38). The amount of the unentrapped or free astaxanthin in the external aqueous phase of all formulations depended on the rate of astaxanthin expulsion from the lipid matrix as well as the rate of astaxanthin degradation in the external aqueous system. It was possible that the degradation of astaxanthin might occur with the unentrapped astaxanthin in the external aqueous phase rather than in the lipid matrix.

Although the ASX-SLNs developed in this study showed the increase in particle size and decrease in entrapment efficiency due to insufficient stability of the lipid phase which resulted in particle fusion and astaxanthin expulsion, ASX-SLNs were still able to protect free astaxanthin from physical and chemical degradation better than the control solution. Among seven ASX-SLNs formulations that were chosen from physical stability result in Section 4.2, the formulations showed entrapment efficiency higher than 70% at 3 months (D10TI30, D10CI30) were selected for *in vitro* release and skin permeation studies.
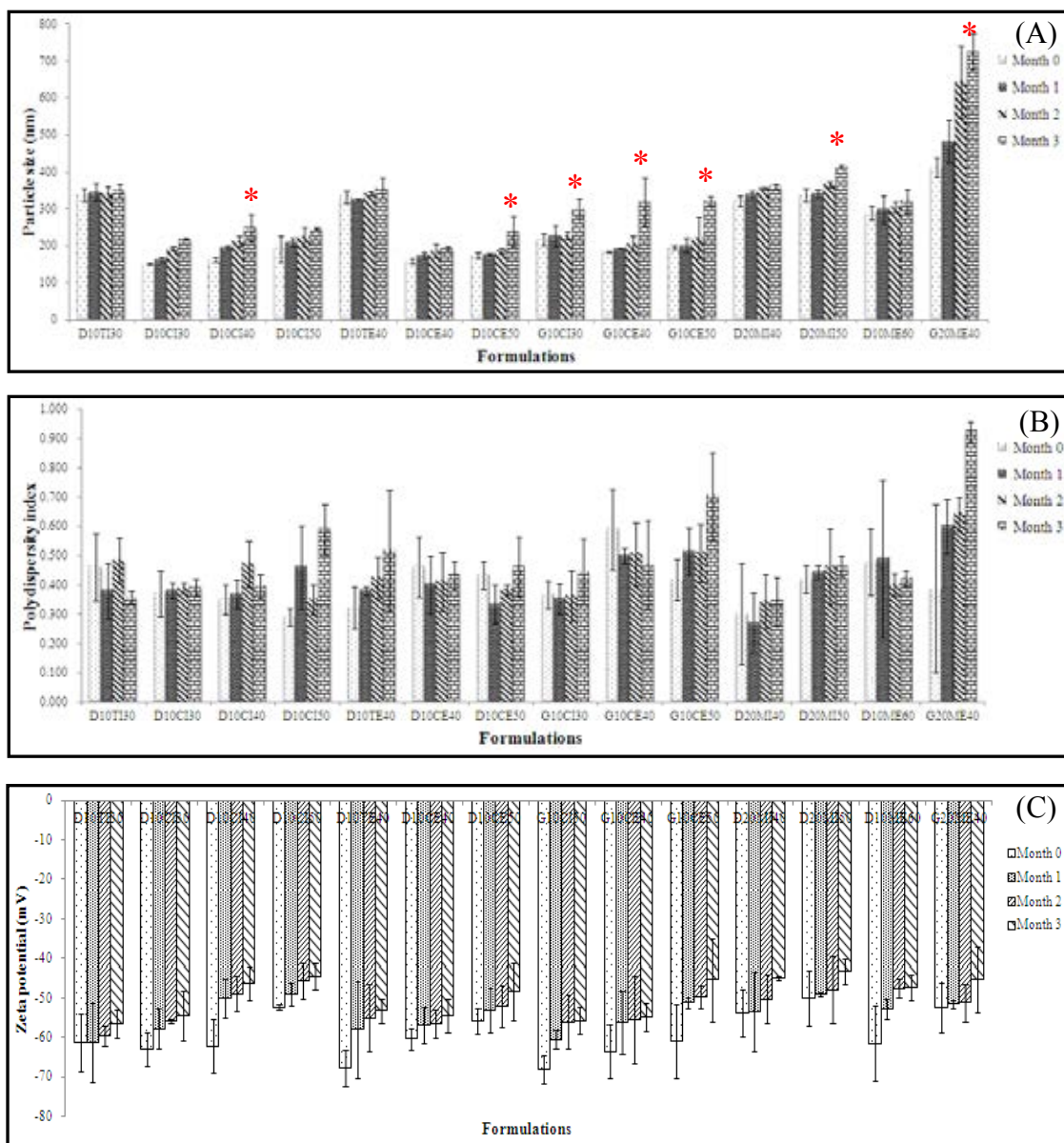
Figure 37 Effect of storage time on particle size (A), size distribution (B), and zeta potential (C) of ASX-SLNs formulations (* means significantly different between ASX-SLNs month 0 and month 3, $p<0.05$).
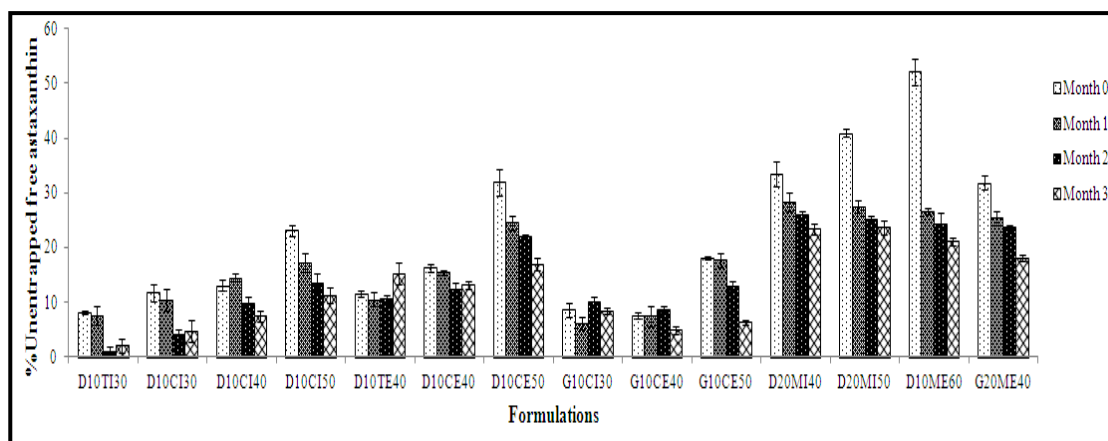
Figure 38 The percentage of unentrapped astaxanthin of ASX-SLNs formulations during storage at room temperature and protected from light.

Table 5 The chemical stability (%recovery and %entrapment efficiency) of all ASX-SLNs formulations and control solution after storage for 3 months.

Formulations	Parameters	Month 0	Month 1	Month 2	Month 3
D10TI30-ASX	%Recovery	98.41±2.26	95.12±1.80	85.46±0.48	80.54±0.15
	%Entrapment efficiency	90.18±1.19	87.52±1.08	84.46±0.50	78.54±1.67
D10CI30-ASX	%Recovery	99.78±1.23	95.54±0.87	86.24±1.00	80.12±1.29
	%Entrapment efficiency	88.08±0.37	85.23±0.24	82.21±2.64	75.32±1.81
D10CI40-ASX	%Recovery	98.29±1.07	95.12±1.66	87.56±0.42	79.54±0.12
	%Entrapment efficiency	85.21±1.26	80.65±0.19	77.63±0.39	72.14±0.33
D10CI50-ASX	%Recovery	99.93±1.24	88.35±1.13	82.98±1.52	76.65±0.57
	%Entrapment efficiency	76.87±0.71	71.12±0.32	69.34±2.41	65.31±1.55
D10TE40-ASX	%Recovery	98.94±0.84	94.32±0.47	84.35±0.45	80.54±0.62
	%Entrapment efficiency	87.32±2.14	83.82±0.23	73.70±1.84	65.35±0.60

Table 5 (Cont.) The chemical stability (%recovery and %entrapment efficiency) of all ASX-SLNs formulations and control solution after storage for 3 months.

Formulations	Parameters	Month 0	Month 1	Month 2	Month 3
D10CE40-ASX	%Recovery	100.04±0.44	96.78±0.28	86.85±0.11	80.75±0.66
	%Entrapment efficiency	83.72±2.16	81.36±0.33	74.51±1.46	67.54±1.91
D10CE50-ASX	%Recovery	99.85±0.90	89.68±0.72	82.12±0.50	75.16±0.25
	%Entrapment efficiency	67.99±2.82	65.11±0.68	60.12±1.06	58.21±0.93
G10CI30-ASX	%Recovery	99.42±0.58	94.85±1.06	88.14±0.53	79.47±0.90
	%Entrapment efficiency	90.84±0.84	88.69±0.81	78.17±0.46	71.12±0.62
G10CE40-ASX	%Recovery	98.21±0.85	97.12±0.57	85.12±1.34	79.38±0.70
	%Entrapment efficiency	90.58±0.77	89.59±0.65	76.41±1.53	74.49±1.44
G10CE50-ASX	%Recovery	99.93±0.81	96.57±0.93	86.36±0.62	78.24±0.55
	%Entrapment efficiency	81.82±2.39	78.79±0.43	73.46±0.66	71.95±1.92
D20MI40-ASX	%Recovery	97.38±1.08	84.84±0.90	77.24±0.61	72.25±0.32
	%Entrapment efficiency	63.86±1.00	56.57±2.62	51.23±2.27	48.83±0.48
D20MI50-ASX	%Recovery	97.90±0.75	78.21±0.27	71.65±0.88	63.78±0.48
	%Entrapment efficiency	56.97±1.81	50.76±0.64	46.34±0.81	40.12±1.03
D10ME60-ASX	%Recovery	98.03±0.96	67.65±1.69	59.54±1.19	51.19±0.95
	%Entrapment efficiency	45.85±2.72	40.99±0.88	35.32±0.43	30.12±2.41
G20ME40-ASX	%Recovery	99.84±1.53	87.51±1.35	82.24±0.27	72.52±0.89
	%Entrapment efficiency	68.01±2.66	62.13±5.40	58.50±1.58	54.45±1.29
Propylene glycol in ethanol (1:1 v/v)	%Recovery	100.99±2.93	76.44±0.71	53.13±0.28	33.12±0.68

4.4 Thermal analysis by differential scanning calorimetry (DSC)

The DSC parameters and thermograms of ASX-SLNs formulations were determined at 0, 1, 2, and 3 months as shown in Table 6 and Appendix D, respectively. All ASX-SLNs formulations showed the slightly increase in melting peak, enthalpy endotherm, and %CI at 0, 1, 2, and 3 months respectively. This result could be correlated with the more ordered crystal lattice, in which the substance required more energy than the less ordered crystal lattice to melt. The less ordered crystal form is easier to transform to more perfect ordered during storage. Astxanthin expulsion may occur and leak from carriers. These DSC results were in agreement with the results of the entrapment efficiency that showed the decrease in amount of astaxanthin in the lipid phase due to the expulsion during storage.

Moreover, the melting point of the ASX-SLNs during storage was lower than the physical mixture (freshly prepared) and pure solid lipid, respectively (Appendix D). It referred to a less ordered structure in SLNs matrix compared to the physical mixtures and bulk lipid. This is in accordance with the literature reports (Burra et al., 2013; Huang et al., 2013) which demonstrated that the melting temperature and enthalpy of SLNs formulations were lower than their corresponding physical mixtures.

From physical and chemical stability result obtained, two stable formulations during storage were selected for *in vitro* release and skin permeation study. The formulations were D10TI30 and D10CI30 because they showed the insignificant increase of particle size, high entrapment efficiency, and slowly increase of %CI over other formulations at the same storage condition.

Table 6 DSC results of lyophilized ASX-SLNs formulations during storage.

| Code | Month | Endotherm | | | | %CI |
		Enthalpy (J/g)	Peak (°C)	Onset (°C)	Endset (°C)	
Bulk Dynasan®118	0	173.0	60.8	41.9	67.8	-
Bulk GMS	0	162.0	63.1	43.6	71.7	-
Myrj®52	0	159.0	50.4	34.6	58.2	-
D10TI30-ASX	0	27.5	43.4	28.1	55.3	31.79
	1	28.1	44.1	28.5	57.3	32.49
	2	32.0	45.6	28.8	53.3	33.17
	3	35.7	47.2	29.5	59.7	36.99
D10CI30-ASX	0	23.6	40.1	28.1	51.7	27.28
	1	25.2	44.9	29.4	52.7	29.13
	2	30.6	48.4	30.7	55.4	31.70
	3	30.9	49.5	30.8	55.6	32.02
D10CI40-ASX	0	19.8	39.9	27.2	50.2	22.89
	1	21.2	44.9	33.5	52.8	24.51
	2	24.3	45.1	32.3	54.3	25.18
	3	25.2	46.2	30.8	57.2	26.14
D10CI50-ASX	0	14.5	41.2	27.2	47.7	16.76
	1	14.9	47.7	32.7	53.1	17.23
	2	17.5	48.5	31.3	55.0	18.10
	3	19.3	49.8	30.6	55.7	19.98
D10TE40-ASX	0	15.9	40.9	25.0	53.6	18.38
	1	17.1	44.9	30.4	53.3	19.77
	2	21.5	47.8	30.9	53.4	22.30
	3	24.3	48.9	28.7	55.3	25.25
D10CE40-ASX	0	8.7	40.9	27.0	53.5	10.02
	1	9.7	47.2	32.6	64.6	11.21
	2	11.0	48.5	32.8	56.1	11.37
	3	13.9	49.6	30.0	55.8	14.41
D10CE50-ASX	0	11.3	42.0	26.3	54.2	13.09
	1	12.8	48.8	32.0	53.3	14.80
	2	14.9	49.0	29.5	56.4	15.49
	3	16.4	50.5	32.1	58.0	17.03
G10CI30-ASX	0	25.7	40.5	24.5	50.3	31.73
	1	26.3	47.7	36.3	56.3	32.47
	2	32.2	50.2	31.4	60.8	33.46
	3	33.6	52.2	31.7	57.5	34.91

Table 6 (Cont.) DSC results of lyophilized ASX-SLNs formulations during storage.

| Code | Month | Endotherm | | | | CI (%) |
		Enthalpy (J/g)	Peak (°C)	Onset (°C)	Endset (°C)	
G10CE40-ASX	0	19.3	38.7	25.1	52.4	23.83
	1	20.1	43.2	30.3	50.3	24.86
	2	25.8	45.0	28.5	53.4	26.82
	3	26.4	48.2	30.2	57.2	27.43
G10CE50-ASX	0	19.2	39.9	28.2	46.3	23.70
	1	19.5	41.9	32.8	48.7	24.07
	2	23.9	45.9	32.6	53.1	24.81
	3	25.6	52.8	33.0	59.2	26.60
D20MI40-ASX	0	78.2	40.9	27.2	55.2	45.20
	1	85.0	44.1	32.2	58.8	49.13
	2	100.7	45.0	30.0	58.9	52.25
	3	107.1	47.9	30.2	59.7	55.55
D20MI50-ASX	0	72.4	40.9	27.2	58.9	41.85
	1	83.2	44.2	32.0	57.2	48.09
	2	105.2	47.5	30.3	60.5	54.55
	3	108.9	47.9	32.5	58.7	56.50
D10ME60-ASX	0	55.5	43.9	26.9	47.4	64.16
	1	58.0	44.6	26.5	58.9	67.05
	2	68.0	45.2	28.3	54.5	70.55
	3	84.5	50.5	35.7	60.4	87.63
G20ME40-ASX	0	63.2	44.1	34.3	67.4	39.01
	1	69.2	48.3	34.0	65.2	42.72
	2	89.6	49.3	33.7	67.9	46.54
	3	95.2	50.2	32.4	63.6	49.48

5. Evaluation of *in vitro* release and pig skin permeation of ASX-SLNs

    5.1 *In vitro* release study

        The ASX-SLNs formulations (D10TI30 and D10CI30), which showed the good property both of physical and chemical stability, were selected to investigate the *in vitro* release profile in comparison to the control solution (the solution of astaxanthin from hydrolyzed extract in Tween®80 2%w/v, isopropanol 2%w/v, and water 96%w/v). The equivalent amount of astaxanthin from hydrolyzed extract (1 mg/mL) was loaded into each formulation in order to maintain sink condition.

        The effective topical formulation should present an ability to release active ingredient at the appopriate extent and rate. Owing to the low water solubility of astaxanthin, the release of astaxanthin was mostly assumed to happen from the lipid matrix of SLNs. ASX-SLNs showed the prolonged release when compared to its solution. In Figure 39, the free astaxanthin exhibited a rapid release almost of 90% from solution within 8 hours, while the release profiles of two ASX-SLNs formulations showed a sustained release over 24 hours. The sustained release pattern could be explained by the deposition of astaxanthin from the outer layer of SLNs. An accumulation of astaxanthin in the external layer of SLNs may appear during the SLNs solidification after dispersion of hot o/w microemulsion into the excess cold water (4°C). The Dynasan®118 may start crystallizing earliest, organizing an inside lipid core. After that, a solid astaxanthin solution may be generated surrounding this core causing an accumulation of astaxanthin in the external region. Sanad et al. (2010) also reported that the subsistence of surfactant could increase the solubility of astaxanthin in water phase, resulting in the repartitioning of astaxanthin into the water phase. This phenomenon made spots of the astaxanthin to be formed on the surface of the SLNs. The sustained release pattern might be occurred from free astaxanthin in lipid matrix which gradually diffused from the inner to the outer layer. The possible model of SLNs is shown in Figure 40.

        Moreover, slight difference in the percentage of cumulative amount of free astaxanthin at 24 hours exhibited between two D10CI30 and D10TI30 ($p>0.05$). This finding could be attributed to the larger specific surface of the smaller particles of D10CI30 affected the increasing of release rate. This is in accordance with the

evidences reported from Wissing et al. (2004) that the larger surface area and the smaller molecular size (high diffusion coefficient) promoted a faster release profile.
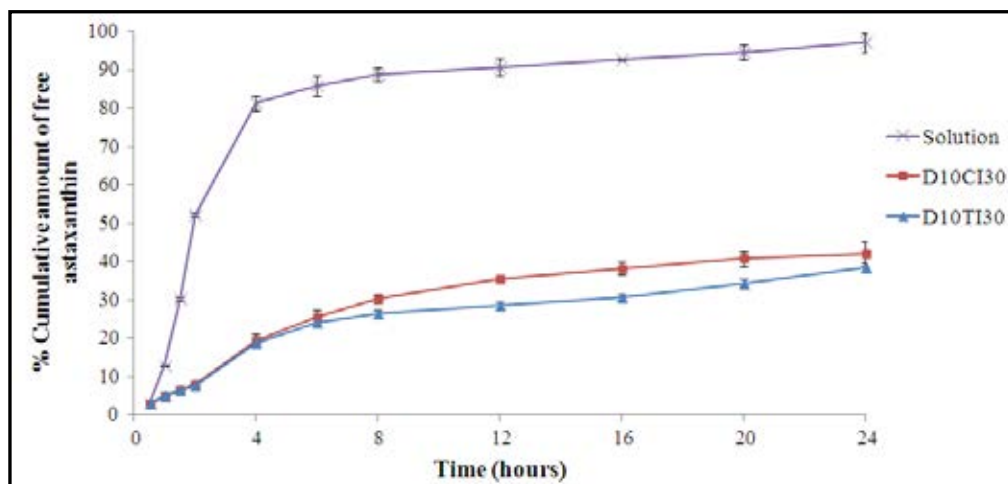
Figure 39 *In vitro* release profiles of free astaxanthin from ASX-SLNs (D10TI30 and D10CI30) and solution. Each point represents the mean±SD (n=3).
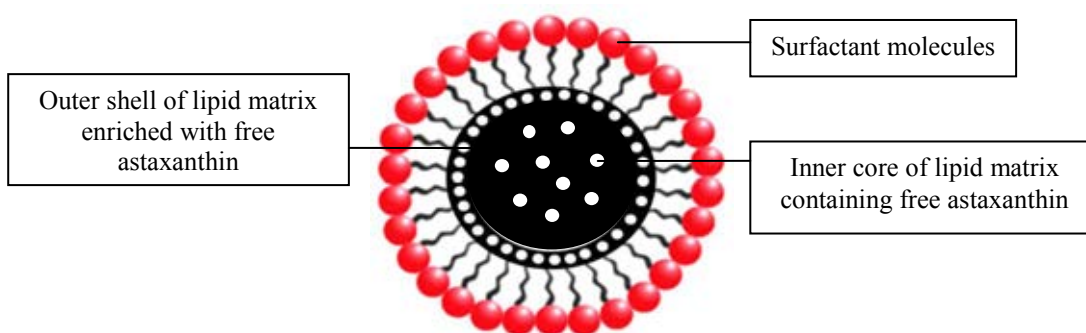
Figure 40 The possible model of ASX-SLNs formulations.

The cumulative release data over 24 hours were plotted to different order kinetic equations including zero-order, first-order, and ig uchi's e ua tion (equation 10, 11, 12, respectively) for prediction the release mechanism of astaxanthin from SLNs.

$$_t \quad k\ t \qquad\qquad uation$$

$$\ln \frac{\ \ }{t} \quad k\ t \qquad\qquad uation$$

$$_t \quad k\ \sqrt{t} \qquad\qquad uation$$

Where, Q_t is the cumulative amount of free astaxanthin release at any time, Q_0 is the beginning amount of free astaxanthin in the formulation, t is the release time, k_0, k_1, k_H are the release rate constant of zero-order, first-order, and Higuchi, respectively.

The coefficient of determination value (R^2) for each equation is listed in Table 7 and Figure 41 shows the Higuchi plots of free astaxanthin released from SLNs. The best fit of ASX-SLNs release profile was found with Higuchi kinetics which explained the diffusion of astaxanthin from matrix system whereas the first-order was the best fit kinetic model for solution. The release profiles exhibited that SLNs demonstrated retarded release of free astaxanthin from lipid matrix in comparison to the solution. In this study, the sustained release property of SLNs was corresponded with many publications (Souto and Muller 2008; Venkateswarlu and Manjunath, 2004; Hao et al., 2011) which showed that the prolonged release could be attributed to embedment of active compound in solid lipid matrix.

Table 7 Coefficient of determination values (R^2) for zero-order, first-order, and Higuchi kinetics.

Formulations	Zero-order	First-order	Higuchi	Higuchi release rate constant ($\mu gcm^{-2}h^{-1/2}$)
D10TI30	0.8963	0.6967	0.9732	137.15
D10CI30	0.8962	0.7222	0.9779	174.40
Solution	0.6924	0.9564	0.8444	-
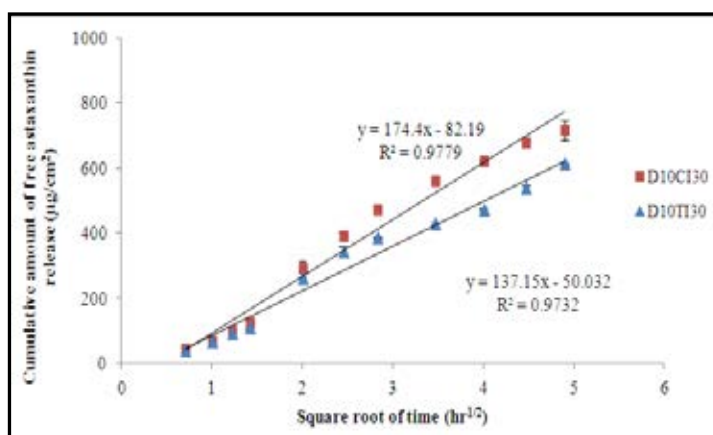
Figure 41 Higuchi plot of ASX-SLNs formulations.

5.2 *In vitro* **permeation study**

As shown in Figure 42, the cumulative amount per unit area of astaxanthin permeated through skin after 24 hours from SLNs formulations (0.2503 ± 0.0049 $\mu g/cm^2$ for D10TI30 and 0.3576 ± 0.0043 $\mu g/cm^2$ for D10CI30) was much higher than that of control solution (0.0739 ± 0.0025 $\mu g/cm^2$) ($p<0.05$). The recovery of free astaxanthin in the skin from D10CI30 was found to be highest followed by D10TI30 and solution as shown in Table 8. The permeation profiles per unit area of free astaxanthin from SLNs are shown in Figure 43. The values of flux and permeation coefficient of free astaxanthin at steady state were computed from the slope of linear regression and are summarized in Table 9. D10CI30 displayed the flux and permeation coefficient higher than D10TI30. Such values of the solution could not be calculated because the free astaxanthin was detected in receptor fluid only 2 time points. These results indicated that SLNs could enhance the skin permeation and retention of free astaxanthin leading to the efficiency in topical delivery system. The mechanisms by which this occurred are ambiguous and different assumptions have been put forth. These include the large surface area owing to the nanometer size, an expulsion of active molecule from SLNs, and penetration enhancer effect.

When comparing the percentage of cumulative amount of free astaxanthin from ASX-SLNs, D10CI30 was significantly greater than D10TI30 ($p<0.05$). It might be due to the smaller particle size of D10CI30 (120.23 ± 4.23 nm) than D10TI30 (226.47 ± 8.12 nm). The small particle sizes can increase the penetration of active compound into skin. Kogan and Garti (2006) explained that the small particle size could intimately contact with the stratum corneum and increase the drug penetrating through skin. Furthermore, the interaction of lipid matrix particle and skin surface can facilitate penetration of active compound from SLNs. Kuchler et al. (2009) examined the interaction of nile red-SLNs and skin surface by scanning electron microscopy and also found the change of lipid particles over 4 hours when having contact with the pig skin surface. SLNs had lost the primary structure, looked to have melted, and declined the number of visual nanoparticles during 4 hours.

Moreover, the two ASX-SLNs formulations were composed of the non-ionic surfactants. Tween®80 and Cremophor®RH40 might give the permeation enhancer effect that increased the skin permeation of free astaxanthin. Due to the

structure of non-ionic surfactant, allowing it to partition between lipophilic mortar and hydrophilic domain of skin. Shokri et al. (2001) investigated the effect of surfactant on the percutaneous permeation of diazepam in rat skin and found that the highest permeation rate (5.68 fold-over control) at the concentration 1%w/w of Tween$^®$80. Nokhodchi et al. (2003) explained the possible mechanisms of non-ionic surfactants to corneocyte disruption by the extraction lipid components or binding with keratin filaments. During this experiment, all formulations were put on the pig skin without occlusion and water evaporation was permitted. This phenomenon affected lipid transformation of SLNs into semisolid gel which induced astaxanthin expulsion. Muller et al. (2002) found that the loss of water influencing the modification of SLNs matrix which might accelerate drug expulsion and penetration. The transformation of α, β′ forms of lipid to stable β ones would contribute to the drug expulsion which was available for permeation (Muller et al., 2000; Jenning and Gohla, 2000).
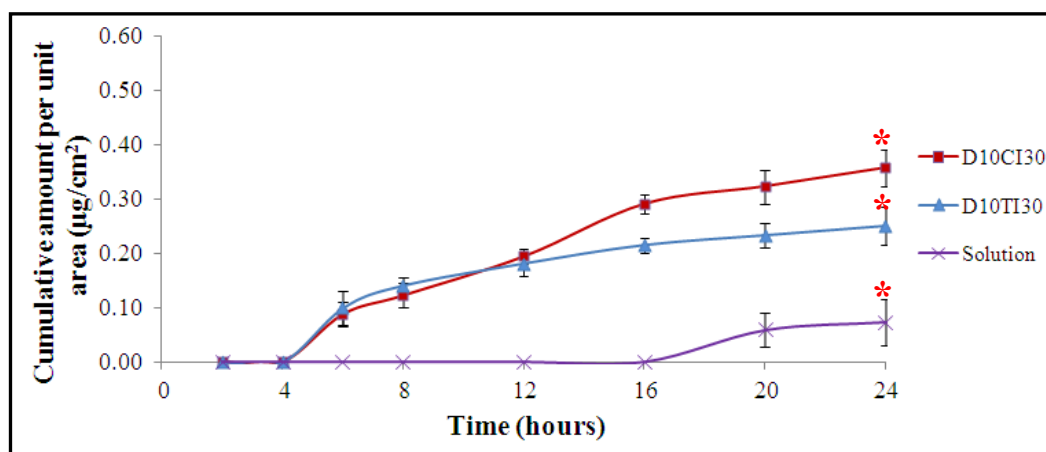
Figure 42 *In vitro* cumulative amount-time profiles of free astaxanthin permeated through pig skin from various formulations (* means significantly different among D10TI30, D10CI30, and solution at 24 hours, $p<0.05$).
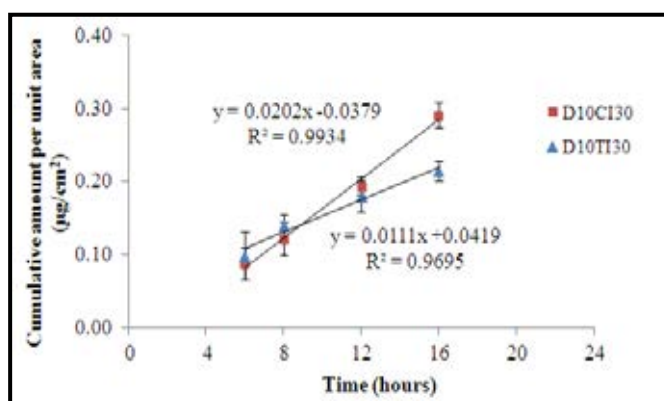
Figure 43 The permeation profiles per unit area of free astaxanthin from ASX-SLNs formulations (mean±SD, n=6).

Table 8 The amount recovery of free astaxanthin from different formulations after the end of pig skin permeation study at 24 hours. Data are expressed as % of total free astaxanthin in the applied dose (mean±SD, n=6).

Formulations	Amount recovery (% of the applied dose)			
	Donor compartment	Pig skin	Receptor compartment	Total
D10TI30	89.60±2.72	1.13±0.23	0.0180±0.0005	90.75±2.88
D10CI30	90.67±4.72	1.34±0.11	0.0265±0.0004	92.04±4.71
Solution	98.77±2.08	0.45±0.04	0.0060±0.0002	99.23±2.09

Table 9 The values of flux and permeation coefficient of free astaxanthin from skin permeation study (*UC = uncalculated).

Formulations	Flux ($\mu g/cm^2 hr$)	Permeation coefficient ($x10^{-5}cm/hr$)
D10TI30	0.0111	5.2885
D10CI30	0.0202	9.5513
Solution	*UC	*UC

From the data, it revealed that the SLNs containing astaxanthin from shrimp shell extract was possible to deliver the active compound into the skin acquiring from the permeation profiles compared to the solution. This finding exhibited the potential

of astaxanthin from shrimp shell extract containing in SLNs can be applied for anti-aging formulation. Furthermore, there are many factors related to the skin permeation *in vivo* and many factors in the realistic situation were not investigated in this study such as mechanically apply, the biological systemic clearance of skin, the efficacy *in vivo*, irritation of formulation, etc. It attributed to the real effect of these preparations as anti-aging for topical formulation should be further examined.

CHAPTER V

CONCLUSIONS

The present study focused on the development of astaxanthin from shrimp shell extract loaded in SLNs for skin delivery. The effect of components in the formulation and astaxanthin extract on SLNs formation by microemulsion method and its stability were also investigated. The release and the skin permeation profiles of free astaxanthin from SLNs were also examined. The results of these investigations were summarized as follows:

1.   The concentration of methanolic NaOH solution was found to be crucial in promoting the hydrolysis of astaxanthin esters and minimizing the degradation of free astaxanthin during saponification. In the present experiment, 0.03 N NaOH resulted in a mild saponification of crude extract that gave the highest percentage yield with very little astaxanthin degradation. The hydrolyzed extract (0.03N NaOH) was composed of the actual free astaxanthin as 21.66%w/w. The antioxidant activity from DPPH assay was 0.7297 μmole/mL which was more than the standard astaxanthin and apocarotenal.

2.   The factors affecting SLNs formation by microemulsion technique were types and concentrations of solid lipids, surfactants, and co-surfactants. Blank-SLNs formulations made from GMS gave a larger particle size than Dynasan®118. Whereas the use of solid surfactants (Myrj®52 and Brij®S721) resulted in the bigger size of SLNs than the use of liquid surfactants (Tween®80 and Cremophor®RH40). Increasing the percentage of solid lipid, surfactant, and co-surfactant also resulted in the augmentation of mean particle size.

3.   Fourteen ASX-SLNs formulations showed the particle sizes in nanometer ranges. The astaxanthin from hydrolyzed extract entrapped in SLNs was 46-91% depending on each formulation. The ASX-SLNs turned to less ordered crystal form after preparation process when compared to physical mixture by using PXRD. ASX-SLNs formulations prepared using the solid surfactant (Myrj®52) displayed the ability to accommodate free astaxanthin less than the group of liquid surfactants

(Tween$^®$80 and Cremophor$^®$RH40) and were in agreement with the lower value of entrapment efficiency.

4.   The stability testing at room temperature and protected from light exhibited that SLNs had a more efficient protective effect on free astaxanthin than the control solution. The percentage of entrapment efficiency of ASX-SLNs gradually decreased with slowly increasing crystallinity index during 3 months.

5.   SLNs manifested the prolonged release profile of free astaxanthin and the permeation profile of ASX-SLNs also displayed remarkably higher permeation through the skin than solution.

However, further studies regarding investigation of the mechanism of topical delivery, *in vivo* test of anti-aging efficacy may be performed to determine the possibility for human use.

REFERENCES

ภาษาไทย

สกุลคุณ มากคุณ. 2546. การสกัดและผลของ astaxanthin จากเปลือกกุ้งต่อการเปลี่ยนแปลงค่าสีและค่า TBA ของ
    ปลาทับทิม (*Oreochromis sp.*) แช่เย็น. วิทยานิพนธ์ปริญญามหาบัณฑิต, สาขาวิชาผลิตภัณฑ์ประมง ภาควิชา
    ผลิตภัณฑ์ประมง มหาวิทยาลัยเกษตรศาสตร์.

ภาษาอังกฤษ

Affandi, M.M., Julianto, T. and Majeed, A. 2011. Development and stability
    evaluation of astaxanthin nanoemulsion. Asian Journal of Pharmaceutical and
    Clinical Research. 4: 142-148.

Allais, C., Keller, G., Lesieur, P., Ollivon, M. and Artzner, F. 2003. X-Ray
    diffraction/calorimetry coupling a tool for polymorphism control. Journal of
    Thermal Analysis and Calorimetry. 74: 723–728.

Amar, I., Aserin, A. and Garti, N. 2003. Solubilization patterns of lutein and lutein
    esters in food grade nonionic microemulsions. Journal of Agricultural and
    Food Chemistry. 51: 4775–4781.

Anajarn, N., Mirhosseini, H., Baharin, B.S. and Tan, C.P. 2010. Effect of processing
    conditions on physicochemical properties of astaxanthin nanodispersions.
    Food Chemistry. 123: 477-483.

Anurak, L., Gaysorn, C., Peankit, D. and Somlak, K. 2011. Griseofulvin solid lipid
    nanoparticles based on microemulsion technique. Advanced Materials
    Research. 197-198: 47-50.

Armenta, R.E., Guerrero, I. and Huertas, I. 2002. Asaxanthin extraction from shrimp
    waste by lactic acid fermentation and enzymatic hydrolysis of the
    carotenoprotein complex. Journal of Food Science. 67: 1002-1006.

Armenta, R.E. and Guerrero, I. 2009. Stability studies on astaxanthin extracted from
    fermented shrimp byproducts. Journal of Agricultural and Food Chemistry. 57:
    6095-6100.

Azeem, A., Ahmad, F., Khar, R. and Talegaonkar, S. 2009a. Nanocarrier for the
    transdermal delivery of an antiparkinsonian drug. AAPS PharmSciTech. 10:
    1093-1103.

Brigger, I., Dubernet, C. and Couvreur, P. 2002. Nanoparticles in cancer therapy and diagnosis. Advanced Drug Delivery Reviews. 54: 631-651.

Burra, M., Jukanti, R., Janga, K.Y., Sunkavalli, S., Velpula, A., Ampati, S. et al. 2013. Enhanced intestinal absorption and bioavailability of raloxifene hydrochloride via lyophilized solid lipid nanoparticles. Advanced Powder Technology. 24: 393-402.

Bunjes, H. and Siekmann, B. 2006. Manufacture, characterization, and applications of solid lipid nanoparticles as drug delivery systems. In S. Benita (ed.), Microencapsulation methods and industrial applications, pp. 213-268. New York: Taylor&Francis

Calo, P., De, M.T., Velazquez, J. and Villa, T. 1995. Mevalonic acid increases trans-astaxanthin and biosynthesis in *Phaffia rhodozyma*. Biotechnology Letters. 17: 575–578.

Camargo, A.P., Meireles, M.A., Ferreira, A.L. and Saito, E. 2012. Extraction of ω-3 fatty acids and astaxanthin from Brazillian redspotted shrimp waste using supercritical CO_2+ethanol mixtures. The Journal of Supercritical Fluids. 61: 71-77.

Charcosset, C., El, H.A. and Fessi H. 2005. Preparation of solid lipid nanoparticles using a membrane contactor. Journal of Controlled Release. 108: 112-120.

Chen, H.M. and e ers, . . . nsil age treatment of crawfish waste for improvement of astaxanthin pigment extraction. Journal of Food Science. 48: 1516–1520.

Chen, X., Yang, S., Xing, R., Yu, H., Liu, S. and Li, P. 2011. Recovery of astaxanthin from discharged wastewater during the production of chitin. Journal of Ocean University of China. 11: 249-252.

Ciapara, I.H., Valenzuela, F., Goycoolea, F.M. and Monal W.A. 2004. Microencapsulation of astaxanthin in a chitosan matrix. Carbohydrate Polymers. 56: 41–45.

Cilurzo, F., Minghetti, P. and Sinico, C. 2007. Newborn pig skin as model membrane *in vitro* drug permeation studies: A technical note. AAPS PharmSciTech. 8: E1-E4.

Coral, H.G. and Bjerkeng, B. 2002. Astaxanthin from the red crab langostilla (*Pleuroncodes planipes*): optical R/S isomers and fatty acid moieties of astaxanthin esters. Comparative Biochemistry and Physiology Part B. 133: 437-444.

Coral, H.G., Huberman, A., De la Lanza, G. and Monroy, R.J. 1997. Pigmentation of the rainbow trout (*Oncorhynchus mykiss*)with oil-extracted astaxanthin from the langostilla (*Pleuroncodes planipes*). Archivos Latinoamericanos de Nutricion. 47: 237–241.

Das, S., Ng, W.K. and Tan, R.B.H. 2012. Are nanostructured lipid carriers (NLCs) better than solid lipid nanoparticles (SLNs): Development, characterizations and comparative evaluations of clotrimazole-loaded SLNs and NLCs?. European Journal of Pharmaceutical Sciences. 47: 139–151.

Dietrich, P. and Anne, K.L. 2006. Tissue distribution of astaxanthin in rats following exposure to graded levels in the feed. Comparative Biochemistry and Physiology. 145: 202-209.

Dingler, A. 1998. Feste Lipid-Nanopartikel als kolloidale Wirstofftragersysteme zur dermalen Applikation. Institut fur Pharmazie. Freie Universitat, Berlin.

Dingler, A., Blum, R.P., Niehus, H. and Müller, R.H. 1999. Solid lipid nanoparticles (SLN^{TM}/Lipopearls^{TM}) a pharmaceutical and cosmetic carrier for the application of vitamin E in dermal products. Journal of Microencapsulation. 16: 751-767.

Dong, Z.H., Chang, S.X., Kai, J.H. and Chang, H.Z. 2003. The production and characteristics of solid lipid nanoparticles (SLNs). Biomaterials. 24: 1781-1785.

Effat, S.F., Saman, A.N. and Zahra, T. 2011. Novel formulation and evaluation of a Q10-loaded solid lipid nanoparticle cream: *in vitro* and *in vivo* studies. International Journal of Nanomedicine. 6: 611-617.

Ekambaram, P. and Abdul, H.S. 2011. Formulation and evaluation of solid lipid nanoparticles of ramipril. Journal of Young Pharmacists. 3: 216-220.

Fang, J.Y., Fang, C.L., Liu, C.H. and Su, Y.H. 2008. Lipid nanoparticles as vehicles for topical psoralen delivery: Solid lipid nanoparticles (SLN) versus nanostructured lipid carriers (NLC). European Journal of Pharmaceutics and Biopharmaceutics. 70: 633-640.

Freitas, C. and Muller, R.H. 1998. Effect of light and temperature on zeta potential and physical stability in solid lipid nanoparticle (SLN) dispersions. International Journal of Pharmaceutics. 168: 221–229.

Freitas, C. and Muller, R.H. 1999. Correlation between long-term stability of solid lipid nanoparticles (SLN) and crystallinity of the lipid phase. European Journal of Pharmaceutics and Biopharmaceutics. 47: 125–132.

Friberg, S.E. and Kayali, I. 1991. Surfactant assocaiation structures, microemulsions, and emulsions in foods: An overview. In: Microemulsions and Emulsions in Foods. E.N. Magda and D. Cornell (eds). ACS Symposium Series 448, American Chemical Society, Washington DC. 7-24.

Gao, Z.G., Choi, H.G., Shin, H.J., Park, K.M., Lim, S.J., Kim, C.K. 1998. Physicochemical characterization and evaluation of a microemulsion system for oral delieery of cyclosporin A. International Journal of Pharmaceutics. 161: 75–86.

Gasco, M.R. 1993. Method of producing solid lipid microspheres having a narrow size distribution. United States Patent. USS 188837.

Goppert, T. and Muller, R. 2005. Protein adsorption patterns on poloxamer- and poloxamine-stabilized solid lipid nanoparticles (SLN). European Journal of Pharmaceutics and Biopharmaceutics. 60: 361–372.

Goto, S., Kogure, K., Abe, K., Kimata, Y., Kitahama, K., Yamashita, E., et al. 2001. Efficient radical trapping at the surface and inside the phospholipids membrane is responsible for highly potent antioxidative activity of the carotenoid astaxanthin. Biochemica et Biophysica Acta. 1521: 251-258.

Gulbake, A., Jain, A., Khare, P. and Jain, S.K. 2010. Solid lipid nanoparticles bearing oxybenzone: In-vitro and in-vivo evaluation. Journal of Microencapsulation. 27: 226-233.

Gulcin, I. 2006. Antioxidant and antiradical activities of L-carnitine. Life Sciences. 78: 803 – 811.

Han, F., Li, S., Yin, R., Liu, H.Z. and Xu, L. 2008. Colloids and Surfaces A: Physicochemical and Engineering Aspects. 315: 210.

Hao, J., Fang, X., Zhou, Y. and Wang, J. 2011. Development and optimization of solid lipid nanoparticle formulation for ophthalmic delivery of chloramphenicol using a Box-Behnken design. International Journal of Nanomedicine. 6: 683–692.

Helgason, T., Awad, T.S., Kristbergsson, K., McClements, D.J. and Weiss, J. 2009. Effect of surfactant surface coverage on formation of solid lipid nanoparticles (SLN). Journal of Colloid and Interface Science. 334: 75-81.

Heurtault, B., Saulnier, P., Pech, B., Proust, J.E. and Benoit, J.P. 2003. Physico-chemical stability of colloidal lipid particles. Biomaterials. 24: 4283–4300.

Hinostroza, G.N. and Bjerkeng, B. 2002. Astsxanthin from the red crab langostilla (*Pleuroncodes planipes*): optical R/S isomers and fatty acid moieties of astaxanthin esters. Comparative Biochemistry and Physiology Part B. 133: 437-444.

Holanda, H.D. and Netto, F.A. 2006. Recovery of components from shrimp (*Xiphopenaeus kroyeri*) processing waste by enzymatic hydrolysis. Journal of Food Science. 71: 298-303.

Hsu, C.H., Cui, Z., Mumper, R.J. and Jay, M. 2003. Preparation and characterization of novel coenzyme Q10 nanoparticles engineered from microemulsion precursors. AAPS Pharmaceutical Sciences Technology. 4: E32.

Hu, L., Tang, X. and Cui, F. 2004. Solid lipid nanoparticles (SLNs) to improve oral bioavailability of poorly soluble drugs. Journal of Pharmacy and Pharmacology. 56: 1527-1535.

Huang, X., Chen, Y.J., Peng, D.Y., Li, Q.L., Wang, X.H., Wand, D.L., et al. 2013. Solid lipid nanoparticles as delivery systems for gambogenic acid. Colloids and Surfaces B: Biointerfaces. 102: 391-397.

Huang, Z.R., Hua, S.C., Yang, Y.L. and Fang, J.Y. 2008. Development and evaluation of lipid nanoparticles for camptothecin delivery: A comparison of solid lipid nanoparticles, nanostructured lipid carriers, and lipid emulsion. Acta Pharmacologica Sinica. 29: 1094-1102.

Izumi, Y., Sato, M., Ueda, F., Sudo, Y., Ujiie, K., Nagata, K., et al. 2009.
e velopment of the dietar supplements, "Astalift supplement" and "Astalift drink". Fujifilm Research and Development. 54: 24-28.

Jacobs, P.B., LeBoeuf, R.D., McCommas, S.A. and Tauber, J.D. 1982. The cleavage of carotenoid esters by cholesterol esterase. Comparative Biochemistry and Physiology. 72B: 157-160.

James, M., Hunter, R.J. and Brien, R. 1992. Effect of particle size distribution and aggregation on electroacoustic measurements of zeta potential. Langmuir. 8: 420-423.

Jenning, V. and Ghola, S. 2000. Solid lipid nanoparticles (SLN) based on the binary mixtures of liquid and solid lipids: a ^{1}H-NMR study. International Journal of Pharmaceutics. 205: 15-21.

Jenning, V., Thunemann, A.F. and Ghola, S. 2000. Characterization of a novel solid lipid nanoparticles carrier system based on binary mixtures on liquid and solid lipids. International Journal of Pharmaceutics. 199: 167-177.

Jingfei, G., Matthew, J.J. and Joachim U. 2010. Polymorphism of 3,3'-dihydroxy-β-β'-carotene-4,4'-dione (Astaxanthin). Chemical Engineering Research and Design.88: 1648-1652.

Jochen, W., Eric, A., Kristberg, K., Thrandur, H. and Tarek, A. 2008. Solid lipid nanoparticles as delivery systems for bioactive food components. Food Biophysics. 3: 146-154.

Johnson, E.A. and An, G.H. 1991. Astaxanthin from microbial sources. Critical Reviews in Biotechnology. 11: 297-326.

Joshi, M.D. and Patravale, V.B. 2006. Formulation and evaluation of Nanostructured Lipid Carrier (NLC) based gel of valdecoxib. Drug Development and Industrial Pharmacy. 32: 911–918.

Khanafari, A., Saberi, A., Azar, M., Vosooghi, G., Jamili, S. and Sabbaghzadeh, B. 2007. Extraction of astaxanthin esters from shrimp waste by chemical and microbial methods. Iranian Journal of Environmental Health Science and Engineering. 4: 93-98.

Kim, D.M., Hyun, S.S., Yun, P., Lee, C.H. and Byun, S.Y. 2012. Identification of an emulsifier and conditions for preparing stable nanoemulsions containing the antioxidant astaxanthin. International Journal of Cosmetic Science. 34: 64–73.

Kobayashi, M. and Sakamoto, Y. 1999. Singlet oxygen quenching ability of astaxanthin esters from the green algae *Haematococcus pluvialis*. Biotechnology Letters. 21: 265–269.

Kogan, A. and Garti, N. 2006. Microemulsions as transdermal drug delivery vehicles. Advances in Colloid and Interface Science. 123-126: 369-385.

Krichnavaruk, S., Shotipruk, A., Goto, M. and Pavasant, P. 2008. Supercritical carbon dioxide extraction of astaxanthin from *Haematococcus pluvialis* with vegetable oils as co-solvent. Bioresource Technology. 99: 5556–5560.

Kuchler, S., Radowski, M.R., Blaschke, T. and Kramer, K.D. 2009. Nanoparticles for skin penetration enhancement-A comparison of a dendritic core-multishell-nanotransporter and solid lipid nanoparticles. European Journal of Pharmaceutics and Biopharmaceutics. 71: 243-250.

Kudo, Y., Nakajima, R. and Matsumoto, N. 2002. Effects of astaxanthin on brain damages due to ischemia. Carotenoid Science. 5: 25.

Kumar, S. and Randhawa, J.K. 2013. Preparation and characterization of paliperidone loaded solid lipid nanoparticles. Colloids and Surfaces B: Biointerfaces. 102: 562-568.

Kusuda, F., Kubo, T., Sudo, Y., Kawabuchi, T., Orikasa, A. and Nakamura, Y. 2010. Development of functional cosmetics "Astalift whitening essence". Fujifilm Research and Development. 55: 33-37.

Lambertsen, G. and Braekkan, O.R. 1971. Method of analysis of astaxanthin and its occurrence in some marine products. Journal of the Science of Food and Agriculture. 22: 99-101.

Lee, G.S., Lee, D.H., Kang, K., Pyo, H. and Choi, T. 2007. Preparation and characterization of bis-ethylhexylphenolmethoxyphenyltriazine (BEMT) loaded solid lipid nanoparticles (SLN). Journal of Industrial and Engineering Chemistry. 13: 1180-1187.

Lim, B.P., Nagano, A. and Terao, J. 1992. Antioxidant activity of xanthophylls on peroxyl radical-mediated phospholipid peroxidation. Biochimica et Biophysica Acta. 1126: 178-184.

Liu, J., Hu, W., Chen, H., Ni, Q., Xu, H. and Yang, X. 2007. Isotretinoin-loaded solid lipid nanoparticles with skin targeting for topical delivery. International Journal of Pharmaceutics. 328: 191–195.

Lorenz, R.T. and Cysewsky, G.R. 2000. Commercial potential for *Haematococcus* microalgae as a natural source of astaxanthin. Trends in Biotechnology. 18: 160–167.

Luo, Y., Chen, D., Ren, L., Zhao, X. and Qin, J. 2006. Solid lipid nanoparticles for enhancing vinpocetine's oral bioavailabilit . Journal of Controlled Release. 114: 53-59.

Ma, Q., Xia, Q., Lu, Y.Y., Hao, X.Z., Gu, N., Lin, X.F., et al. 2007. Preparation of tea polyphenols-loaded solid lipid nanoparticles based on the phase behaviors of hot microemulsions. Solid State Phenomena. 121-123: 705-708.

Machmudah, S., Shotipruk, A., Goto, M., Sasaki, M. and Hirose, T. 2006. Extraction of astaxanthin from *Haematococcus pluvialis* using supercritical CO_2 and ethanol as entrainer. Industrial and Engineering Chemistry Research. 45: 3652–3657.

Manosroi, A., Jantrawut, P., Akazawa, H., Akihasa, T., Manosroi, K. and Manosroi, J. 2011. Transdermal absorption enhancement of gel containing elastic niosomes loaded with gallic acid from *Terminalia chebula* galls. Pharmaceutical Biology. 49: 553-562.

Martin, G., Mark, E.H. and Miguel, O. 2003. *Haematococcus* astaxanthin: applications for human health and nutrition. Trends in Biotechnology. 21: 210-216.

Matsuno, T. 1992. Structure and characterization of carotenoids from various habitats and natural sources. Methods in Enzymology. 21: 22-25.

Mizutani, Y., Sakata, O., Hoshino, T., Honda, Y., Yamashita, M., Arakane, K., et al. 2005. Preventive effects of carotenoids on photoaging and its application for cosmetics. Journal of Japanese Cosmetic Science Society. 29: 9-19.

Mehnert,W. and Mader, K. 2001. Solid lipid nanoparticles: production, characterization and applications. Advanced Drug Delivery Reviews. 47: 165-196.

Morel, S., Ugazio, E., Cavalli, R. and Gasco, M. R. 1996. Thymopentin in solid lipid nanoparticles. International Journal of Pharmaceutics. 132: 259-261.

Muhlen, A., Schwarz, C. and Mehnert, W. 1998. Solid lipid nanoparticles (SLN) for controlled drug delivery-Drug release and release mechanism. European Journal of Pharmaceutics and Biopharmaceutics. 45: 149–155.

Muller, R.H., Radtke, M. and Wissing, S.A. 2002. Solid lipid nanoparticles (SLN) and nanostructured lipid carriers (NLC) in cosmetic and dermatological preparations. Advanced Drug Delivery Reviews. 54: 131-155.

Muller, R.H. Mader, K. and Hohla, S. 2000. Solid lipid nanoparticles (SLN) for controlled drug delivery-a review of the state of the art. European Journal of Pharmaceutics and Biopharmaceutics. 50: 161–178.

Negi, J.S., Chattopadhyay, P., Sharma, A.K. and Ram, V. 2012. Development of solid lipid nanoparticles (SLNs) of lopinavir using hot self nano-emulsification (SNE) technique. European Journal of Pharmaceutical Sciences. 48: 231-239.

Nokhodchi, A., Shokri, J., Dashbolaghi, A., Hassan,Z.D., Ghafourian, T. and Barzegar, J.M. 2003. The enhancement effect of surfactants on the penetration of lorazepam through rat skin. International Journal of Pharmaceutics. 250: 359–369.

Ogawa, M., Maia, A., Fernandes, A., Nunes, M., Oliveira, M. and Freitas, S. 2007. Residuos do beneficiamento do camarao cultivado: obtencao de pigmentos carotenoides. Ciencia e Tecnologia de Alimentos. 27: 333–337.

Ohgami, K. and Shiratori, K. 2003. Effects of astaxanthin on lipopolysaccharide-induced inflammation *in vitro* and *in vivo*. Investigative Ophthalmology and Visual Science. 44: 2694-2701.

Oryza. Astaxanthin. Oryza Oil and Fat Chemical Co., Ltd. [Online]. 2006. Available from : www.oryza.co.jp./html [2011, September 10]

Paliwal, R., Rai, S., Vaidya, B., Khatri, K. and Goyal, A.K. 2009. Effect of lipid core material on characteristics of solid lipid nanoparticles designed for oral lymphatic delivery. Nanomedicine. 5: 184-191.

Palozza, P. and Krinsky, N.I. 1992a. Antioxidant effects of carotenoids *in vivo* and *in vitro*: An overview. Methods in Enzymology. 213: 403-420.

Panida Borisut. 2011. Anti-tyrosinase and antioxidant activities of *Morinda citrifolia* fruit extract and development of nanoemulsions. aste r's Thesis, e partment of Pharmaceutics and Industrial Pharmacy, Faculty of Pharmaceutical Sciences, Chulalongkorn University.

Pasquel, L.J. and Babbitt, J.K. 1991. Isolation and partial characterization of a natural antioxidant from shrimp (*Pandalus jodani*). Journal of Food Science. 58: 143-145.

Pathak, P. and Nagarsenker, M. 2009. Formulation and evaluation of lidocaine lipid nanosystems for dermal delivery. AAPS PharmSciTech. 10: 985-992.

Pattani, A.S., Mandawgade, S.D. and Patravale, V.B. 2006. Development and comparative anti-microbial evaluation of lipid nanoparticles and nanoemulsion of Polymyxin B. Journal of Nanoscience and Nanotechnology. 6: 1–5.

Peng, C.H., Chang, C.H., Peng, R.Y. and Chyau, C.C. 2010. Improved membrane transport of astaxanthine by liposomal encapsulation. European Journal of Pharmaceutics and Biopharmaceutics. 75: 154–161.

Ponsuk Jithavech. 2005. Anti-oxidant, anti-collagenase and anti-tyrosinase activities of extracts of *Phyllanthus emblica* (amla) locally grown in Thailand for use in cosmetic products. aste r's Thesis, Department of Pharmaceutical Technology, Faculty of Pharmaceutical Sciences, Chulalongkorn University.

Rowe, R.C., Sheskey, J.P. and Owen, S.C. 2006. Handbook of Pharmaceutical Excipients, 4th ed. London: The Pharmaceutical Press.

Sachindra, N.M., Bhaskar, N., Siddegowda, G.S., Sathista, A.D. and Suresh, P.V. 2007. Recovery of carotenoids from ensilaged shrimp waste. Bioresource Technology. 98: 1642–1646

Samuel, S.P. and David, B. 1981. Characterization of astaxanthin pigments from heat-processed crawfish waste. Journal of Agricultural and Food Chemistry. 29: 505-508.

Sanad, R.A., Malak, N.S., Bayoomy, T.S. and Badawi, A.A. 2010. Preparation and characterization of oxybenzone-loaded solid lipid nanoparticles (SLNs) with enhanced safety and sunscreening efficacy: SPF and UVA-PF. Drug Discoveries and Therapeutics. 4: 472-483.

Schwarz, C. and Mehnert, W. 1999. Solid lipid nanoparticles (SLN) for controlled drug delivery II. drug incorporation and physicochemical characterization. Journal of Microencapsulation. 16: 205-213.

Seki, T., Sueki, H., Kohno, H., Suganuma, K. and Yamashita, E. 2001. Effects of astaxanthin from *Haematococcus pluvialis* on human skin-patch test, skin repeated application test, effect on wrinkle reduction. Fragnance Journal. 12: 98-103.

Severino, P., Pinho, S.C., Souto, E.B. and Santana, M.H.A. 2011. Polymorphism, crystallinity and hydrophilic-lipophilic balance of stearic acid and stearic acid-capric/caprylic triglyceride matrices for production of stable nanoparticles. Colloids and Surfaces B: Biointerfaces. 86: 125–130.

Shah, K.A., Date, A.A., Joshi, M.D. and Patravale, V.B. 2007. Solid lipid nanoparticles (SLN) of tretinoin: Potential in topical delivery. International Journal of Pharmaceutics. 345: 163–171.

Shiratori K., Ogami K. and Nitta T. 2005. The effects of astaxanthin on accomodation and asthenopia-Efficacy identification study in healthy volunteers. Clinical Medicine. 21: 637-650.

Shokri, J., Nokhodchi, A., Hassan, Z.D, Ghafourian, T. and Barzegar, J.M. 2001. The effect of surfactants on the skin penetration of diazepam. International Journal of Pharmaceutics. 228: 99–107.

Siekmann, B. and Westesen, K. 1992. Submicron sized parenteral carrier systems based on solid lipids. Pharmaceutical and Pharmacological Letters. 1: 123-126.

Silva, A.C., Garcia, M.L., Egea, M.A., Fonseca, J., Silva, R., Santos, D., et al. 2011. Preparation, characterization and biocompatibility studied on risperidone-loaded solid lipid nanoparticles (SLN): High pressure homogenization versus ultrasound. Colloids and Surfaces B: Biointerfaces. 86: 158–165.

Song, C. and Liu, S. 2005. A new healthy sunscreen system for human: Solid lipid nanoparticles as carrier for 3,4,5-trimethoxybenzoylchitin and the improvement by adding Vitamin E. International Journal of Biological Macromolecules. 36: 116–119.

Souto, E.B. and Muller, R.H. 2008. Cosmetic features and applications of lipid nanoparticles (SLN®, NLC®). International Journal of Cosmetic Science. 30: 157-165.

Sowmya, R. and Sachindra, N.M. 2012. Evaluation of antioxidant activity of carotenoid extract from shrimp processing byproducts by in vitro assays and in membrane model system. Food Chemistry. 134: 308-314.

Spernath, A., Yaghmur, A., Aserin, A., Hoffman, R.E. and Garti, N. 2002. Food-Grade microemulsions based on nonionic emulsfiers: Media to enhance lycopene solubilization. Journal of Agricultural and Food Chemistry. 50: 6917–6922.

Stecova, J., Mehnert, W., Blaschke, T., Kleuser, B., Sivaramakrishnan, R., Zouboulis, C. C., et al. 2007. Cyproterone acetate loading to lipid nanoparticles for topical acne treatment: particle characterisation and skin uptake. Pharmaceutical Research. 24: 991-1000.

Suratchawadee Amorndechawat. 2009. Development of solid lipid nanoparticles containing Artocarpus lakoocha heart wood extract (Puag-Haad) for whitening and anti-wrinkle effects. aste r's Thesis, e partment of Pharmaceutics and Industrial Pharmacy, Faculty of Pharmaceutical Sciences, Chulalongkorn University.

Sylvia, A. and Muller, R.H. 2003. Cosmetic applications for solid lipid nanoparticles (SLN). International Journal of Pharmaceutics. 254: 65–68.

Tachaprutinun, A., Udomsup, T., Luadthong, C. and Wanichwecharungruang, S. 2009. Preventing the thermal degradation of astaxanthin through nanoencapsulation. International Journal of Pharmaceutics. 374: 119–124.

Tiyaboonchai, W., Tungpradit, W. and Pliannangchang, P. 2007. Formulation and characterization of curcuminoids loaded solid lipid nanoparticles. International Journal of Pharmaceutics 337: 2-306.

Tominage, K., Hongo, N., Karato, M. and Yamashita, E. 2012. Cosmetic benefits of astaxanthin on human subjects. Acta Biochimica Polonica. 59: 43-47.

Torrisen, O., Tidemann, E., Hansen, F. and Raa, J. 1981. Ensiling in acid. A method to stabilize astaxanthin in shrimp processing by-products and improve uptake of this pigment by rainbow trout (*Salmo gairdneri*). Aquaculture. 26: 77–83.

Tsuchiya, M., Scita, G., Freisleben, H.J., Kagan, V.E. and Packer, L. 1992. Antioxidant radical scavenging activity of carotenoids and retinoids as compared to α-tocopherol. Methods in Enzymology. 213: 460-472.

United States Pharmacopeial Convention: The United States Pharmacopeia 35- The National Formulary 30. Mack Pulishing: Pensylvania. 2012

Venkateswarlu, V. and Manjunath, K. 2004. Preparation, characterization and *in vitro* release kinetics of clozapine solid lipid nanoparticles. Journal of Controlled Release. 95: 627– 638.

Vitorino, C., Carvalho, F.A., Almeida, A.J., Sousa, J.J. and Pais, A. 2011. The size of solid lipid nanoparticles: An interpretation from experimental design. Colloids and Surfaces B: Biointerfaces. 84: 117–130.

Wang, J.J., Liu, K.S., Sung K.C., Tsai, C.Y. and Fang, J.Y. 2009. Skin permeation of buprenorphine and its ester prodrugs from lipid nanaoparticles: lipid emulsion, nanostructured lipid carriers and solid lipid nanoparticles. Journal of Microencapsulation. 26: 734-747.

Wang, Y., Deng, Y., Mao, S., Jin, S., Wang, J. and Bi, D. 2005. Characterization and body distribution of β-elemene solid lipid nanoparticles (SLN). Drug Development and Industrial Pharmacy. 31: 769-778.

Wataru, M. 1991. Biological functions and activities of animal carotenoids. Pure and Applied Chemistry. 63: 141-146.

Westesen, K., Bunjes, H. and Koch, M.H.J. 1997. Physicochemical characterization of lipid nanoparticles and evaluation of their drug loading capacity and sustained release potential. Journal of Controlled Release 48: 223-236.

Wissing, S.A., Kayser, O. and Muller, R.H. 2004. Solid lipid nanoparticles for parenteral drug delivery. Advanced Drug Delivery Reviews. 56: 1257–1272.

Wissing, S.A. and Muller, R.H. 2002. Solid lipid nanoparticles as carrier for sunscreens: *In vitro* release and *in vivo* skin penetration. <u>Journal of Controlled Release</u>. 81: 225-233.

Wissing, S.A. and Muller, R.H. 2002. The influence of the crystallinity of lipid nanoparticles on their occlusive properties. <u>International Journal of Pharmaceutics</u>. 242: 377-379.

Wissing, S. A. and Muller, R. H. 2003. Cosmetic applications for solid lipid nanoparticles (SLN). <u>International Journal of Pharmaceutics</u>. 254: 65–68.

Wissing, S. A. and Muller, R. H. 2003. The influence of solid lipid nanoparticles on skin hydration and viscoelasticity-*in vivo* study. <u>European Journal of Pharmaceutics and Biopharmaceutics</u>. 56: 67-72.

Wolfgang, M. and Karsten, M. 2001. Solid lipid nanoparticles production, characterization and applications. <u>Advanced Drug Delivery Reviews</u>. 47: 165-196.

Yamashita, E. 2006. The effects of a dietary supplement containing astaxanthin on skin condition. <u>Carotenoid Science</u>. 10: 91-95.

Yuan, H., Miao, J., Du, Y.Z., You, J., Hu, F.Q. and Zeng, S. 2008. Cellular uptake of solid lipid nanoparticles and cytotoxicity of encapsulated paclitaxel in A549 cancer cells. <u>International Journal of Pharmaceutics</u>. 348: 137-145.

Yuan, J.P. and Chen, F. 1998. Chromatographic separation and purification of trans-astaxanthin from the extracts of *Haematococcus pluvialis*. <u>Journal of Agricultural and Food Chemistry</u>. 46: 3371-3375.

Yuan, J.P. and Chen, F. 1999. Hydrolysis kinetics of astaxanthin esters and stability of astaxanthin of *Haematococcus pluvialis* during saponification. <u>Journal of Agricultural and Food Chemistry</u>. 47: 31-35.

Zhang, J., Fan, Y. and Smith, E. 2009. Experimental design for the optimization of lipid nanoparticles. <u>Journal of Pharmaceutical Sciences</u>. 98: 1813-1819.

Zhao, Y., Wang, C., Chow, A.H., Ren, K., Gong, T., Zhang, Z., et al. 2010. Self-nanoemulsifying drug delivery system (SNEDDS) for oral delivery of Zedoary essential oil: Formulation and bioavailability studies. <u>International Journal of Pharmaceutics</u>. 383: 170–177.

APPENDICES

APPENDIX A

The Percentage yields of shrimp shell crude extract

Table 10 The percentage yields of shrimp shell crude extract after passive extraction by various organic solvents.

Organic solvents	%Yield (w/w)
Acetone	3.70
Ethanol	5.22
n-hexane	3.04
Isopropanol	9.22
Methanol	2.14

Note: The percentage yields of crude extract was calculated from:

$$ie\ ld\quad \frac{a\ ss\ of\ crude\ extract\ g}{a\ ss\ of\ homogenized\ shrimp\ powder\ g}\ x\qquad ua\ tion$$

APPENDIX B

Validation of HPLC method

Validation for the quantitative analysis of free astaxanthin by HPLC method

The analytical parameters used in the assay validation for HPLC method were specificity, linearity, accuracy and precision.

1. **Specificity**

The specificity of HPLC method was evaluated by comparing the assay results of spiked free astaxanthin in SLNs, receptor medium, and skin extract with the standard solution. The peak of free astaxanthin must be completely separated from and not be interfered by the peaks of other components in the sample.

2. **Linearity**

Linearity was evaluated with different amounts of diluted stock standard solutions to form working solutions containing 0.0125-2.500 µg/mL of free astaxanthin. Three sets of seven standard solutions were prepared and analyzed. Linear regression analysis of the peak areas versus their concentrations was performed. The linearity was defined from the coefficient of determination (R^2).

Acceptance criteria:

The coefficient of determination (R^2) should be more than 0.9990.

3. **Accuracy**

The accuracy of the method was determined from the percentage of analytical recovery. Five sets of three concentrations of free astaxanthin at 0.0125, 1, and 2 µg/mL were prepared and analyzed. The percentage of recovery of each concentration was calculated.

Acceptance criteria:

The percentage of analytical recovery should be within 98.0-102.0% of each nominal concentration.

4. **Precision**

4.1 **Intraday precision**

The intraday precision was determined by analyzing five sets of three concentrations of free astaxanthin at 0.0125, 1, and 2 µg/mL in the same day. The relative standard deviation (%RSD) of the peak area responses at each concentration were determined.

4.2   Interday precision

The interday precision was determined by analyzing three concentrations of free astaxanthin at 0.0125, 1, and 2 μg/mL on five different days. The relative standard deviation (%RSD) of the peak area responses at each concentration were determined.

Acceptance criteria:

The relative standard deviation (%RSD) for both intraday and interday precision should be less than 2%.

Validation for the quantitative analysis of free astaxanthin by HPLC method

The developed HPLC system was applied to analyze the free astaxanthin content in SLNs containing astaxanthin from shrimp shell extract. The method validation was performed in the topic below.

1. **Specificity**

The specificity is a capability to measure the analyte correctly and with specificity in the existence of other ingredients in the sample.

The methanol/dichloromethane/acetonitrile/water (85:5:5:5 v/v) was used as the mobile phase. The typical chromatograms of free astaxanthin standard solution, blank-SLNs, ASX-SLNs, and other chromatograms are shown in Figures 44-54. All chromatograms are shown under the same attenuation and scale. The solvent used to prepare the final solution before HPLC injection was methanol and dichloromethane (1:1 v/v).
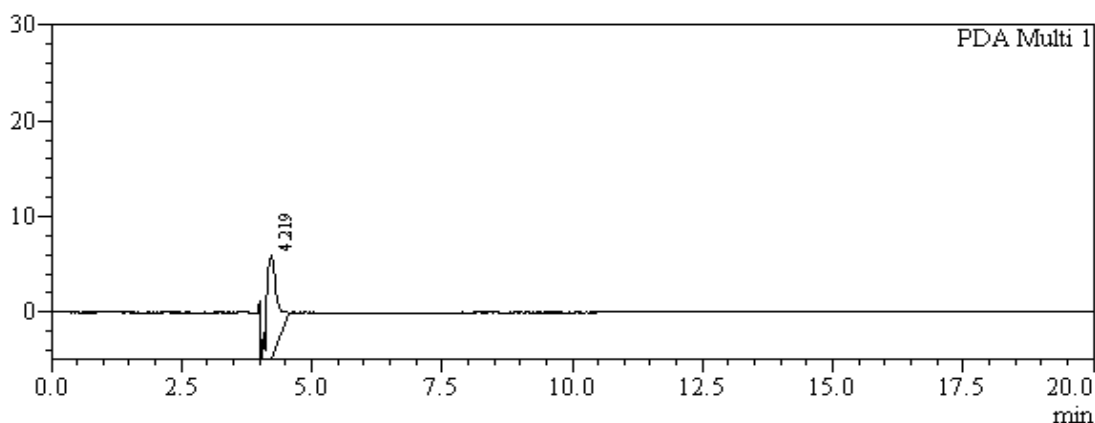

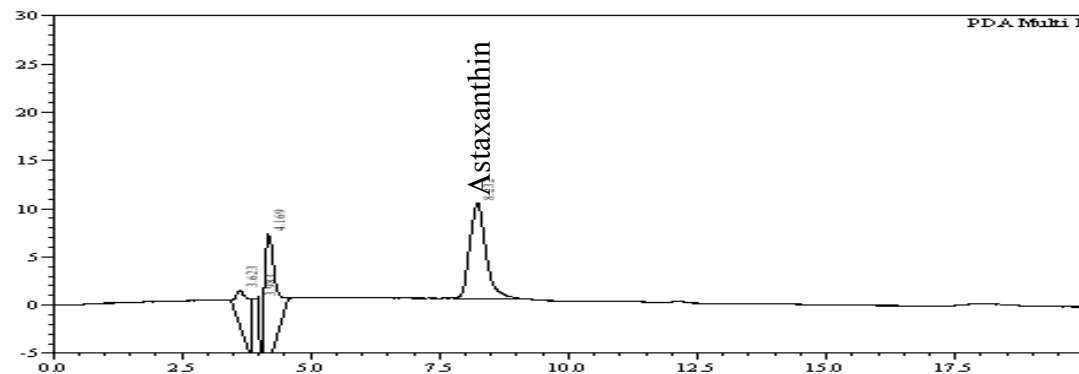Figure 44 HPLC chromatogram of methanol and dichloromethane medium (1:1 v/v)

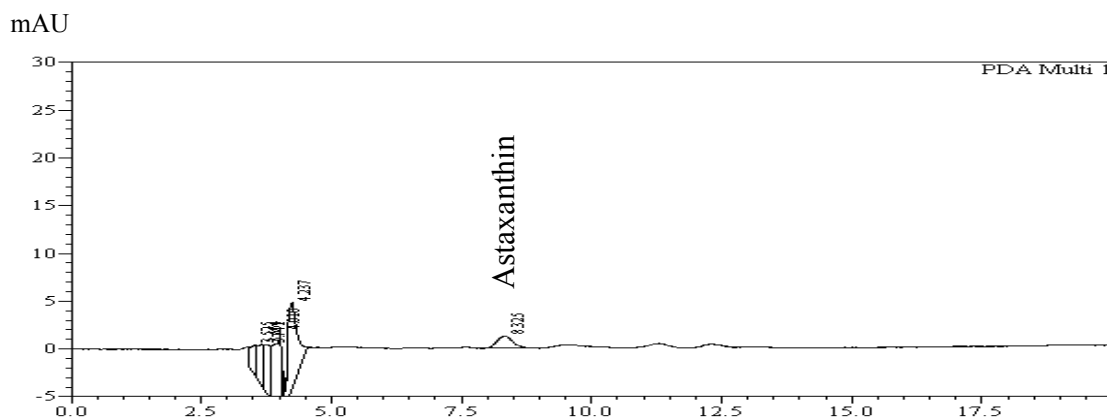Figure 45 HPLC chromatogram of free astaxanthin standard solution (final concentration of free astaxanthin = 0.125 µg/mL).

Figure 46 HPLC chromatogram of hydrolyzed extract (0.03N NaOH) (final concentration of free astaxanthin = 0.05 µg/mL).
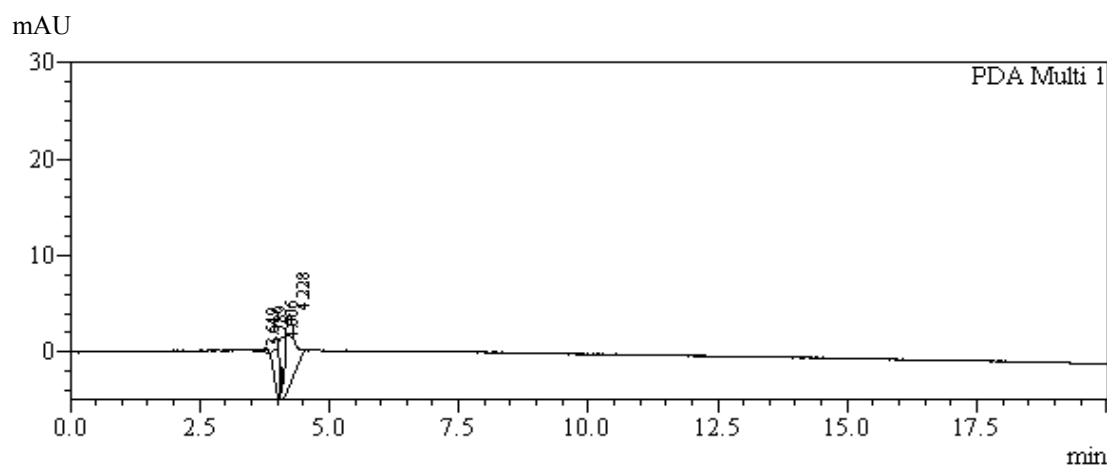

Figure 47 HPLC chromatogram of blank-SLNs (D10TI30-Blank).

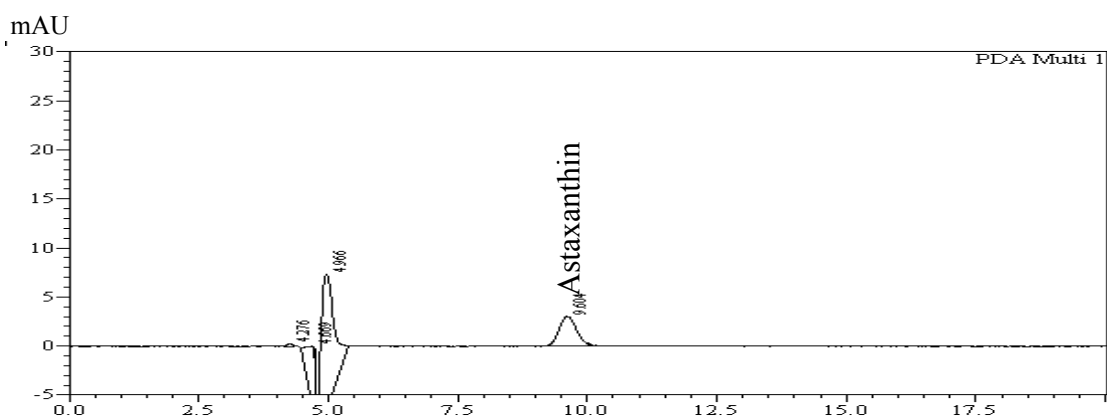Figure 48 HPLC chromatogram of ASX-SLNs (D10TI30-ASX, final concentration of free astaxanthin = 0.05 µg/mL).
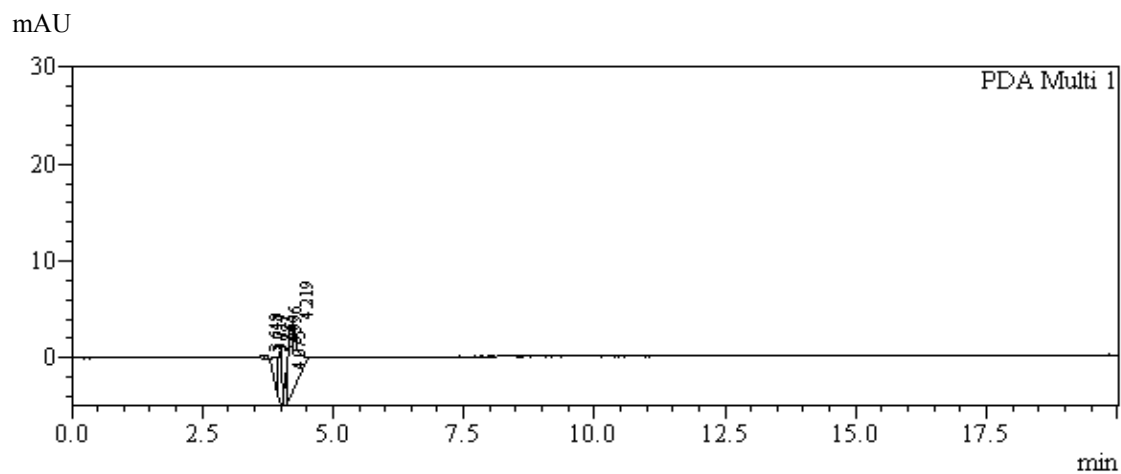
mAU

Figure 49 HPLC chromatogram of blank-SLNs (G10CE40-Blank).

mAU
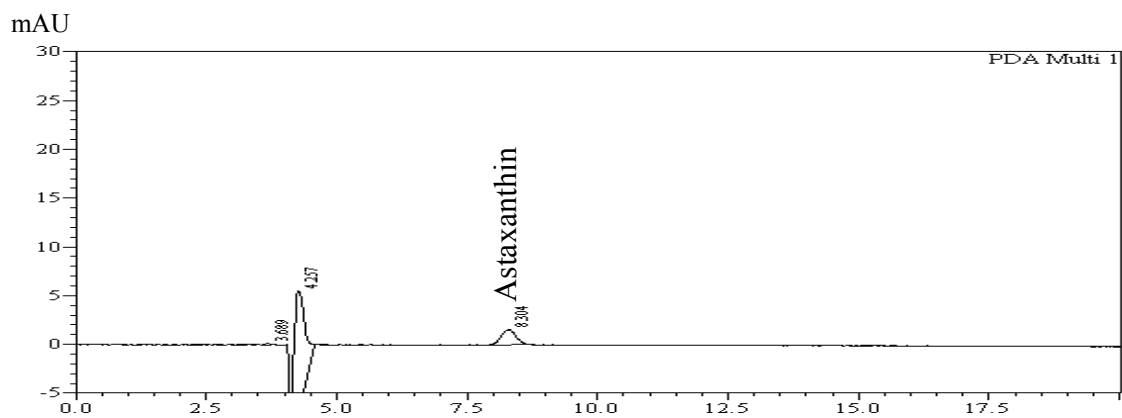
Figure 50 HPLC chromatogram of ASX-SLNs (G10CE40-ASX, final concentration of free astaxanthin = 0.05 μg/mL).

mAU

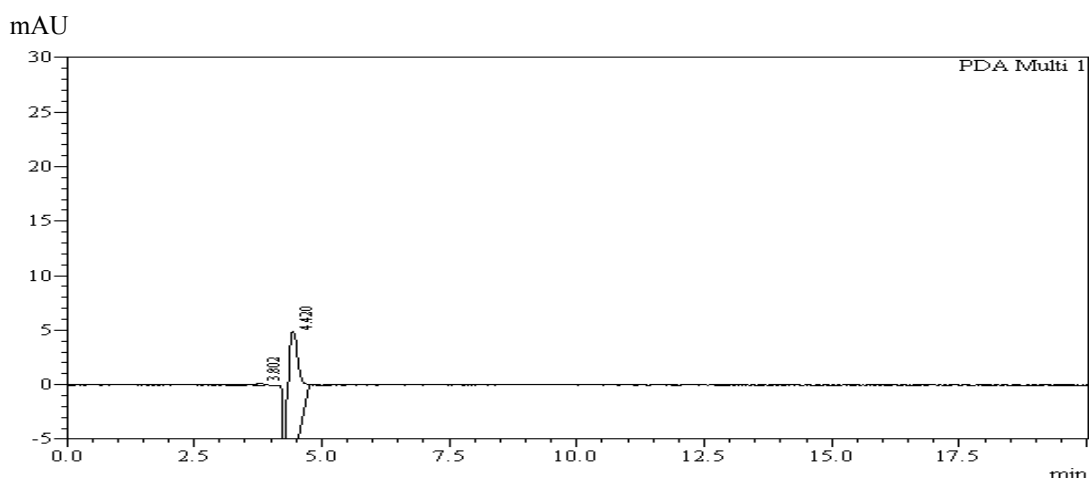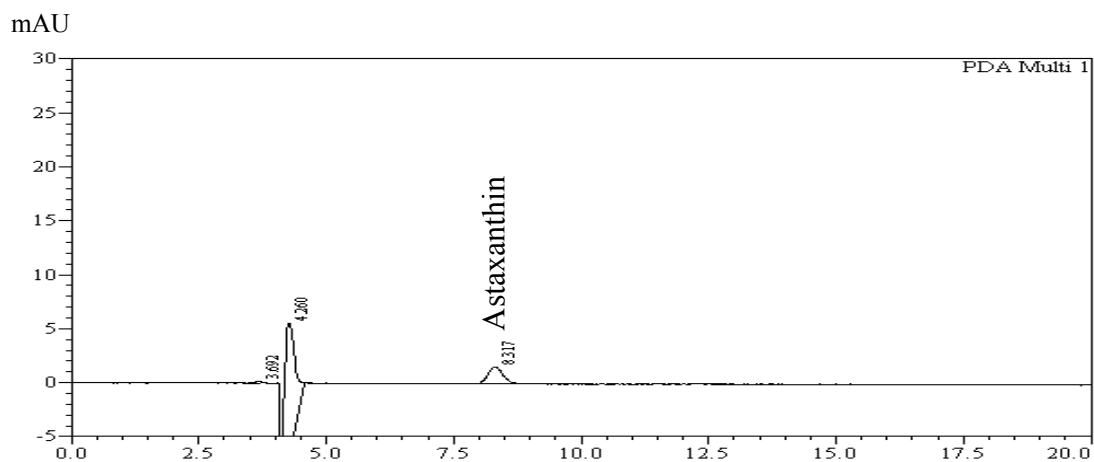Figure 51 HPLC chromatogram of blank receptor medium.

Figure 52 HPLC chromatogram of free astaxanthin and receptor medium (final concentration of free astaxanthin = 0.05 µg/mL).
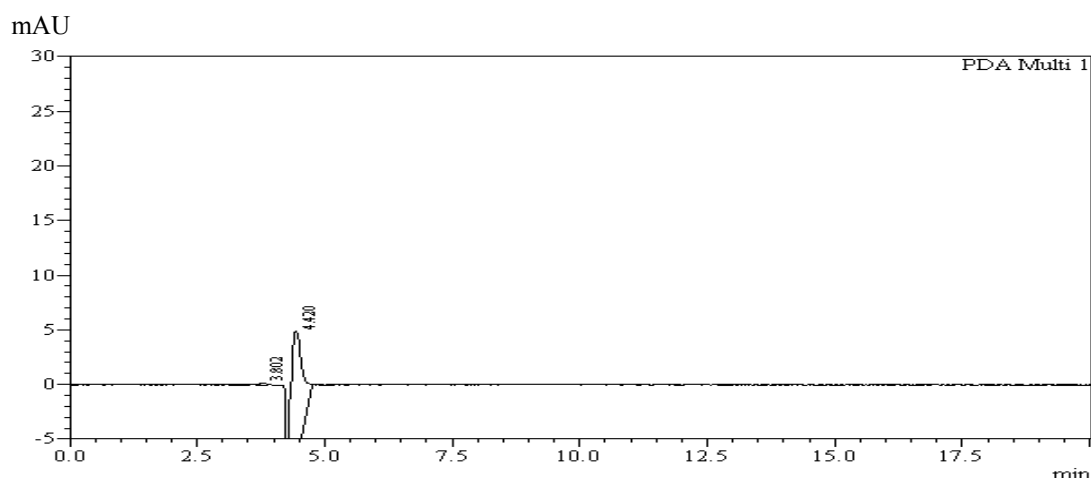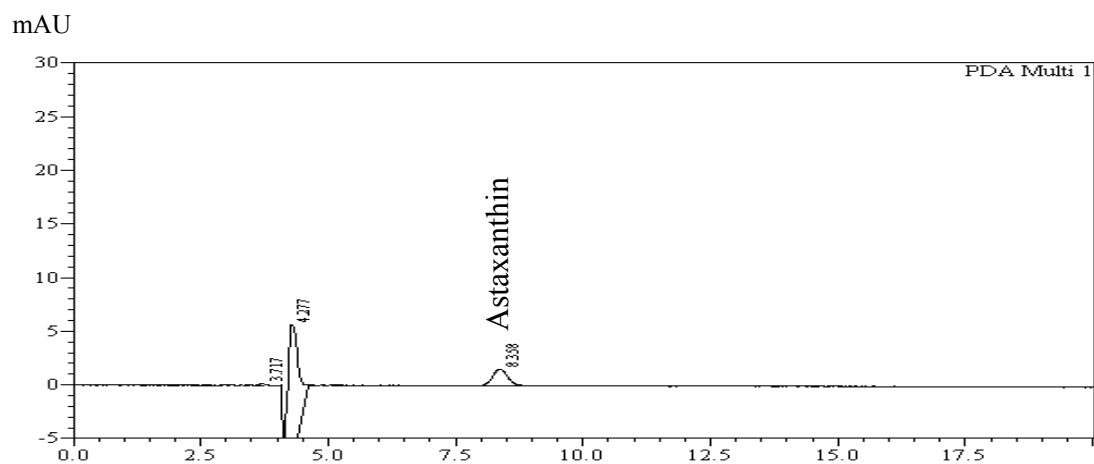

Figure 53 HPLC chromatogram of blank skin extract.

Figure 54 HPLC chromatogram of free astaxanthin and skin extract (final concentration of free astaxanthin = 0.05 µg/mL).

From Figures 44-54, the retention time of free astaxanthin peak was eluted at about 8.30 minutes. It was found that there was no interference from other components in the chromatogram including solid lipids, surfactants, skin extract, receiver fluid, solvent, and mobile phase. Hence, the HPLC method was acceptable for specificity.

2. Linearity

The linearity is the ability of the method to show test results that are directly equivalent to the concentration of analyte in the samples within a given range. The linearity is normally showed in the terms of variance around the slope of the regression line computed according to an established mathematical equation from the peak area gained by the analysis of test samples with different concentrations of analyte. The representative calibration curve data of free astaxanthin standard solution with methanol and dichloromethane (1:1 v/v) is shown in Table 11. The plot of free astaxanthin concentrations versus the peak areas illustrated the linear correlation in the concentration range of 0.0125-2.5000 µg/mL (Figure 55). The coefficient of determination (R^2) of this line was 1.0000. These results indicated that the HPLC method was acceptable for quantitative analysis of free astaxanthin in the range studied.

Table 11   Data for calibration curve of free astaxanthin by HPLC method.

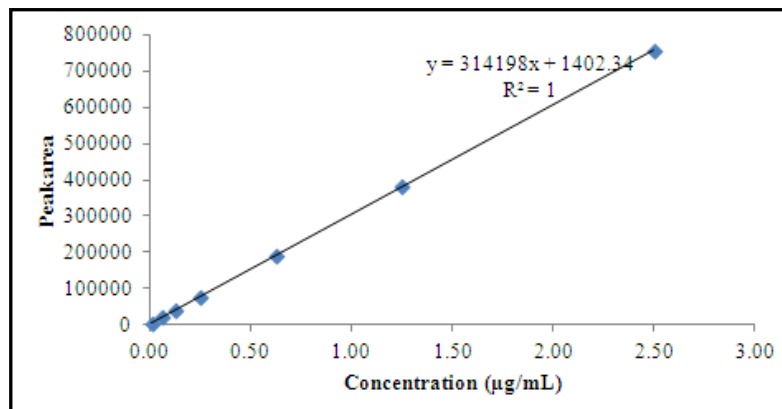| Concentration of astaxanthin (µg/mL)	Peak area			Mean	SD
	Set 1	Set 2	Set 3		
0.0125	3929	3348	3356	3544	333
0.0625	18960	18675	19540	19058	441
0.1250	40689	38966	38324	39326	1223
0.2500	76362	77273	76355	76663	528
0.6250	187530	187249	189480	188086	1215
1.2500	368973	374774	382528	375425	6801
2.5000	733977	747546	754039	745188	10237
R^2	1.0000	1.0000	1.0000	1.0000	-

Figure 55   Calibration curve of free astaxanthin by HPLC method.

3.   Accuracy

The accuracy is percent recovery obtained from the mean of observed concentrations calculated from the calibration curve divided by the mean of actual concentrations and multiplied by 100. The determination of accuracy was performed by analyzing fives sets of three concentrations (0.0125, 1, and 2 µg/mL) of free astaxanthin in methanol and dichloromethane medium (1:1 v/v). The percentages of analytical recovery were in the range of 98-102%, which pointed that this method could be used for analysis of free astaxanthin at all concentrations studied with high accuracy (the data is shown in Table 12).

Table 12   The percentage of analytical recovery of free astaxanthin by HPLC method.

Concentration of astaxanthin (µg/mL)	%Analytical recovery					Mean±SD
	Set 1	Set 2	Set 3	Set 4	Set 5	
0.0125	101.43	98.55	100.83	101.50	100.97	100.66±1.21
1.0000	99.35	101.06	98.49	99.44	101.50	99.97±1.26
2.0000	98.60	98.51	98.79	100.31	101.75	99.59±1.41

4.   Precision

The precision was determined in terms of percent coefficient of variation (%CV) or relative standard deviation (%RSD) of series of measurements.

Tables 13 and 14 illustrate the data of intraday precision and interday precision, respectively, of free astaxanthin in methanol and dichloromethane medium (1:1, v/v). All relative standard deviation values were small, 0.96–1.64% and 0.94–1.73%, respectively. Relative standard deviation of an analytical method should generally be less than 2%. Therefore, the HPLC method was precise for the quantitative analysis of free astaxanthin in the range studied.

Table 13   Data of intraday precision by HPLC method.

Concentration of astaxanthin (µg/mL)	Estimated concentration (µg/mL)					Mean±SD	%RSD
	Set 1	Set 2	Set 3	Set 4	Set 5		
0.0125	0.0129	0.0125	0.0126	0.0128	0.0124	0.0126±0.0002	1.6405
1.0000	0.9935	1.0262	0.9869	1.0069	0.9934	1.0014±0.0157	1.5646
2.0000	2.0024	2.0007	1.9798	2.0315	1.9917	2.0012±0.0192	0.9573

Table 14   Data of interday precision by HPLC method.

Concentration of astaxanthin (µg/mL)	Estimated concentration (µg/mL)					Mean±SD	%RSD
	Set 1	Set 2	Set 3	Set 4	Set 5		
0.0125	0.0123	0.0123	0.0126	0.0128	0.0126	0.0125±0.0002	1.7316
1.0000	1.0000	0.9987	1.0284	1.0308	0.9991	1.0114±0.0166	1.6455
2.0000	1.9781	1.9685	1.9908	2.0176	1.9956	1.9901±0.0187	0.9392

In conclusion, the analysis of free astaxanthin content by HPLC method validated in this research exhibited good specificity, linearity, accuracy and precision. The limit of quantitation (LOQ) or the lowest concentration at which free astaxanthin can be detected with agreeable accuracy, and precision was 0.0125 µg/mL. Thus, this HPLC method was used for computation of the free astaxanthin content in SLNs.

APPENDIX C

Titration results to form microemulsion boundary line within each phase diagram

Table 15   The titration results to form microemulsion boundary line within the phase diagram of cetyl palmitate, isopropanol, different surfactants, and water at 70°C.

Types of co-surfactants	Types of surfactants	The ratios of solid lipid and mixed surfactants	Solid lipid	Mixed surfactants	Water
Isopropanol	Tween®80	1:6	12.94	77.62	9.44
		1:3	21.65	64.94	13.42
		1:1	42.02	42.02	15.97
		3:1	63.03	21.01	15.97
		6:1	74.53	12.42	13.04
	Poloxamer®188	1:6	12.61	75.66	11.73
		1:3	20.83	62.50	16.67
		1:1	42.02	42.02	15.97
		3:1	61.22	20.41	18.37
		6:1	76.43	12.74	10.83
	Brij®S721	1:6	12.90	77.42	9.68
		1:3	23.75	71.26	4.99
		1:1	42.74	42.74	14.53
		3:1	62.50	20.83	16.67
		6:1	74.77	12.46	12.77
	Cremophor®RH40	1:6	13.09	78.53	8.38
		1:3	22.78	68.34	8.88
		1:1	42.92	42.92	14.16
		3:1	60.98	20.33	18.70
		6:1	73.85	12.31	13.85
	Myrj®52	1:6	13.02	78.13	8.85
		1:3	21.93	65.79	12.28
		1:1	41.49	41.49	17.01
		3:1	64.94	21.65	13.42
		6:1	74.30	12.38	13.31

Table 16 The titration results to form microemulsion boundary line within the phase diagram of Dynasan®118, isopropanol, different surfactants, and water at 70°C.

Types of co-surfactants	Types of surfactants	The ratios of solid lipid and mixed surfactants	Solid lipid	Mixed surfactants	Water
Isopropanol	Tween®80	1:6	3.43	20.60	75.97
		1:3	8.15	24.45	67.40
		1:1	28.99	28.99	42.02
		3:1	69.44	23.15	7.41
		6:1	79.58	13.26	7.16
	Poloxamer®188	1:6	12.67	76.05	11.28
		1:3	21.65	64.94	13.41
		1:1	38.91	38.91	22.18
		3:1	68.03	22.68	9.29
		6:1	81.08	13.51	5.41
	Brij®S721	1:6	4.92	29.53	65.55
		1:3	11.48	34.44	54.08
		1:1	35.84	35.84	28.32
		3:1	61.86	20.62	17.52
		6:1	81.19	13.53	5.28
	Cremophor®RH40	1:6	7.23	43.38	49.39
		1:3	8.62	25.86	65.52
		1:1	41.84	41.84	16.32
		3:1	68.97	22.99	8.04
		6:1	81.30	13.55	5.15
	Myrj®52	1:6	10.42	62.50	27.08
		1:3	12.52	37.55	49.93
		1:1	41.15	41.15	17.70
		3:1	68.81	22.94	8.25
		6:1	80.86	13.48	5.66

Table 17 The titration results to form microemulsion boundary line within the phase diagram of Dynasan®118, benzyl alcohol, different surfactants, and water at 70°C.

Types of co-surfactants	Types of surfactants	The ratios of solid lipid and mixed surfactants	Solid lipid	Mixed surfactants	Water
Benzyl alcohol	Tween®80	1:6	11.66	69.93	18.41
		1:3	19.46	58.37	22.17
		1:1	41.67	41.67	16.66
		3:1	66.52	22.17	11.31
		6:1	81.30	13.55	5.15
	Poloxamer®188	1:6	13.37	80.21	6.42
		1:3	22.27	66.82	10.91
		1:1	40.82	40.82	18.36
		3:1	70.09	23.36	6.55
		6:1	80.97	13.50	5.53
	Brij®S721	1:6	11.74	70.42	17.84
		1:3	20.88	62.63	16.49
		1:1	38.91	38.91	22.18
		3:1	66.67	22.22	11.11
		6:1	80.75	13.46	5.79
	Cremophor®RH40	1:6	12.20	73.17	14.63
		1:3	20.92	62.76	16.32
		1:1	45.45	45.45	9.10
		3:1	67.42	22.47	10.11
		6:1	81.52	13.59	4.89
	Myrj®52	1:6	11.22	67.34	21.44
		1:3	19.88	59.64	20.48
		1:1	42.19	42.19	15.62
		3:1	68.49	22.83	8.68
		6:1	82.53	13.76	3.71

Table 18 The titration results to form microemulsion boundary line within the phase diagram of Dynasan®118, ethanol, different surfactants, and water at 70°C.

Types of co-surfactants	Types of surfactants	The ratios of solid lipid and mixed surfactants	Solid lipid	Mixed surfactants	Water
Ethanol	Tween®80	1:6	6.06	36.36	57.58
		1:3	12.77	38.31	48.92
		1:1	34.25	34.25	31.50
		3:1	68.03	22.68	9.29
		6:1	81.30	13.55	5.15
	Poloxamer®188	1:6	12.95	77.72	9.33
		1:3	21.79	65.36	12.85
		1:1	42.19	42.19	15.62
		3:1	69.12	23.04	7.84
		6:1	81.63	13.61	4.76
	Brij®S721	1:6	7.91	47.47	44.62
		1:3	15.38	46.15	38.47
		1:1	40.65	40.65	18.70
		3:1	62.50	20.83	16.67
		6:1	80.75	13.46	5.79
	Cremophor®RH40	1:6	6.08	36.45	47.47
		1:3	12.00	36.01	51.99
		1:1	41.84	41.84	16.32
		3:1	68.81	22.94	8.25
		6:1	81.19	13.53	5.28
	Myrj®52	1:6	7.39	44.31	48.30
		1:3	13.37	40.11	46.52
		1:1	32.26	32.26	35.48
		3:1	68.49	22.83	8.68
		6:1	81.08	13.51	5.41

Table 19   The titration results to form microemulsion boundary line within the phase diagram of GMS, isopropanol, different surfactants, and water at 70°C.

Types of co-surfactants	Types of surfactants	The ratios of solid lipid and mixed surfactants	Solid lipid	Mixed surfactants	Water
Isopropanol	Tween®80	1:6	3.35	20.09	76.56
		1:3	11.53	34.60	53.87
		1:1	38.31	38.31	23.38
		3:1	63.83	21.28	14.89
		6:1	78.12	13.02	8.86
	Poloxamer®188	1:6	11.89	71.34	16.77
		1:3	21.14	63.42	15.44
		1:1	40.65	40.65	18.70
		3:1	63.03	21.01	15.96
		6:1	75.19	12.53	12.28
	Brij®S721	1:6	5.29	31.71	63.00
		1:3	12.27	36.81	50.92
		1:1	36.36	36.36	27.28
		3:1	64.66	21.55	13.79
		6:1	77.42	12.90	9.68
	Cremophor®RH40	1:6	1.89	11.35	86.76
		1:3	9.19	27.57	63.24
		1:1	41.67	41.67	16.66
		3:1	65.93	21.98	12.09
		6:1	79.79	13.30	6.91
	Myrj®52	1:6	4.57	27.43	68.00
		1:3	9.80	29.41	60.79
		1:1	38.46	38.46	23.08
		3:1	65.79	21.93	12.28
		6:1	76.92	12.82	10.26

Table 20 The titration results to form microemulsion boundary line within the phase diagram of GMS, benzyl alcohol, different surfactants, and water at 70°C.

Types of co-surfactants	Types of surfactants	The ratios of solid lipid and mixed surfactants	Solid lipid	Mixed surfactants	Water
Benzyl alcohol	Tween®80	1:6	11.93	71.60	16.47
		1:3	20.49	61.48	18.03
		1:1	42.55	42.55	14.90
		3:1	68.49	22.83	8.68
		6:1	78.84	13.14	8.02
	Poloxamer®188	1:6	12.39	74.35	13.26
		1:3	21.14	63.42	15.44
		1:1	42.92	42.92	14.16
		3:1	65.50	21.83	12.67
		6:1	78.02	13.00	8.98
	Brij®S721	1:6	11.86	71.17	16.97
		1:3	20.33	60.98	18.69
		1:1	36.23	36.23	27.54
		3:1	62.76	20.92	16.32
		6:1	76.34	12.72	10.94
	Cremophor®RH40	1:6	11.49	68.97	19.54
		1:3	19.34	58.03	22.63
		1:1	40.82	40.82	18.36
		3:1	64.38	21.46	14.16
		6:1	77.72	12.95	9.33
	Myrj®52	1:6	11.29	67.72	20.99
		1:3	19.19	57.58	23.23
		1:1	42.37	42.37	15.26
		3:1	63.42	21.14	15.44
		6:1	77.62	12.94	9.44

Table 21 The titration results to form microemulsion boundary line within the phase diagram of GMS, ethanol, different surfactants, and water at 70°C.

Types of co-surfactants	Types of surfactants	The ratios of solid lipid and mixed surfactants	Solid lipid	Mixed surfactants	Water
Ethanol	Tween®80	1:6	5.87	35.19	58.94
		1:3	12.39	37.17	50.44
		1:1	37.45	37.45	25.10
		3:1	63.97	21.32	14.71
		6:1	77.82	12.97	9.21
	Poloxamer®188	1:6	12.47	74.81	12.72
		1:3	21.23	63.7	15.07
		1:1	42.02	42.02	15.96
		3:1	63.97	21.32	14.71
		6:1	77.32	12.89	9.79
	Brij®S721	1:6	7.72	46.33	45.95
		1:3	15.06	45.18	39.76
		1:1	34.48	34.48	31.04
		3:1	63.03	21.00	15.97
		6:1	76.05	12.67	11.28
	Cremophor®RH40	1:6	5.95	35.71	58.34
		1:3	12.59	37.78	49.63
		1:1	42.02	42.02	15.96
		3:1	64.52	21.51	13.97
		6:1	77.32	12.89	9.79
	Myrj®52	1:6	6.39	38.31	55.30
		1:3	14.53	43.60	41.87
		1:1	35.71	35.71	28.58
		3:1	63.42	21.14	15.44
		6:1	77.92	12.99	9.09

APPENDIX D

DSC thermograms
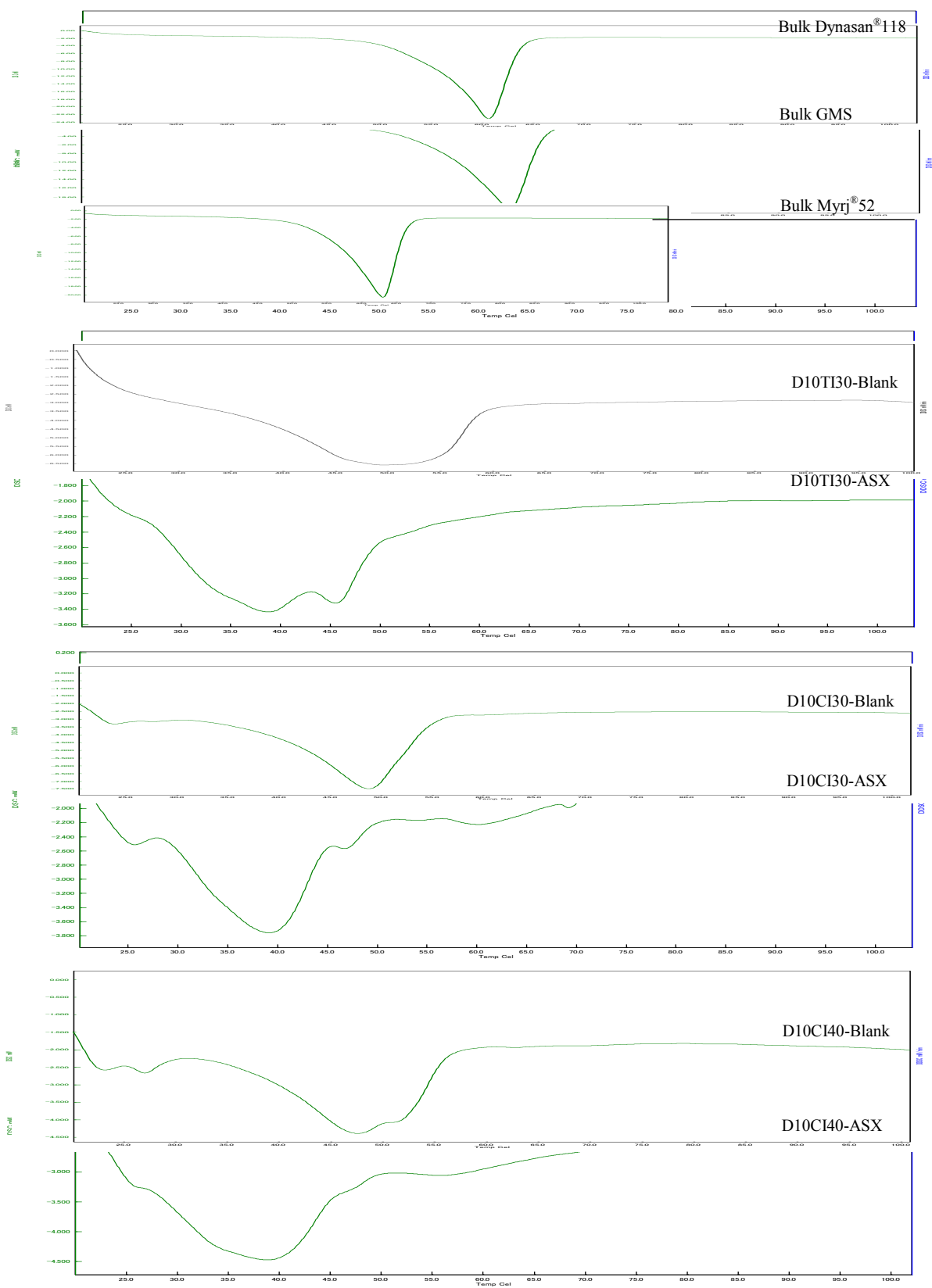
Figure 56 DSC thermograms of bulk materials, lyophilized blank-SLNs, and ASX-SLNs formulations.
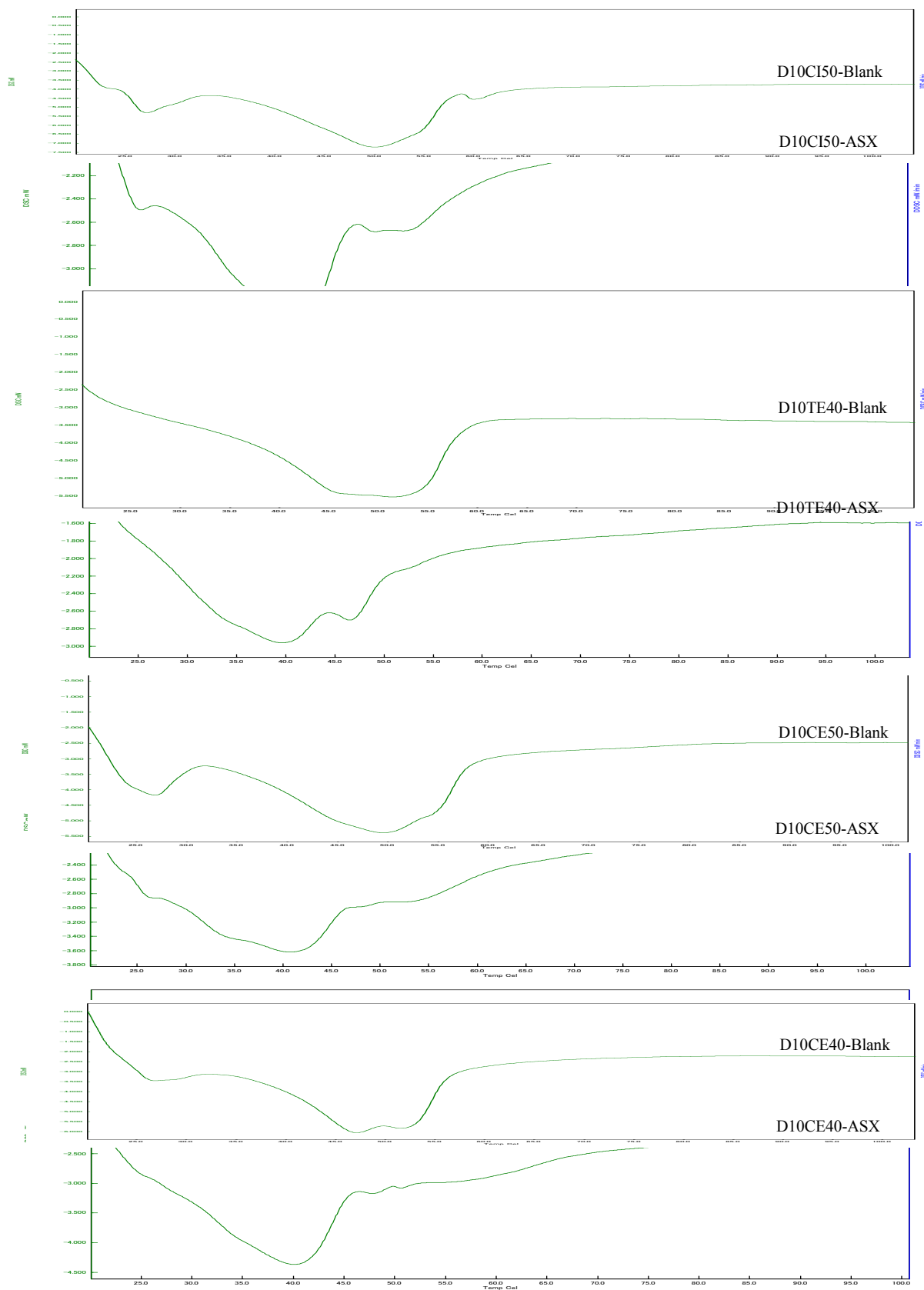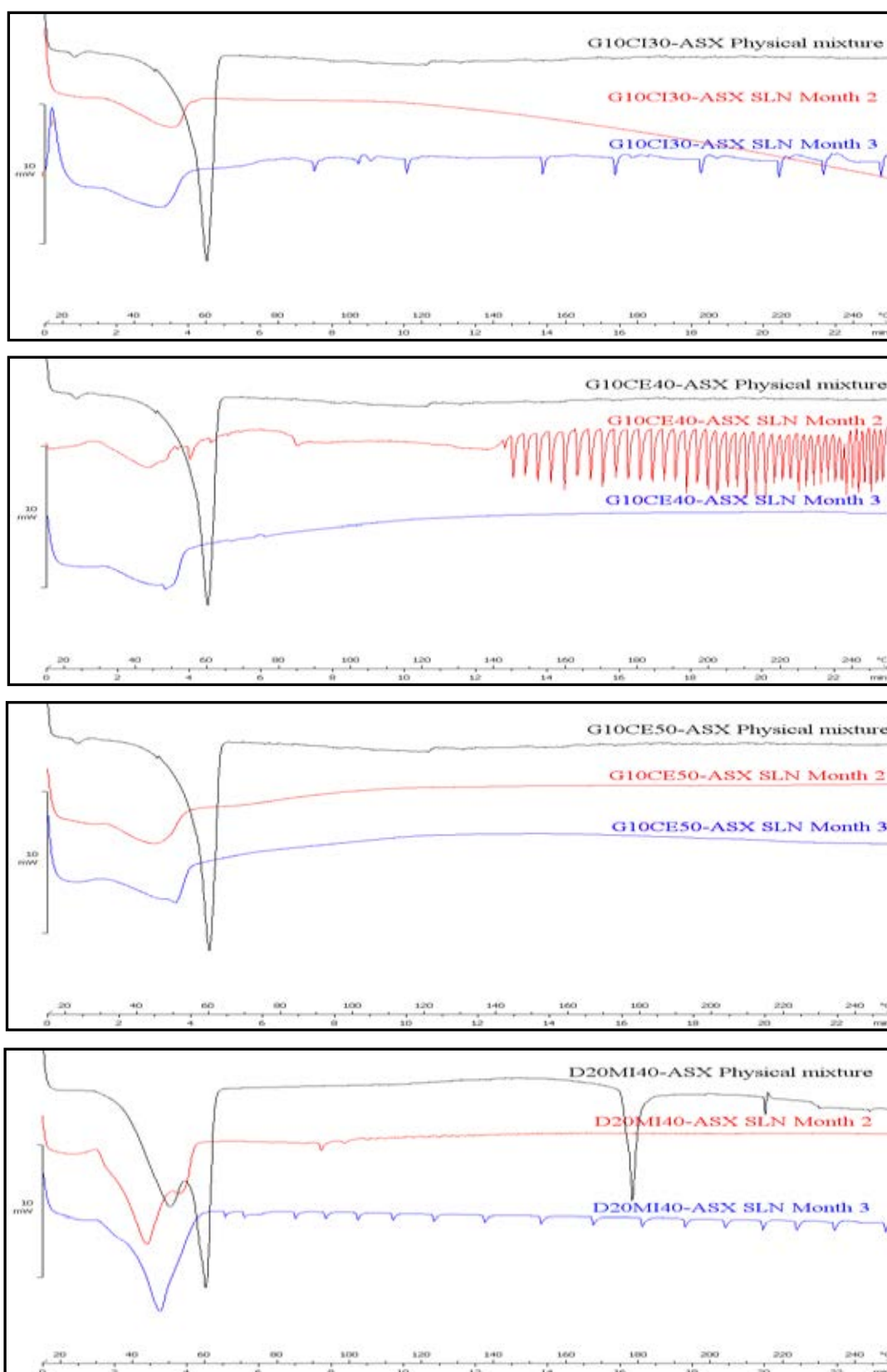
Figure 56 (Cont.) DSC thermograms of bulk materials, lyophilized blank-SLNs, and ASX-SLNs formulations.
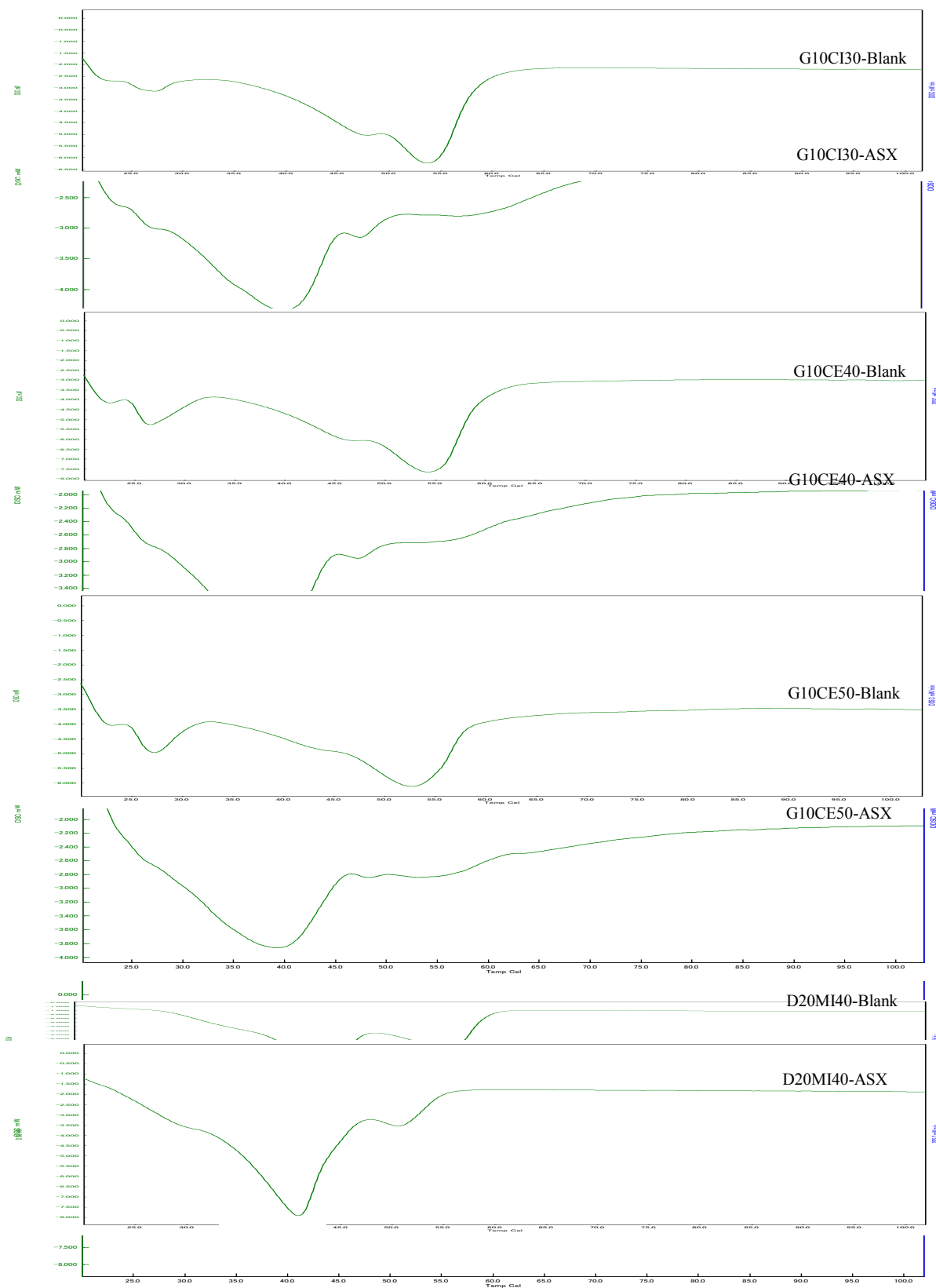
Figure 56 (Cont.) DSC thermograms of bulk materials, lyophilized blank-SLNs, and ASX-SLNs formulations.
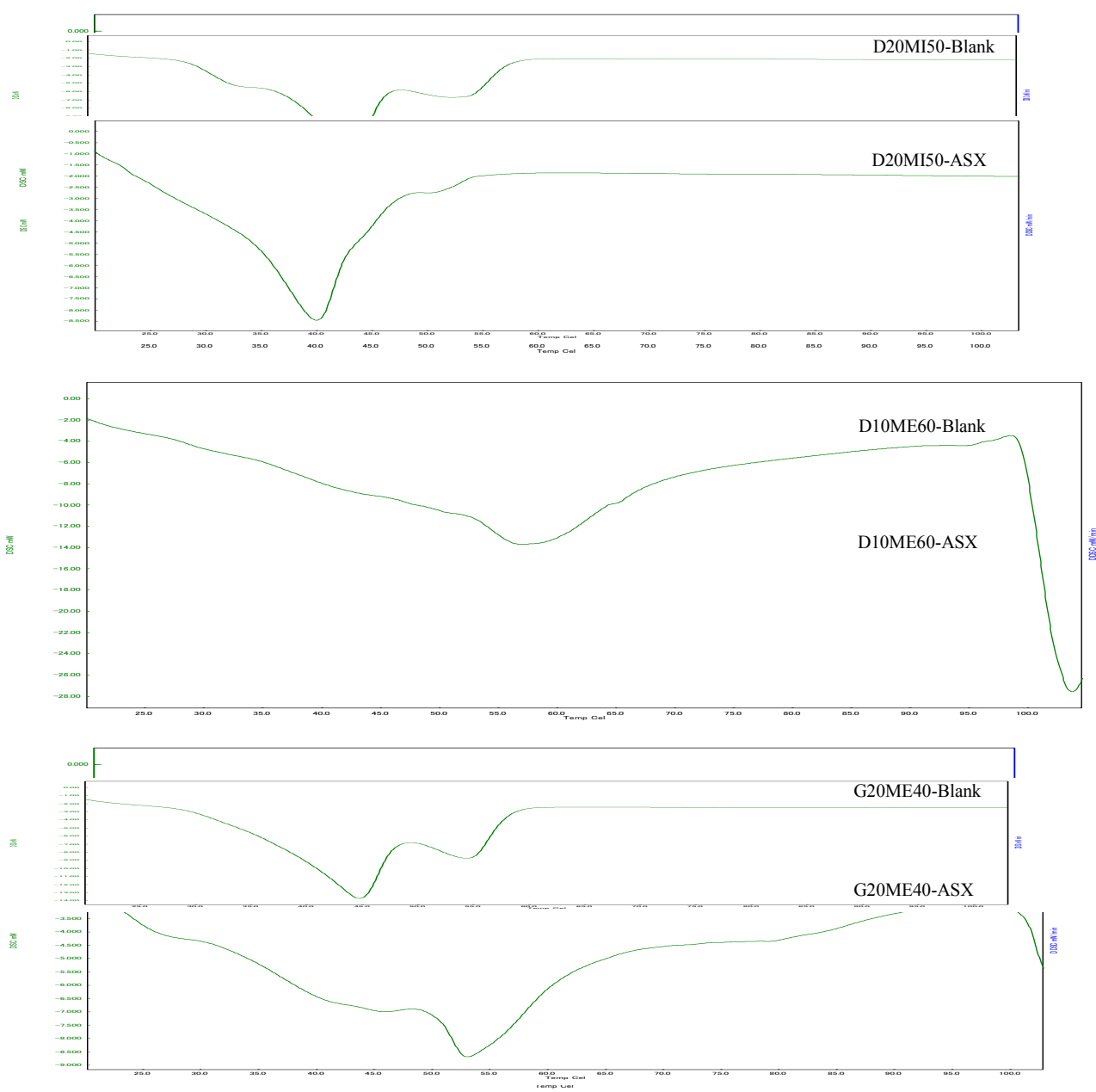
Figure 56 (Cont.) DSC thermograms of bulk materials, lyophilized blank-SLNs, and ASX-SLNs formulations.
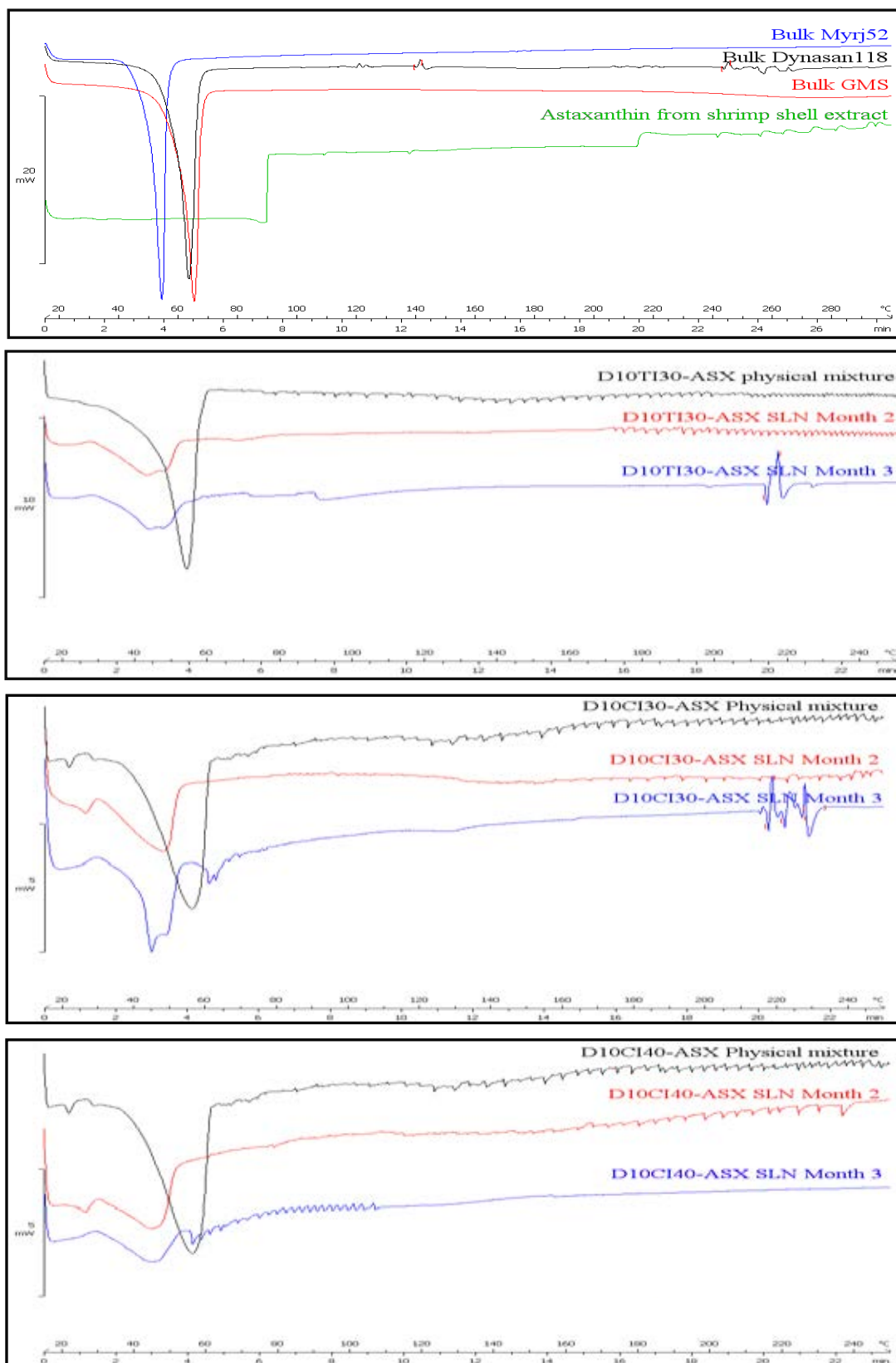
Figures 57 DSC thermograms of bulk materials, ASX-physical mixture, lyophilized ASX-SLNs formulations during storage.
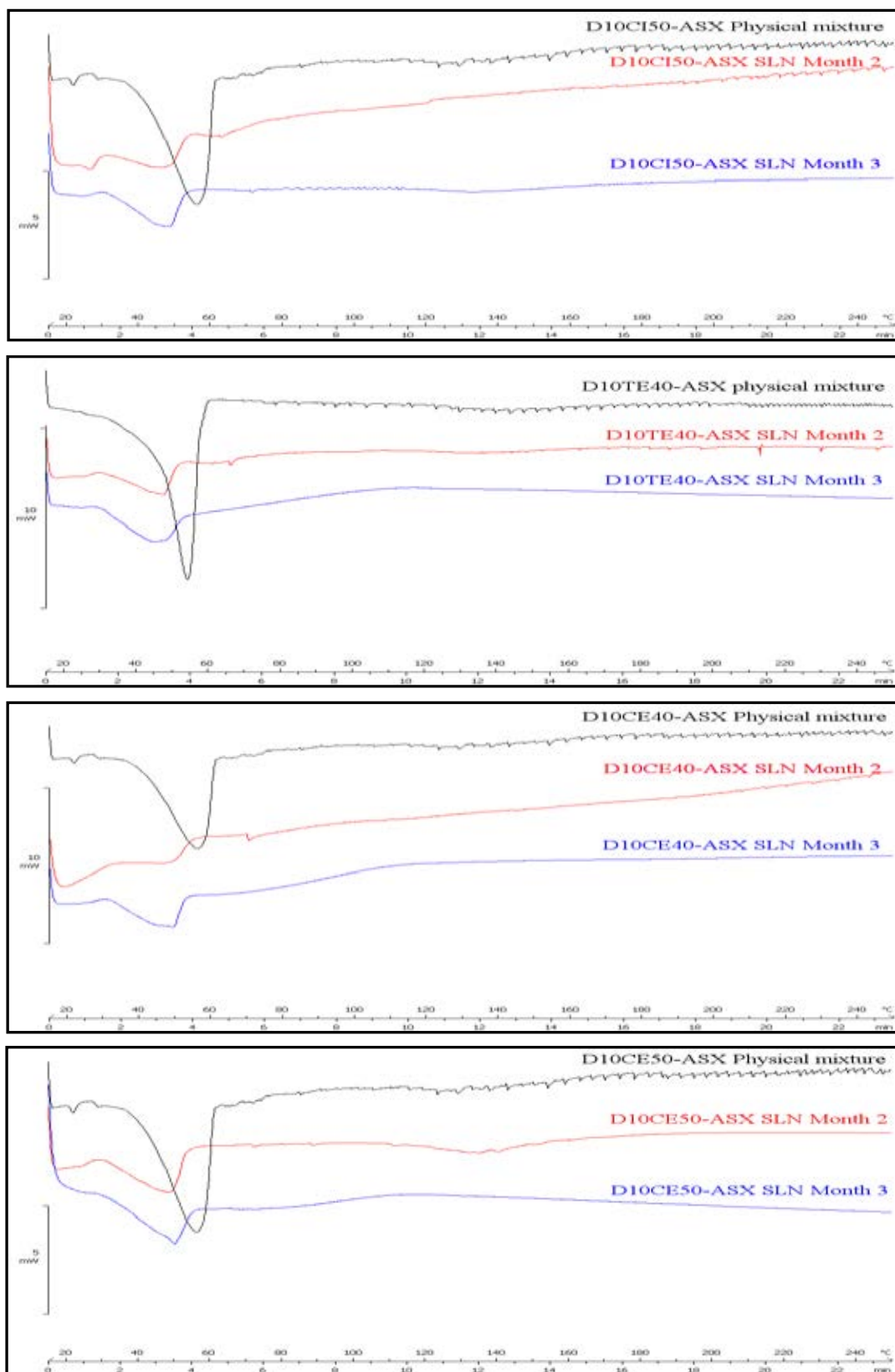
Figures 57 (Cont.) DSC thermograms of bulk materials, ASX-physical mixture, lyophilized ASX-SLNs formulations during storage.

Figures 57 (Cont.) DSC thermograms of bulk materials, ASX-physical mixture, lyophilized ASX-SLNs formulations during storage.
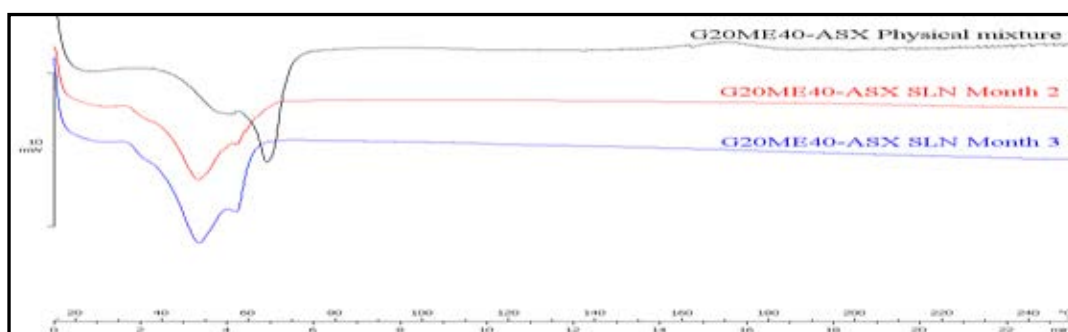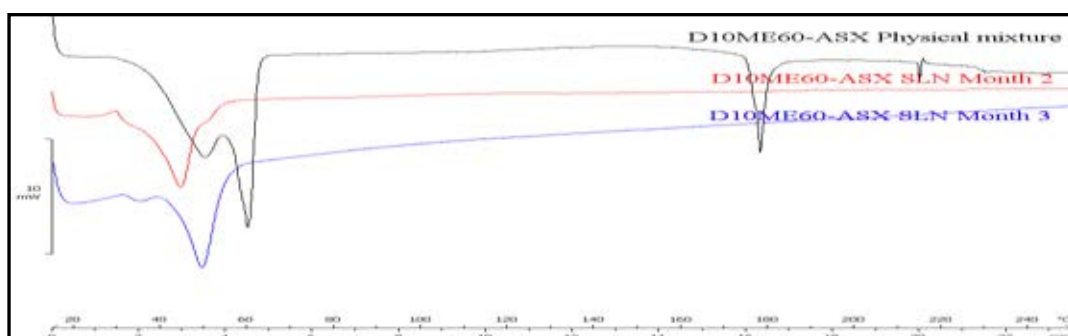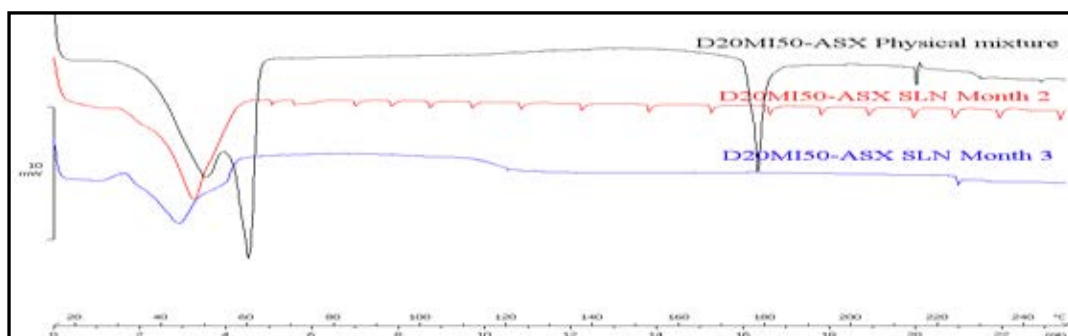
Figures 57 (Cont.) DSC thermograms of bulk materials, ASX-physical mixture, lyophilized ASX-SLNs formulations during storage.

APPENDIX E

Molecular structure and physical properties
of some materials

Properties of some materials used in this study

1.   Brij®S721

Synonyms: polyoxyethylene (21) stearyl ether, steareth 21

Structural formula:
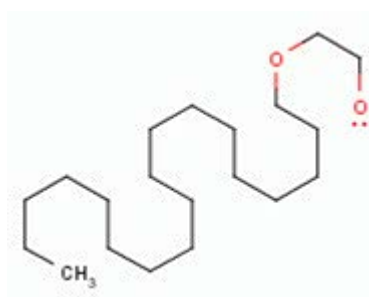
HLB value: 16

Melting point: 43°C

2.   Cetyl palmitate

Synonyms: hexadecyl hexadecanoate, palmityl palmitate, hexadecyl ester

Structural formula:
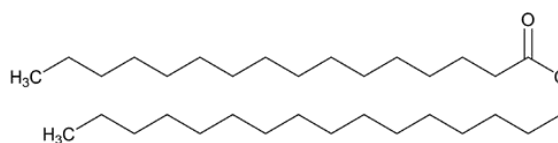
HLB value: 10

Melting point: 54°C

3.   Compritol®ATO 888

Synonyms: glyceryl behenate, glycerol dibehenate

Structural formula:
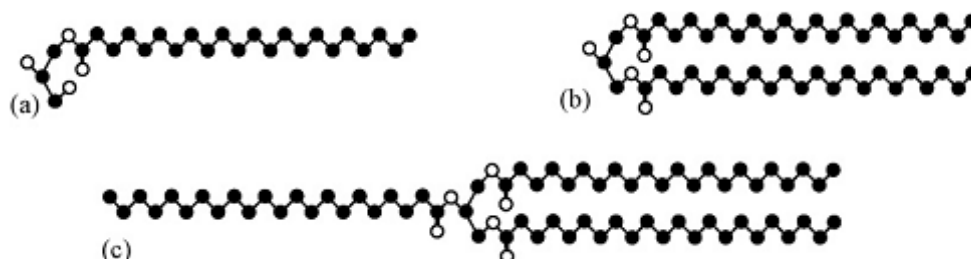
Where, (a) monobehenate, (b) dibehenate, and (c) tribehenate

HLB value: 2

Melting point: 65-77°C

4. Cremophor®RH40

Synonyms: polyoxyl 40 hydrogenated castor oil, macrogol-glycerolhydroxystearate, polyoxyethylenglycerol trihydroxystearate, Kolliphor®RH40, glycerol-polyethylene glycol oxystearate (hydrogenated) castor oil
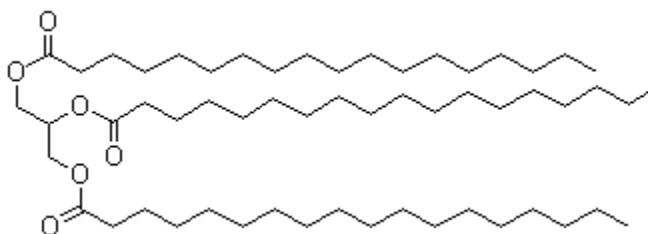
HLB value: 14-16

Melting point: 20°C

5. Dynasan®118

Synonyms: tristearin, stearic acid triglyceride, glycerol tristearate
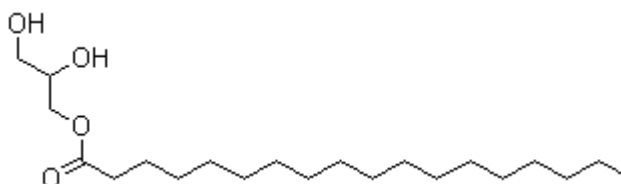
Structural formula:

HLB value: 3

Melting point: 72°C

6. Glyceryl monostearate

Synonyms: monostearin, glycerin monostearate, glycerol monostearate
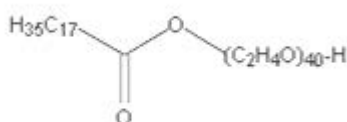
Structural formula:

HLB value: 3.8

Melting point: 55-60°C

7. Myrj®52

Synonyms: Polyoxyethylene 40 stearate, fatty acid glycol, PEG-20 stearate, polyoxyethylene glycol 40 monostearate, polyoxyl 40 stearate
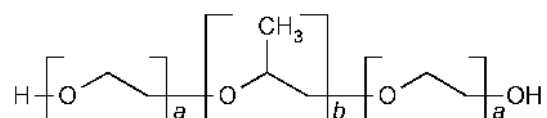
Structural formula:

HLB value: 16.9

Melting point: 38°C

### 8.	Poloxamer®188

Synonyms: Pluronic®F-68, Lutrol, polyethylene-propylene glycol copolymer, polyoxyethylene-polyoxypropylene copolymer
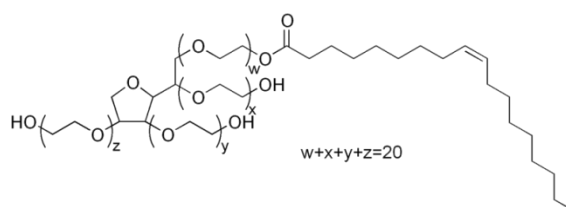
Structural formula:

Where, a=80, b=27

HLB value: 29

Melting point: 52-57°C

### 9.	Tween®80

Synonyms: polysorbate 80, polyoxyethylene sorbitan (20) monooleate, polyoxyethylenesorbitan monooleate, PEG (80) sorbitan monooleate

Structural formula:

HLB value: 15

APPENDIX F

The protocol from Ethics Committee

VITA

Mr. Kritsada Roopyai was born on June 26, 1987 in Chanthaburi, Thailand. He graduated with a Bachelor of Science Degree in Pharmacy (first-class honors) from the Faculty of Pharmacy, Mahidol University in 2009. Before the enrollment in the Master degree program in Pharmacy at Chulalongkorn University in 2011, he worked at Silom Medical Co., Ltd. as a pharmacist in the department of research and development for 1 year.